Ultrasound Measurement in Metal Melts:

Microscale Mechanisms and Improvements

by

Bitong Wang

Submitted in Partial Fulfillment of the

Requirements of the Degree

Doctor of Philosophy

Supervised by

Professor Douglas H. Kelley

Materials Science Program

Arts, Sciences and Engineering

Edmund A. Hajim School of Engineering and Applied Sciences

University of Rochester

Rochester, New York

2022

Table of Contents

Biographical Sketch

The author was born in Baoding, a small city in China, and spent his childhood there. In 2011, the author attended Sichuan University, China as an undergrad, and earned a Bachelor of Engineering degree in Metal Material Engineering in 2015. In the fall of 2015, the author came to the United States and began studying at the University of Rochester as a graduate student in the Materials Science Program.

In September 2016, the author met his advisor, Professor Douglas H. Kelley, and joined the Mixing Lab. Then, he started the research on ultrasound and liquid metals. During that time, the author was deeply attracted by the beauty of liquid metals, the magic of ultrasound, and the creativity of scientific research. So, after he obtained a Master of Science degree in 2017, the author decided to continue pursuing a Doctorate in Materials Science at the University of Rochester, under the supervision of Prof. Kelley. During the period of doctoral study, the author served as the research assistant and has participated in multiple projects, spanning the fields of ultrasound measurement, liquid metal battery, and wetting assessment of molten metals and molten salts.

Besides research activity, the author has served as a teaching assistant at the University of Rochester for the classes Solar Cell and Practical Electron Microscopy during the period 2019-2020. The author was also served as the vice president of the Materials Research Society - University of Rochester Chapter during the period 2019-2021.

List of Publications:

1. **B. Wang** and D.H. Kelley. Microscale mechanisms of ultrasound velocity measurement in metal melts, Flow Measurement and Instrumentation, Volume 81, 2021, ISSN 0955-5986, https://doi.org/10.1016/j.flowmeasinst.2021.102010.

2. **B. Wang** and D.H. Kelley. Optimal Vessel Materials for Indirect-contact Ultrasound Measurements. Proceedings of 13th International Symposium on Ultrasonic Doppler Methods for Fluid Mechanics and Fluid Engineering. 2021. Zürich, Switzerland.

3. **B. Wang**, A. Caldwell, A. Allanore, D.H. Kelley. Investigation of Echo Source and Signal Deterioration in Ultrasound Measurement of Metal Melt. In: TMS 2022 151st Annual Meeting & Exhibition Supplemental Proceedings. The Minerals, Metals & Materials Series. Springer, Cham. https://doi.org/10.1007/978-3-030-92381-5_46.

4. J. S. Cheng, **B. Wang**, I. Mohammad, G. M. Horstmann, and D. H. Kelley. UDV methods for characterizing flows in liquid metal batteries. Proceedings of 13th International Symposium on Ultrasonic Doppler Methods for Fluid Mechanics and Fluid Engineering. 2021. Zürich, Switzerland.

5. J. S. Cheng, **B. Wang**, I. Mohammad, J. M. Forer, and D. H. Kelley. Laboratory model of electrovortex flow with thermal gradients, for liquid metal batteries. arXiv preprint arXiv:2108.01648, 2021. Submitted.

6. J. S. Cheng, I. Mohammad, **B. Wang**, D. F. Keogh, J. M. Forer, and D. H. Kelley. Oscillations of the large-scale circulation in experimental liquid metal convection at aspect ratios 1.4-3. 2022: Under consideration for publication in J. Fluid Mech.

Acknowledgments

In the journey of my graduate study, as well as in the seven years of my life at Rochester, many people have helped me, supported me, and encouraged me to keep going forward.

Firstly, I would like to thank my advisor Douglas Kelley for his continuous support and guidance, both in research and in my daily life. Prof. Kelley is a great teacher, brilliant scientist, and trusted leader. He loves reading, sporting, and enjoying life, which deeply influenced me. He is the most energetic person I have ever met, and always full of passion for learning and trying new things. He always encouraged us to attend conferences, share our knowledge, and learn from the community. I am very grateful for all his help with respect to my study, research, presentation and writing skills, and English.

I also want to acknowledge my colleagues and friends from the Mixing Lab. Every one of them is so special and incredible. I want to thank all current and prior team members I have worked with: Ibrahim Mohammad, Ruy Ibanez, Yiming Gan, Aditya Raghunandan, Kimberly Boster, Keelin Quirk, Jarod Forer, Nikola Raicevic, Helena Schreder, Jonathan Cheng, Jia Liu, Jeff Tithof, Rakan Ashour, Thomas Nevins, Gerrit Horstmann, Fatima Min Rivas, Logan Bashford, Mira Bodek, Andrew Fianu, Kimberly Llajaruna Peralta, Frederico Hama, Beauclaire Mbanya, Rebeca Toro Garza, and Jinge Wang. These creative people have offered me tremendous support and help. I have also learned and appreciated different cultures from them. The daily group lunch, group dinners every summer and

winter, team sports, as well as conference experiences, will be fond memories in my heart forever. I would like to particular gratitude the liquid metal battery crew; they made me realize how powerful and productive teamwork can be!

Many faculties and staff around the University of Rochester have provided me with immeasurable help. I would like to thank Professor Yates Matthew for providing me with the summer research opportunity in 2016. I want to thank Brian McIntyre for coaching me on SEM, EDS, and various coating methods; he always shares all kinds of skills with me selflessly. I want to thank James Alkins for training me in machining works. I want to thank Christine Pratt for teaching me various instruments in the material lab and providing me with all kinds of supplemental support. I want to thank Mike Pomerantz and Omar Soufan for helping me with some machining and characterization works. I want to thank Gina Eagan for all her help with administrative assistance throughout my graduate career, from my first day of admission to the later day of defense preparation. I also want to thank the staff in the ME office for their assistance. I will always remember the warm and wonderful ME Christmas party, the delicious food, and the drink Jill and Ibrahim made!

In addition, I would like to say thanks to my roommates and some friends in Rochester and from my hometown. I want to thank Siyuan Liu, Yifan Li, Haowen Zhu, Wentao Hu, Jiawei Sun, and Yawen Tian. Their accompany brings a lot of pleasure to my daily life.

In the last, I want to thank my father and mother, my grandparents, my cousins, and all members of my big family. Their constant encouragement and deep love made me stronger and inspired me to be a better person.

Abstract

Ultrasound Doppler velocimetry (UDV) is one of the few techniques enabling real-time imaging and flow measurement in metal melts. However, ultrasound measurement in metal melts is difficult reliable because its operation depends on phenomena that are poorly understood. This thesis focuses on ultrasound measurement in liquid gallium, one of the liquid metals most common in laboratory studies. To establish the UDV measurement as a reliable technique, I investigated the underlying mechanisms of ultrasound measurement in liquid gallium and explored ways to improve the quality and accuracy of UDV measurement.

To understand the mechanisms of ultrasound measurement in liquid gallium, I performed experimental investigations on the source of bulk echoes in gallium. I present evidence from microscopy examinations and ultrasound measurements that oxide inclusions are mainly responsible for bulk echoes in gallium. I explored the ultrasound scattering mechanisms of oxide inclusions with a novel size estimation method and demonstrated that ultrasound waves in liquid gallium are mainly scattered by gallium oxide inclusions in agglomerated form, primarily via Mie scattering. In summary, UDV utilizes the backscattering echoes from gallium oxides to obtain consecutive bulk echoes and thus enable flow velocity measurements in gallium.

To improve the quality and accuracy of UDV measurements, I conducted the indirect-contact ultrasound measurement in gallium. I systematically investigated the effect of vessel wall material, including the material type, thickness, and wetting properties, on ultrasound measurements, and found that acrylic is the best common vessel material for liquid gallium. In addition, I studied ultrasound signal deterioration in gallium and found two distinct causes: the loss of scattering particles from the bulk due to density difference, and the degradation of wetting at the UDV transducer surface that occurs with ultrasound emission. I further discussed ultrasound-induced cavitation in gallium, a possible underlying mechanism causing the degradation of wetting. I show evidence that indirect-contact ultrasound measurements through a material that wets the melt well not only improve the accuracy and quality of ultrasound measurements, but also mitigate the signal deterioration caused by wetting degradation.

The outcome of this work not only provides us with more comprehensive knowledge and insights concerning ultrasound and metal melts, but also enables us to better use the UDV measurement in other studies involving metal melts, for instance, the study of liquid metal batteries.

Contributors and Funding Sources

This work was supported by a dissertation committee consisting of Professor Douglas H. Kelley (advisor) and Professor Niaz Abdolrahim of the Department of Mechanical Engineering, and Professor Diane Dalecki of the Department of Biomedical Engineering. Professor Danielle Benoit of the Department of Biomedical Engineering served as the chair of the defense committee. The committee members have offered constructive advice and a tremendous help to this thesis.

The research work in this thesis was funded by the National Science Foundation (NSF) under grant numbers CMMI-1562545 and CBET-1552182. Professor Douglas H. Kelley was the principal investigator of both projects. Additional support was provided through the University of Rochester.

Professor Antoine Allanore and Andrew Caldwell of Massachusetts Institute of Technology contributed to Chapter 4 of this thesis, with their collaboration on studying the dissolved gas and ultrasound-induced cavitation in liquid gallium. Jonathan Cheng and Ibrahim Mohammad contributed to the liquid metal battery experiments in Appendix A. The rest was the author's independent work.

List of Tables

List of Figures

—— Chapter 1 ——

Introduction

1.1 Research background-study of liquid metals and metal melts

Over the thousands of years of human history, metals and their alloys are among the most important materials promoting the evolution of human society. Since the development of modern science and technology, there are various advanced techniques and tools available for us to characterize and examine the properties of metal materials when they are in the solid state. However, even up to now, there are only a few methods allowing us to ‘look’ the inside of metals when they are in the liquid state. Generally, metal in the liquid state is termed as liquid metal or metal melt.

In many engineering fields, monitoring the internal conditions and measuring the flows inside metal melts are important. For example, in the metal casting process, the impurity level and the flow pattern of the metal melt inside the casting mold will affect the quality of the final cast product [1]. For many years, the electromagnetic stirrer and electromagnetic brake have been considered effective ways to enhance the casting quality and productivity during the continuous casting process [2]. However, for the current casting technology, the characterization and inspection of casting products are carried out only after solidification, so there is no real-time feedback on the impurity levels or the effects of electromagnetic control. In addition to traditional fields such as alloy casting, research and applications related to liquid metals or metal melts are developing rapidly in many emerging fields. For instance, liquid gallium and its alloys are widely applied to novel

flexible electronics and wearable devices, in which the liquid metal's behaviors directly determine their safety and performance [3]. Lead-bismuth (PbBi) is commonly used as the coolant in nuclear reactors and accelerator-driven systems, where the internal conditions of PbBi need to be closely monitored in order to avoid possible leakage [4]. In liquid metal batteries, both the anode and cathode electrodes consist of molten metals such as lithium or antimony, where various fluid flows introduced by thermal gradients and electric currents can affect the performance and lifetime of the battery [5, 6]. In geophysical studies, liquid metals like gallium or sodium are often used in lab-scale models, and thus measuring their flow structures is essential [7-9]. Therefore, techniques that enable real-time characterization, especially flow measurement, of metal melts are urgent and important.

Unlike transparent liquids, such as water, the opacity of metal melts makes it difficult to use conventional optical techniques, such as Particle Image Velocimetry (PIV), to measure the flow inside metal melts directly. Besides the opaqueness, the high temperature and chemical aggressiveness often involved in metal melts limit the development of measurement techniques for metal melts. Reviews of flow measurement techniques for liquid metals list some available methods [10, 11]. In general, there are invasive methods, such as Force Reaction Probes [12], and non-invasive methods, like Radioscopic techniques [13]. Among those methods, ultrasound-related techniques have broad prospects and could be performed in various types of fluids in either invasive ways or non-invasive ways.

1.2 Ultrasound metrology and ultrasound Doppler velocimetry

Ultrasound is a kind of acoustic wave with a frequency above 20 kHz. As an acoustic wave, an ultrasound wave propagates in media in the form of mechanical vibration; if the propagation medium is liquid, then the ultrasound wave can be treated as a longitudinal wave [14]. When ultrasound propagates in media, transmission, reflection, scattering, and attenuation occur, and the information and energy conversion involved in those processes allow people to utilize the ultrasound as a tool in various applications.

1.2.1 Ultrasound metrology

Ultrasound-related techniques such as ultrasound diagnostic imaging and various ultrasound therapeutic treatments have been widely used in medical and biomedical fields [15, 16]. Ultrasound measurement and characterization techniques are also extensively applied to various water-based fluid studies [17, 18]. In addition, the application of ultrasound techniques in the field of metallic materials has a long history. In ultrasonic non-destructive testing, high-frequency ultrasound is used to detect defects or measure the thickness of solid metal parts [19]. In ultrasonic melt processing, high-power ultrasound has been used to treat and degas metal melts for nearly a century [20]. In this work, in order to distinguish from those ultrasound techniques for solid material testing, and from those for melt treatment, we refer to the ultrasound techniques intended for measuring and characterizing metals in liquid state as ultrasound metrology.

For ultrasound metrology, the ultrasound frequency being used is typically from one to tens of MHz, in order to achieve a higher measurement resolution. In ultrasound metrology, the measurement of echo is the core. When an ultrasound wave propagates in a medium, echoes are produced if there is an echoing object with different acoustic impedance

present in the ultrasound beam path. The acoustic impedance Z is an intrinsic property of a material, which is determined by the sound speed c and the density ρ of that material: $Z = \rho \cdot c$. If the size of the echoing object is much larger than the ultrasound wavelength, then the strength of the echo is given by the Intensity Reflection Coefficient R_I.

$$R_I = \left(\frac{Z_2 - Z_1}{Z_2 + Z_1}\right)^2 \tag{1.1}$$

where Z_1 is the acoustic impedance of the medium the ultrasound passes through, and Z_2 is the acoustic impedance of the echoing object. Although there are many different types of ultrasound metrology techniques, for example, the ultrasound transit time technique (UTTT) [21], echo reflection/backscattering technique [18], ultrasound Doppler technique [22], etc., they are all based on analyzing the information contained in echoes.

Ultrasound metrology techniques can also be categorized according to the type of ultrasound wave used, i.e., continuous-wave or pulsed-wave. For the continuous-wave ultrasound, continuous sinusoidal waves are emitted by an ultrasound transducer, and echoes are received by another transducer(s). For the pulsed-wave ultrasound, short pulses consisting of a few cycles of sinusoidal waves are emitted periodically by an ultrasound transducer, and echoes are received by the same and/or another transducer(s). The ultrasound metrology techniques used and discussed in the present work are mainly focused on the pulsed wave ones.

1.2.2 Ultrasound doppler velocimetry

Ultrasound doppler velocimetry (UDV), or ultrasonic velocity profile (UVP), is one type of ultrasound metrology technique developed for flow measurement based on the principle

of the Doppler effect. This technique enables real-time flow velocity measurements in transparent or opaque fluids. The Doppler ultrasound technique was originally developed and extensively used in medical and clinical fields for measuring the blood flow [22]. In 1986, Yasushi Takeda for the first time applied and validated this ultrasound Doppler technique in fluid mechanics study [23]. Since the UDV was demonstrated to have the capability of real-time flow measurements in liquid mercury [24], this method has been widely applied to fluid mechanics studies of various liquid metals or metal melts over the past forty years.

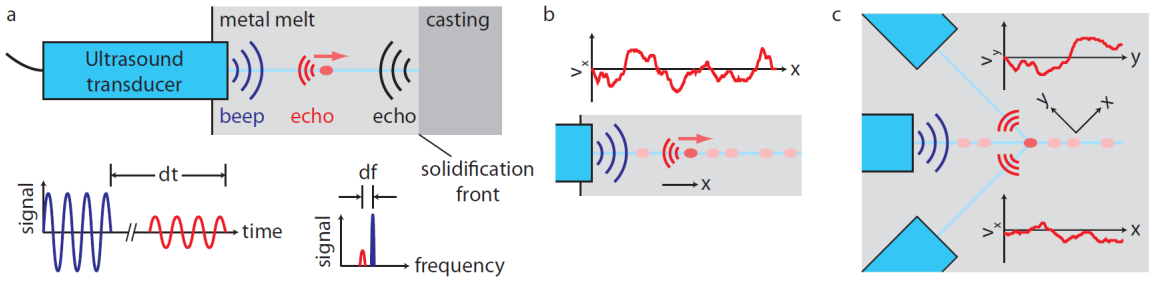

Figure 1.1 The working principle of UDV technique. (a) An UDV ultrasound transducer emits a pulse of ultrasound waves and listens for echoes. Echoes from small moving objects (red) or large interface (black) reveal the position of the echoing object. The Doppler shift *df* reveals one component of velocity. (b) When many echoing objects are present, one transducer can measure one component of velocity at many locations along the beam line. (c) Three transducers placed at different angles together can measure two or three components of velocity.

The working principle of UDV in fluids is based on the pulse-echo technique, as shown in figure 1.1. A short pulse of ultrasound is emitted at a certain frequency by an ultrasound transducer, and echoes are received by the same transducer or by another. Echoes could be produced by reflections of ultrasound waves at large interfaces, such as the solid-liquid

interface or liquid-gas interface, and by scattering from small particles or bubbles suspended in the fluid. When receiving an echo, the position of the echoing object with respect to the transducer can be calculated by the time of flight dt of the echo:

$$Position\ (distance\ from\ transducer) = \frac{dt * c}{2} \tag{1.2}$$

where c is the sound speed of the fluid. The velocity of the echoing object can be calculated from the Doppler shift of echo frequency. The movement of the echoing object results in a small shift of the signals: motion away from the transducer lowers the frequency, and motion toward the transducer raises the frequency. This is called the Doppler effect. Based on the Doppler effect, one velocity component (along the wave propagation direction) of the echoing object can be derived from the equation:

$$u = \frac{c * f_d}{2f_e} \tag{1.3}$$

where f_e is the ultrasound emitting frequency, f_d is the Doppler shift frequency, and u is the projection of the echoing object's velocity along the ultrasound propagation direction. Recording echoes with a single transducer accesses a single velocity component; recording echoes with multiple transducers can access multiple velocity components. If the echoing object is a tracer particle that accurately follows the fluid motion, its velocity gives a measure of the fluid velocity at that location. If many tracer particles are present in the ultrasound beam path, a single ultrasound pulse can produce many echoes and therefore many measurements, yielding a velocity profile along a line in the ultrasound propagation direction.

An ultrasound transducer is the key device that converts electric signals into acoustic signals and emits ultrasound waves. There are many different types of ultrasound transducers designed based on different electro-acoustic transduction principles. The piezoelectric transducer is one of the most commonly used transducers in various ultrasound techniques, including the UDV method. The main component of a piezoelectric ultrasound transducer is the piezoelectric element, which is usually made of polarized ceramics [25]. During operation, the piezoelectric element is excited by electrodes inside the transducer, and mechanical pressure is generated inside the piezoelectric element; then, the resonant oscillation of the piezoelectric element results in the emission of ultrasound waves [25]. For a UDV transducer, the thickness of the piezoelectric element determines its resonance frequency, i.e., the emitting frequency or the basic frequency of the transducer. In general, the UDV transducer emits high-intensity, high-frequency ultrasound waves and receives very weak echo waves.

One major advantage of the UDV is that it enables instantaneous velocity measurement in metal melts in respect to both space and time. Before the application of UDV, people study the flow of metal melts either by measuring the time-averaged velocity in space, or by measuring the velocity evolution at a fixed position [10]. Actually, the velocity measured by the UDV method at a certain point is the spatially averaged velocity within a small measuring volume. The measured velocity value thus depends on the size of the measuring volume. For a cylindrical UDV transducer, the measuring volume has a disk shape. The size of the measuring volume is determined by the diameter of the transducer (diameter of the piezoelectric element), the basic ultrasound frequency, and the number of ultrasound cycles in a single pulse. The size of the measuring volume also increases slightly with the propagation distance due to the divergence of ultrasound beam. Multiple

consecutive measuring volumes aligned coaxially together compose a continuous velocity profile along the ultrasound measuring line.

1.3 Application of ultrasound metrology in metal melts - literature review

For the current commercial UDV devices, mainly the ultrasound transducers, their working temperature is usually below 200°C-300°C, depending on suppliers. However, commonly used metals or alloys have very high melting temperatures, such as aluminum (660°C) and steel (>1400°C). Therefore, most UDV studies of metal melts focus on using low melting temperature metals as laboratory model experiments. Conducting UDV measurements in low-temperature metals simplifies experiments significantly. The measurement results not only help us understand the flow behaviors of metal melts under various conditions, but also contribute to the validation of numerical simulations. By calculating some dimensionless parameters, the UDV measurement results could also be applied equivalently to larger-scale fluid flows and high-temperature melts as well. In addition, with the increase of direct applications of low melting temperature metals in various engineering fields nowadays, UDV measurement of low-temperature metals has more practical significance.

In 1986, Takeda et al. first described the principle and characteristics of the UDV measurement for fluid mechanics study [23]. In 1987, they validated the UDV method by successfully measuring the velocity profile of liquid mercury in a T-branch pipe [24]. Since then, the UDV method has started to be applied to many different kinds of metal melts.

In 2001, Brito el al. [26] for the first time enabled UDV measurements in liquid gallium. In their study, a vortex flow was produced in liquid gallium by a spinning disk, and the velocity profile was measured by three ultrasound transducers positioned at different angles. They discussed several experimental issues concerning the ultrasound measurement in gallium, especially the influence of gallium oxides. They also discussed their methods for achieving better UDV measurement, such as cleaning gallium with HCl acid, coating container sidewalls with cataphoretic films, selecting tracer particles for liquid gallium, etc.

In 2002, Eckert and Gerbeth [27] successfully applied UDV measurements to a liquid sodium flow. Since liquid sodium is chemically reactive, the ultrasound measurement was conducted through a stainless steel adapter. They discussed multiple problems encountered during the ultrasound measurements in sodium, like the transmission of the ultrasound beam through the adapter wall, the acoustic coupling between the transducer and the adapter wall, and the wetting between the inner surface of the wall and the liquid sodium.

Also in 2002, Kazys et al. [28] for the first time applied ultrasound velocity measurement in liquid PbBi eutectic alloy, which is used as the coolant in nuclear reactors and accelerator driven systems. In that work, they carefully investigated the acoustic properties of PbBi and discussed the acoustic coupling issues.

In 2004, Cramer et al. [29] first applied the UDV method to flow velocity measurement of eutectic GaInSn alloy. In their experiment, the flow of liquid GainSn was driven by two different kinds of magnetic fields. They discussed the scattering particles and wetting issues concerning the applicability of ultrasound measurement in GaInSn and gave

suggestions for improving ultrasound signal quality. In that study, they emphasized the importance of understanding the mechanisms of ultrasound measurement in liquid metals.

In the past 40 years, the UDV method has been established in more and more different types of metal melts [10, 25]. The application of the UDV in metal melts also impacts various fields, such as electromagnetic flow, alloy casting, solidification process, liquid metal batteries, lab-scale models for geophysical research, etc. According to the measurement principle, those applications can be roughly divided into three categories: flow measurements, bubble or impurity detections, and large interface/solidification front tracking.

1.3.1 Flow measurement

Because UDV was originally designed for the purpose of flow measurement, it has been extensively used to measure various flows of liquid metals. The capability and applicability of UDV in respect to flow measurement has been summarized by Takeda [25, 30, 31] and Eckert [32]. Some specific applications of UDV flow measurement are reviewed below.

The research team from Helmholtz Zentrum Dresden-Rossendorf (HZDR) spent many years studying the flow structures and related mass/heat transport in metal melts during the continuous-casting process [2, 33-36]. They built a small-scale experimental facility named Mini-LIMMCAST, in which GaInSn alloy or SnBi alloy was used for low-temperature model experiments. Through quantitative flow measurements with the UDV method, they investigated various issues, such as the impact of magnetic fields on the outlet flow from the submerged nozzle, the damping effect of electromagnetic brake on the flow velocity in the mold, the interaction between flows driven by a swirling flow nozzle and electromagnetic stirring, the modification of flow structures during argon bubble

injection, etc. In addition, Chaudhary et al. [37] used those ultrasound measurement results to evaluate and validate the performance of computational models of continuous casting. Tasaka el al. [38] investigated a rotating flow of liquid gallium by the UDV method. The spatio-temporal behavior of the large-scale convective motion in gallium was observed from the measured velocity profiles. In their study, they specially designed a vessel for gallium to achieve good wetting. They also discussed the importance of pre-treatment of gallium and the selection of tracer particles. Starace et al. [39] investigated the Tayler instability by UDV flow measurements in a column of GaInSn alloy. The flow motion driven by an electric current passing along the axis of GaInSn was measured by four UDV transducers at one end. Eckert et al. [40] investigated different flow patterns in liquid GaInSn with the UDV method, and thus demonstrated the efficiency of intensive stirring and mixing produced by different types of time-modulated rotating magnetic fields. Gillet et al. [41, 42] investigated thermal convection and magnetoconvection in a rapidly rotating spherical shell by measuring the fluid velocity of liquid gallium with the UDV method. Zhang et al. [43] applied the UDV method to study how the oxide layer covering on the top surface of liquid GaInSn governs the anomalous behavior of the flow. From velocity measurements by five UDV transducers, they revealed that different properties and regimes of the oxide layer have a striking influence on both the primary swirling and the secondary recirculating flow of the liquid metal. Kelley et al. [5, 44] used the UDV method to study the fluid flow in a liquid metal electrode layer. In their experiment configurations, molten PbBi was used as the electrode material contained in a battery vessel, where the current was induced by a negative current collector connected to the PbBi. Ultrasound flow measurements were conducted in the PbBi under argon atmosphere. They also emphasized the effect of oxidation and wetting of PbBi on UDV

signals. Losev et al. [45] applied the UDV method to study the characteristics of an oscillating vortex flow in gallium eutectic alloy. In that work, they found that stirring the liquid metal has a positive influence on the UDV signal quality and measurement accuracy, whereas the temperature change in the liquid metal has a negative influence. They also discussed the optimal operating parameters to achieve UDV measurement reliability. Zurner et al. [46] compared the performance of Local Lorentz force velocimetry and UDV by measuring the flow behavior of vertical convection in liquid GaInSn. In their recent studies [47, 48], they used multiple cross-aligned UDV transducers, combined with temperature measurements, to characterize the three-dimensional dynamics of the single large-scale circulation in a cylindrical convection cell filled with GaInSn, and revealed how the large-scale flow is affected by an increasing magnetic field strength. Vogt et al. [49] used ultrasound to measure the flow topology and the temporal dynamics of turbulent Rayleigh-Bénard convection in liquid gallium. Through their coupled laboratory-numerical experiments, they discovered the so-called jump rope vortex mode in the large-scale circulations of liquid metal flow. Akashi et al. [50] applied UDV flow measurement to study the Rayleigh-Bénard convection in a liquid GaInSn alloy, and they demonstrated that the jump rope vortex flow structures also exist in liquid metals contained in cuboid containers of different aspect ratios.

In addition to using one or more individual transducers to perform UDV measurements, some groups have developed ultrasound transducer array systems. Sven Franke et al. [51] presented a novel ultrasound Doppler system which employs an array of 25 transducer elements. They experimentally validated their system by measuring flows of GaInSn driven by a rotating magnetic field. With a parallel operation mode they developed, they enabled a two-dimensional flow mapping in liquid metals for the first time. In a later

study [52], they also investigated the electro-vortex flows in liquid GaInSn induced by two parallel pencil electrodes immersed at the free surface, in which they utilized a rotatable transducer array consisting of 25 singular ultrasound transducers to measure the two-dimensional flow pattern of GaInSn. Buttner et al. [53] designed a novel UDV system for dual-plane, two-component flow velocity measurements. Their measurement system employs four transducer arrays consisting of total 100 elements. They demonstrated the capability of their transducer arrays by mapping a flow of GaInSn inside a cubic vessel, where the flow was driven by a rotating magnetic field. By using the dual-plane configuration and the crossed-plane configuration of the transducer arrays, they measured the flow structures of both the primary and secondary flow simultaneously for the first time. Naube and Mader et al. [54-56] developed a phased array flow measurement system based on the pulsed-wave ultrasound Doppler principle. The capabilities of this system were demonstrated on flow measurements of GaInSn, in which they achieved flow measurements in various configurations, like one velocity component measurement in four planes, two velocity components measurement in two planes, and three velocity components in two measuring lines.

1.3.2 Detection of bubbles or impurities

Detection of bubbles by means of ultrasound is based on analyzing the echoes caused by the reflection and/or scattering of ultrasound waves on gas bubbles. T.Vogta et al. [57, 58] applied ultrasound to detect the entrainment of gas into liquid metals. They produced different flow regimes in liquid GaInSn by inducing magnetic fields, and injected gas bubbles from the bottom. They used two types of ultrasound metrology methods to study the mechanisms of bubble entrainment: UDV transducers located at the vessel bottom to

observe the bubble entrainment and free surface deformation, and an ultrasound array located at the vessel sidewall to track the bubble movement. From the measured flow field and the path of the rising gas bubbles, they discovered various interactions among bubbles, metal flows, and magnetic fields. Andruszkiewicz et al. [21] investigated bubble dynamics in a liquid metal-gas flow, through detecting gas bubbles in liquid GaInSn with ultrasound techniques. They combined the ultrasound Doppler method and ultrasound transit time technique together, with ultrasound transducers arranged in either vertical or horizontal orientations, to enable the measurement of positions, velocities, and diameters of bubbles. Wang et al. [59] investigated the rising behavior of isolated bubbles in a liquid GaInSn under different magnetic field intensities. They used the UDV method to measure the terminal velocity of the bubble and thus revealed the influence of the magnetic field on the liquid metal flow around the bubble trajectory. They also discussed the possible effect of oxidations of GaInSn on the bubble ascension velocity.

Comparing to the echo intensity from gas bubbles, the echo from small solid impurities is weaker due to the smaller acoustic impedance mismatch. Thus, the detection of solid impurities depends more on analyzing the change of echo intensities. Smith and Gokelma et al. [60, 61] introduced an inclusion detection system for identifying and quantifying potential sources of inclusions in molten aluminum. Their measurement system utilizes two ultrasound transducers, one transmitter and one receiver, to detect the impurity levels inside aluminum melt by correlating the echo intensity with the size distribution and concentration of inclusions. Achard et al. [62, 63] developed a novel ultrasound sensor for measuring the inclusion levels in aluminum melt based on analyzing echo amplitudes, while simultaneously measuring the flow velocity of the aluminum in the casting trough.

1.3.3 Tracking the solidification front

Tracking the solidification process by ultrasound relies on detecting the reflection of ultrasound waves from the large liquid-solid interface, which is also the solidification front. Zhang et al. [64] investigated the effects of the magnetically induced low-gravity environment on the melting rate and on the profile of the solid/melt interface during the solidification process of gallium, in which ultrasound was used to measure the thickness of solid and liquid phases and capture the shape of their interface. Oborin et al. [65] applied ultrasound to investigate the crystallization processes in a thin layer of liquid gallium. They induced a flow generating by an alternating magnetic field to stir the liquid gallium during the solidification stage. By tracking the solidification front movements with the UDV method, they revealed how the crystallization process and solidification rate are affected by the topology and intensity of the flow inside the liquid metal layer. Dadzis et al. [66] applied the UDV to measure the directional solidification processes of gallium. In their experiment, the liquid gallium was solidified in a container under a vertical temperature gradient and an external traveling magnetic field (TMF). Through the UDV transducer placed on top, they measured that the solid-liquid interface presents a concave shape with an upward TMF and a convex shape with a downward TMF. Thieme et al. [67] utilized a novel measurement system based on the UDV method to characterize the solidification processes and flow phenomena in a liquid gallium layer. In their measurement configuration, nine single ultrasound transducers placed on the top of the gallium container were used for the in-situ tracking of the solid–liquid interface during a directional solidification process, and four linear transducer arrays placed at the sidewall were used for a 2-D vector flow mapping.

1.3.4 Waveguide and high-temperature applications

Although the traditional UDV transducer is restricted to temperatures below 200°C, the development and application of acoustic waveguides allow the UDV technique to be used in high-temperature and chemically reactive metal melts as well. Eckert et al. [68] has developed a new type of ultrasound probe integrating waveguide and UDV techniques. The acoustic waveguide is a buffer rod made of stainless steel, and special care is required for achieving a good acoustic coupling to the piezoelectric transducer as well as to the tested melt. The reliability of the new probe has been demonstrated with successful measurements in PbBi bubbly flows and in CuSn flows. To achieve a long-term ultrasound measurement in the liquid ePbBi alloy, Kazys et al. [69] evaluated the performance of several high-temperature piezoelectric materials, such as PZT, bismuth titanate, lithium niobate, and aluminum nitride. Those transducers were coupled to a stainless steel acoustic waveguide to measure ePbBi flows. In their study, particular attention was given to the acoustic coupling among the piezoelectric element, acoustic waveguide, and the liquid PbBi alloy. In a more recent study, Achard et al. [62] discussed the wettability and durability of waveguides immersed in the metal melt. They developed an innovative system that integrates a power ultrasound transducer and an ultrasound measurement transducer together. The ultrasound measurement transducer is used to measure the impurity levels as well as melt flows. The power ultrasound transducer is excited periodically to restore the wetting between the waveguide and metal melt via releasing microbubbles accumulated on the waveguide surface. Their design enabled in-line and real-time continuous inclusions detections and flow velocity measurements of aluminum melt inside the casting trough. Although many studies have successfully applied acoustic waveguides to the flow measurement of high-temperature metal melts, one big drawback

is that the acoustic waveguide significantly reduces the accuracy of the ultrasound measurement. Further research is required to establish reliable ways for conducting UDV measurements in high-temperature metals.

1.4 Motivation and experimental methods

Although the UDV method has been successfully established in various types of liquids, the application of ultrasound measurement in liquid metals/metal melts is not completely reliable. Indeed, many prior studies have realized that the operation of UDV measurement in metal melts depends on phenomena that are poorly understood. One example is the strong echoes produced throughout the bulk of high-purity metal melts, where the echo source is unknown. Another example is the deterioration of ultrasound signals in metal melts due to unclear causes. Those issues exist because the underlying mechanisms of ultrasound measurement in metal melts are still unclear. In addition, as a measurement tool, the quality and accuracy of the measurement determine the reliability of UDV method. Unfortunately, since almost all commercial UDV devices and transducers are designed for water-based fluid applications, their performance is usually poor when applying them to metal melts. How to obtain accurate and high-quality measurements has always been a major challenge when applying the UDV technique to metal melts.

The goal of this thesis is to establish the UDV measurement as a reliable technique for the study of metal melts, especially with respect to flow measurements, via two primary research aspects: one is to investigate and understand the underlying mechanisms of ultrasound measurement in metal melts, and the other is to explore ways to improve the

quality and accuracy of UDV measurement. The outcome of this thesis work will not only provide us with a more comprehensive knowledge concerning ultrasound and metal melts, but will also enable us to better use the UDV measurement in other studies involving metal melts, for instance, the study on flow structures of liquid metal batteries.

In the present work, the issues and challenges existing in UDV measurements are mainly investigated by performing ultrasound measurements in liquid gallium using a commercial UDV device, DOP3010. In the following sections, some basic information of the DOP3010 instrument and gallium are introduced. After that, example UDV measurements are presented.

1.4.1 The DOP3010 instrument

In this study, a commercial UDV device, DOP3010 (Signal Processing, Switzerland), is used to perform all ultrasound measurements. This instrument was developed for the purpose of flow measurement in various kinds of liquids and has been used by many research groups for the study of metal melts. It should be noted that, although it is called as ultrasound Doppler velocimetry, the working principle of DOP3010 is not based on measuring the Doppler shift anymore. In fact, the velocity of the echoing object is derived from shifts in phase positions between consecutive pulses, and the Doppler effect only plays a minor role. According to the description on the *Signal Processing* website: when many echoing objects are randomly distributed inside the ultrasound beam, echoes from them are in a random fashion; where the velocity information is extracted by algorithms developed based on the correlations existing between echoes of multiple consecutive ultrasound emissions.

The DOP3010 has ten individual channels, each of which can be connected to an ultrasound transducer via a BNC connection. With the multiplexer function, it allows up to ten ultrasound transducers to be used simultaneously for flow measurements. The UDV transducer (Signal Processing, Switzerland) is a single-element circular transducer operating in a piston-like manner; it emits and receives ultrasound pulse waves for measurement (A-scan). Each UDV transducer has a fixed working frequency. There are two types of UDV transducers used throughout this work: TR0405LH and TR0805LH, with a working frequency of 4 MHz and 8 MHz, respectively; they are built with the same dimensions: 5 mm piezo-element diameter, 8 mm housing diameter, 90 mm housing length. Their maximum working temperature is 230°C.

The DOP3010 comes with control software that acquires and displays the measured echo profiles and velocity profiles in real-time. The software allows setting and adjusting several ultrasound parameters. Those parameters directly determine the quality and accuracy of UDV measurements. Some important ultrasound parameters are introduced below.

Emitting frequency. The ultrasound emitting frequency f_e is determined by the selected UDV transducer. In this study, two ultrasound emitting frequencies, 4 MHz and 8 MHz, are mainly used.

Burst length. In UDV, the transducer emits a short ultrasound pulse consisting of several cycles of ultrasound waves. The number of cycles contained in a single pulse is given by the parameter *Burst length*. The burst length and emitting frequency together determine the length of the pulse, which is also the longitudinal dimension of the measuring volume.

Pulse repetition frequency (PRF). The PRF is the frequency at which the ultrasound pulse is emitted. In other words, the PRF determines the interval between two successive

pulse emissions. This interval is also the period during which the UDV transducer receives echoes. From the Nyquist theorem, the value of PRF f_{PRF} determines the maximum measurable depth P_{max} and the maximum measurable velocity u_{max}:

$$P_{max} = \frac{c}{2f_{PRF}} \qquad u_{max} = \frac{c * f_{PRF}}{4f_e} \tag{1.4}$$

Emissions per profile. To obtain statistically reliable results, each velocity profile is computed based on correlations between multiple consecutive pulse emissions. The number of emissions required to derive one velocity profile is determined by the parameter *Emissions per profile*. In general, a higher value of *Emissions per profile* produces a more accurate result, whereas a lower value of *Emissions per profile* allows the measurement of flows involving rapid changes.

More discussions about those parameters and how to choose their values are in Appendix A. More detail introductions of the DOP3010 instrument and its software can be found in the DOP3010 user's manual, available at *www.signal-processing.com*.

1.4.2 Gallium and its properties

In this work, liquid gallium is the main material in which the ultrasound measurements were conducted. Gallium is a metal with a melting temperature about 30°C. Gallium exists in compounds formed in nature and is produced as a by-product of aluminum ore processing. Pure gallium presents a silvery blue appearance in solid state. Liquid gallium is silvery white in color and reflective.

We select gallium for four main reasons. First, the melting temperature of gallium, around 30°C, is suitable for our study. On one hand, this temperature is low enough to simplify

the operating of ultrasound experiments, where commercial ultrasound equipment such as UDV transducers and hydrophones can be readily used. On the other hand, this temperature is high enough to allow the liquid metal to be solidified for the purpose of various solid-state examinations such as the SEM and EDS tests. Second, as can be seen from the literature review section above, more than 80% of the previous UDV studies have been performed in gallium or its alloy GaInSn. Therefore, investigating and understanding the mechanisms of UDV measurement in gallium has more practical implications. Third, since the dissolved gas in liquid gallium is hydrogen, not oxygen, gallium is a good candidate for investigating the roles of dissolved gas and oxide inclusions individually, as well as investigating the potential ultrasound-induced cavitation problems. This part will be fully discussed in Chapter 4. Fourth, since gallium is in the same group with aluminum in the periodic table, and since the hydrogen is also the main dissolved gas in aluminum, gallium is a suitable low-temperature analogy model for aluminum. The data and results of ultrasound measurements in gallium can be used to build the numerical simulation model for aluminum. Thus, studying the mechanisms of ultrasound measurement in gallium also has significance in practical engineering applications. In addition, liquid gallium is non-toxic and environmentally friendly, making it easy to handle in lab-scale experiments.

Some important physical properties of gallium related to ultrasound measurements are listed in Table 1.1. Those parameters are from references [70-74].

Table 1.1 Some physical properties of gallium (under ambient pressure)

Melting point	29.8°C
Boiling point	2400°C
Density (solid)	5910 kg/m^3
Density (liquid at 60°C)	6058 kg/m^3
Viscosity (at 60°C)	1.465 mPa·s
Surface tension (at 60°C)	0.706 N/m
Sound speed (at 60°C)	2860 m/s
Acoustic impedance (at 60°C)	17.3 MRayls
Sound absorption coefficient (at 60°C)	1.67 *10^{-17} Np*s^2/cm

Some notes: All of our ultrasound experiments in gallium were conducted within a small temperature range, from 33°C to 60°C, so the variation of parameters based on functions of temperature is minimal and neglectable [73]. The surface tension of gallium is high, one order of magnitude larger than that of water. The sound absorption coefficient of gallium is one order of magnitude smaller than that of water.

Liquid gallium is easily oxidized once exposed to the air: gallium will react with the oxygen and water vapor in the air to produce gallium oxide. Although there are several different modifications of gallium oxide polymorphs, the β-Ga_2O_3 is the most common and the most stable form over the entire temperature range [75, 76]. Once liquid gallium is oxidized, a gallium oxide film is formed on the free surface of liquid gallium, which shows a wrinkled and matte appearance.

Proper storage of gallium is necessary. In our lab, since liquid gallium attacks most other metals by diffusing into the metal lattice, liquid gallium is contained in a glass beaker when in use. However, as gallium undergoes a 3% volume expansion when transforming from liquid state to solid state [77], the long-term storage of gallium is in stainless steel bowls.

Some gallium is also stored in a PTFE beaker inside an argon glovebox; that gallium is used for experiments that require high purity.

Some acoustic parameters of gallium are presented below.

Near field and far field. For the single-element piston ultrasound transducer used in this work, the theoretical intensity of the acoustic field it produces along the axis of the beam can be described by [78]:

$$\frac{I_x}{I_{max}} = \sin^2\left[\frac{\pi}{\lambda}\left(\sqrt{r^2 + x^2} - x\right)\right] \tag{1.5}$$

where I_x is the is intensity at distance x, I_{max} is the maximum intensity, λ is the ultrasound wavelength, and r is the radius of the transducer. According to this equation, we plot the intensity of an 8 MHz ultrasound field as a function of axial distance from the transducer, in gallium and water (as a comparison), as shown in figure 1.2. In the acoustic field, there is a location of the last maximum of acoustic intensity, whose distance from the transducer is given by:

$$Distance\ of\ I_{max} = \frac{4r^2 - \lambda^2}{4\lambda} \tag{1.6}$$

This location divides the ultrasound field into two regions: the region between the transducer surface and this maximum location is called the near-field, and the region lying beyond the maximum location is called the far-field. In the near-field, the ultrasound intensity oscillates strongly along the axis of the beam, which might induce noises and affect the UDV measurement. Therefore, most UDV studies avoid flow measurements in the near-field region, but more focus on measurements in the far-field region.

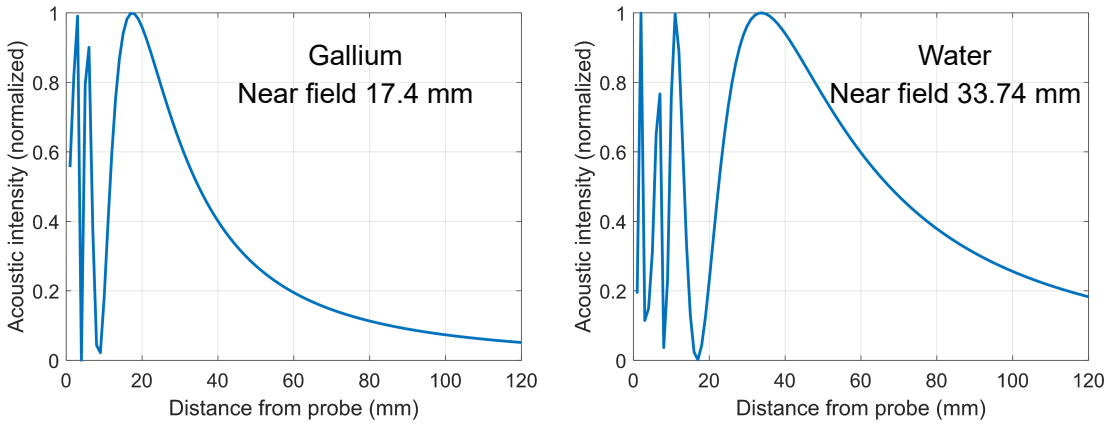

Figure 1.2 Theoretical intensity of the acoustic field along the axis of the transducer, in liquid gallium (left) and water (right). The frequency of the ultrasound wave is 8 MHz, and the diameter of the transducer is 5 mm. The length of near field is indicated in the captions.

Divergence angle. In the far-field region, the ultrasound waves possess small oscillations in the radial direction, and the main acoustic lobe is contained in a cone-like shape. The half-angle divergence (-6dB width) of the main lobe can be calculated by [78]:

$$Divergence\ angle = \sin^{-1}\left(\frac{0.61\lambda}{r}\right) \tag{1.7}$$

For 8 MHz ultrasound waves in liquid gallium, the divergence angle is about 5°.

Ultrasound attenuation. When ultrasound waves propagate in media, ultrasound attenuation happens, limiting the distance the ultrasound waves can travel. The ultrasound attenuation depends on the ultrasound emitting frequency and on the type of propagation media. Typically, the ultrasound attenuation is caused by the acoustic energy lose due to reflection and scattering, and the acoustic energy absorption by the media (conversion of acoustic energy to heat). The ultrasound absorption rate increases exponentially with the ultrasound frequency [79], which is one of the main factors that limits the maximum

ultrasound frequency that can be used. The ultrasound absorption coefficient of gallium is one order of magnitude smaller than that of water.

We have measured the axial distribution of acoustic pressure produced by an 8 MHz UDV transducer in gallium and in water by a hydrophone. The acoustic pressure is measured every 10 mm in-step from the UDV transducer surface. The measured acoustic pressure distribution along the axis of the transducer is shown in figure 1.3. The figure also suggests that the ultrasound energy loss in gallium is smaller than in water.

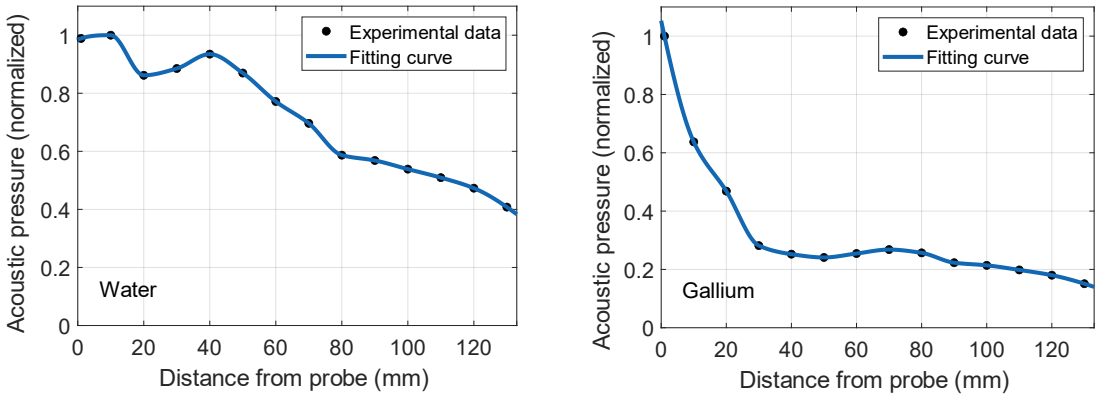

Figure 1.3 The axial distribution of acoustic pressure produced by an 8 MHz UDV transducer in gallium (left) and water (right). The acoustic pressure is measured every 10 mm by a hydrophone.

Measurement volume and spatial resolution. The velocity profile measured by the UDV method consists of multiple consecutive measuring volumes. The spatial resolution of the UDV measurement is thus determined by the size of each measuring volume. The measuring volume has a disk-like shape, where its lateral dimension is determined by the diameter of the transducer and the beam divergence, and its longitudinal dimension is determined by the pulse length. For 8 MHz ultrasound in 60°C liquid gallium, the theoretical lateral size of a single measuring volume is 5 mm to 14 mm (for a measurement

distance of 100 mm) and the longitudinal size is 1~2 mm. In fact, the exact value of spatial resolution is not important with respect to the research objectives of this work. We still learned those dimensions in order to design the size of the vessels used for conducting UDV measurements.

1.4.3 Typical UDV measurement results

In a typical UDV measurement, the DOP3010 performs echo measurements and velocity measurements simultaneously, and thus provides two types of results: the spatial-temporal echo profile and the spatial-temporal velocity profile.

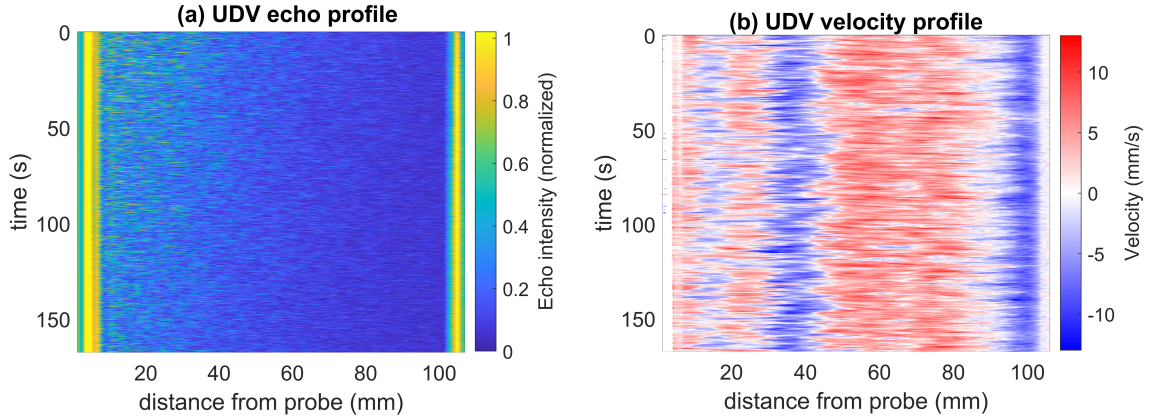

Figure 1.4 An example of UDV measurement results for liquid gallium. (a) Spatial-temporal echo profile measured in gallium. It measures the envelope of echoes. The color indicates the echo intensity amplitude. (b) Spatial-temporal velocity profile measured in gallium. Red colors (positive velocity) signify velocity away from the from the transducer; blue colors (negative velocity) signify velocity toward the transducer.

Figure 1.4 shows an example of UDV measurement results for liquid gallium, in which the measured echo intensities and flow velocities are plotted as functions of time and distance from the transducer. In the spatial-temporal echo profile, echoes were measured

throughout the bulk of high purity liquid gallium (99.99% pure). The strong echoes at around 100 mm are caused by ultrasound reflections from the wall of the gallium container. The strong echoes near the probe surface are resulted from the ultrasound near-field oscillation and the interface between transducer surface and gallium (this will be discussed later). In the spatial-temporal velocity profile, only one velocity component along the ultrasound propagation direction is measured. Red colors (positive velocity) signify velocity away from the transducer; blue colors (negative velocity) signify velocity toward the transducer. In this work, many experiments and discussions are based on analyzing the information extracted from the spatial-temporal profiles, or the results of the spatial-averaged or time-averaged profiles.

1.5 Objectives and thesis overview

To study the ultrasound measurement in liquid gallium, I set three specific objectives for this thesis work: 1) identifying the source of echoes in gallium and exploring the echoing mechanisms; 2) improving the UDV measurement performance, especially for liquid gallium; 3) investigating the ultrasound signal deterioration phenomenon in gallium and its corresponding mechanisms.

Identifying the source of echoes in gallium

UDV requires at least one echoing object in each measuring volume; otherwise, the measured velocity is zero [25]. For UDV measurements in water, echoing objects are usually provided by artificially seeding tracer particles into the water. Interestingly, UDV measurements in gallium, as well as in some other metal melts, do not require seeding of

tracer particles, suggesting that there are natural tracer particles or inhomogeneities existing in the metal melts to provide echoes. However, the source of those natural particles or inhomogeneities had not been identified before the work described in this dissertation. When a test fluid itself includes intrinsic echoing objects, whose size and concentration we cannot control, then the reliability and applicability of UDV measurements might depend mainly on the characteristics of the echoing objects. Therefore, it is essential to identify the echoing object and investigate its characteristics carefully before designing the experiment. Unfortunately, many UDV measurements of metal melts in prior studies were carried out without knowing the exact source of echoes.

In Chapter 2, I experimentally investigate the source of bulk echoes in liquid gallium and its corresponding mechanisms. I start by introducing the importance of bulk echoes in UDV measurements. Then, I determine the source of bulk echoes in gallium by combining scanning electron microscopy (SEM), UDV measurements, and Particle Tracking Velocimeter (PTV) measurements together. I also develop a novel method, based on measuring the terminal velocity, to estimate the mean size of the echoing objects in gallium. Through analogous experiments in water, I further discuss the possible mechanisms by which the echoing objects produce the echoes.

Improving the UDV measurement performance

How to obtain robust and high-quality UDV measurements in metal melts has always been a challenge. UDV measurements can be non-invasive, but not fully contactless: a continuous acoustic path from the transducer to the test liquid is required [25]. However, due to the high surface tension and complex oxidation behavior of metal melts, the wetting and acoustic coupling conditions between the commercial UDV transducer and metal

melts are usually bad, leading to poor signal qualities and unstable measurements. Hence, performing UDV measurements by inserting the transducer directly into the metal melt might not be the best choice.

In Chapter 3, I introduce the concepts of direct-contact ultrasound measurement and indirect-contact ultrasound measurement, and also discuss the differences between them. In order to find the optimal vessel material for indirect-contact ultrasound measurements in water and liquid gallium, I systematically investigate the effect of vessel wall material, including the material type, thickness, and wetting properties, on ultrasound signals. A special focus is given to how the wetting, characterized by contact angles, affects the UDV measurements.

Investigating the ultrasound signals deterioration

UDV signals deterioration over time is an undesirable phenomenon we have observed during UDV measurements in liquid gallium. Many publications also have reported that the ultrasound signals in metal melts are unstable that the signals deteriorate or eventually fail altogether [26, 29, 44, 45]. This phenomenon limits the duration of UDV measurements and makes the measurement results unreliable. However, there has been no unified conclusion to explain this phenomenon.

In Chapter 4, I thoroughly study the UDV signal deterioration in gallium as well as the mechanism behind it. I first introduce how the ultrasound signal deterioration happens and how it affects UDV measurements. Then I discuss two distinct mechanisms causing the signal deterioration through a series of experiments. The experiments and discussions in this chapter build on the knowledge of the previous two chapters. In addition, I further investigate the ultrasound-induced cavitation in liquid gallium, which might be a possible

mechanism causing the deterioration. The research on ultrasound-induced cavitation was conducted in collaboration with Prof. Allanore and Andrew Caldwell from the Massachusetts Institute of Technology.

Appendix A summarize some technical details of the UDV method with respect to flow measurements in liquid metal batteries, as well as some challenges encountered during the liquid metal battery experiments. In the liquid metal battery project, the UDV is the primary tool to characterize the flow structures inside the liquid metal battery's electrode layers.

Appendix B summarizes some of the author's personal experience on the operation of the DOP3010 instrument, as well as some tips for improving the signal quality of UDV measurements.

—— Chapter 2 ——

The Source of Bulk Echoes

To fully understand the mechanisms of UDV measurements in liquid metals, studying the source of ultrasound echoes is necessary. In this chapter, we experimentally investigate the source of bulk echoes in liquid gallium and its corresponding echoing mechanisms. We demonstrate the role of oxide inclusions on UDV measurements, and further discuss possible ways to control it.

Part of the results listed in this chapter have been published in reference [80, 81].

2.1 Introduction: Bulk echoes and UDV measurements

From the working principle of the UDV, we learned that the UDV velocity measurement is based on consecutive echo measurements, especially the echoes coming from the bulk part of a fluid. In other words, all information about the velocity measurement is contained in the echoes [82]. Therefore, the bulk echo measurements directly determine the performance of the UDV.

Figure 2.1(a) shows UDV echo measurements in water with or without adding tracer particles. The strong echo peaks at 70 mm are caused by the specular reflection of ultrasound waves at the back wall of the container, and we call it the backwall echoes. The echoes measured in the bulk part (the part between the transducer surface and container's back wall) of water are called the bulk echoes. The generation of bulk echoes requires inhomogeneities in the liquid to produce acoustic impedance mismatch. In pure

water, no bulk echo is measured because there is no echoing object present. To get bulk echoes, tracer particles must be added to the water, and the bulk echo intensities increase as more tracer particles are added. On the other hand, the backwall echo intensities slightly decrease as more tracer particles are added, because more ultrasound energy is scattered by the tracer particles.

Similarly, UDV measurements in liquid metals also require inhomogeneities like small particles or bubbles acting as reflectors to generate sufficient bulk echoes. In previous studies, people have added zirconium-boride powders into liquid gallium [26, 38, 83], or gold-palladium powders into mercury [25] to generate bulk echoes. Interestingly, we detected strong bulk echoes in liquid gallium even without adding any tracer particles, as shown in figure 2.1(b). Because the liquid gallium is melted from solid gallium of 99.99% purity, where those bulk echoes come from was a mystery.

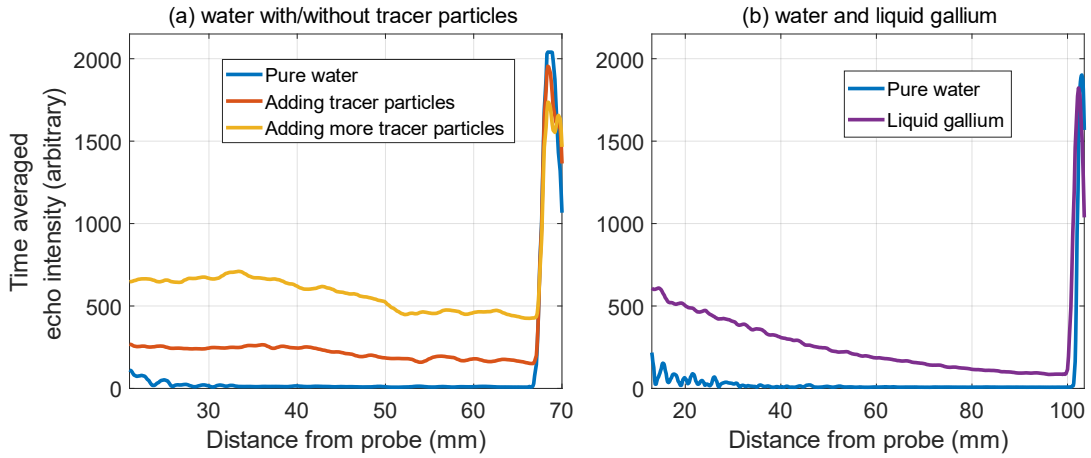

Figure 2.1 UDV echo measurements in (a) water with/without tracer particles and (b) liquid gallium. No bulk echo is measured in pure water. Strong bulk echoes are measured in tracer particle water and liquid gallium.

As the spontaneous bulk echoes are only observed in customary metals like gallium and sodium, but not in noble metals such as mercury, it is reasonable to assume that the naturally occurring metal oxide inclusions are the source of those bulk echoes [10]. For instance, many studies have argued that gallium oxides are responsible for the bulk echoes in gallium and gallium alloys [27, 29, 41, 44, 45, 56, 58, 59, 66, 67]. However, due to the opacity of liquid metals, no direct evidence about the relationship between metal oxides and bulk-echo signals has been provided yet. Besides metal oxides, other inhomogeneities, such as trace metal impurities common in liquid metals, also cause echoes. Cramer et al. have observed that microbubbles generated during the liquid metal filling process may also act as tracer particles to provide bulk echoes [29]. For alloys such as GaInSn, some researchers assumed that microscopic segregations resulting from localized deviations from eutectic compositions would cause bulk echoes as well [39, 51].

Compared to adding artificial tracer particles, naturally existing inhomogeneities are preferable. Several difficulties arise if artificial tracer particles must be added to the liquid metals. On the one hand, the density of the tracer particles should match that of the liquid metal. However, unlike water, each liquid metal has a different density, so tracer particles are not universal. On the other hand, the high surface tension of liquid metals usually hinders the homogeneous mixture of tracer particles, and the separation of tracer particles from the liquid metal is also a challenge [27, 38]. Other than solid tracer particles, prior studies also injected microbubbles into mercury as tracers [25, 84]. The merits are that bubbles do not contaminate the liquid metal and are easy to separate. But the bubbles' size and lifetime are difficult to control. Due to those difficulties, most research groups prefer gallium and its alloy, rather than mercury, as the fluid to conduct UDV studies. However, when the fluid itself includes natural inhomogeneities whose characteristics like

density, concertation, or size distribution are not clear, the experimental system design and parameters might be determined mainly by the characteristics of the inhomogeneities. Therefore, it is necessary to identify the type of inhomogeneities and investigate their characteristics comprehensively before designing the experiments.

In ultrasound measurements, inhomogeneities play the role of echoing objects that provide bulk echoes. There are four reasons why we need to study the characteristics of echoing objects in liquid metals. First, the material composition of the echoing objects determines their acoustic impedance and thus the reflection coefficients in the fluid. Second, the density of the echoing objects determines whether they can closely follow the fluid flow without slip. If the density mismatch between the fluid and echoing objects is large, then the measured velocity does not reflect the real fluid flow, and the echoing objects separate from the fluid over time. Third, the size of echoing objects determines the echoing mechanisms, which further determines the received echo intensity and thus the signal quality. Empirically, the ideal size of tracer particles in UDV measurements should be around 1/4 – 1/2 of the ultrasound wavelength; if too small, the bulk echoes are too weak that the signal-to-noise ratio is low; if too large, multiple reflections between tracer particles might distort the measurement [25]. Fourth, the concentration of echoing objects determines the reliability of UDV measurements. It also depends on the specific flow conditions to be measured: UDV requires at least one particle in each measuring volume [25], thus, high-velocity flows require lower concentrations of tracer particles, while low-velocity flows such as natural convection require higher concentrations.

Apparently, a comprehensive study on the source of bulk echoes in liquid metals such as gallium is a prerequisite for establishing UDV measurements in liquid metals. Unfortunately, there is a lack of systematic study about the source of bulk echoes in liquid

metals. Further, the mechanisms by which ultrasound waves are echoed in liquid metals have not been explained. In this chapter, we experimentally investigate the source of ultrasound bulk echoes during UDV measurements in liquid gallium and its characteristics. Through SEM examinations and ultrasound measurements, we determined that gallium oxide inclusions are the source of bulk echoes in liquid gallium. Through a novel size estimation method and analogous experiments, we demonstrated that ultrasound waves in gallium are primarily scattered by gallium oxide inclusions in agglomeration form, and Mie scattering is the dominant mechanism.

2.2 SEM and EDS examination

In general, echoes are caused by acoustic impedance mismatches, which implies that impurities might be present in liquid gallium to produce the observed bulk echoes. To find the impurities in gallium, we solidified the liquid gallium and characterized the solid gallium sample by scanning electron microscopy (SEM) and energy dispersive x-ray spectroscopy (EDS).

Under the SEM, gallium oxide inclusions with different sizes and morphologies have been found mainly from the sample's top surface and cross-section, as shown in figure 2.2 and figure 2.3, respectively. SEM images reveal that the gallium oxide inclusions exist either as single particles or as agglomerates. As a result, the size of the gallium oxide inclusions varies from one to tens of microns. The typical size of a single gallium oxide particle is about one micron.

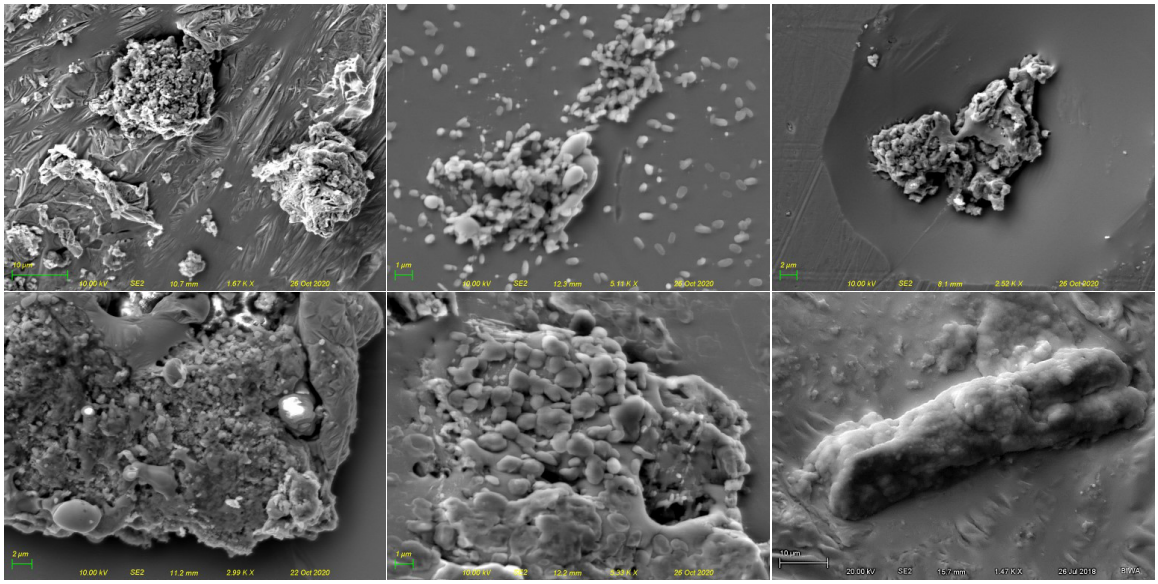

Figure 2.2 SEM images of gallium oxide inclusions found from the top surface of the gallium sample.

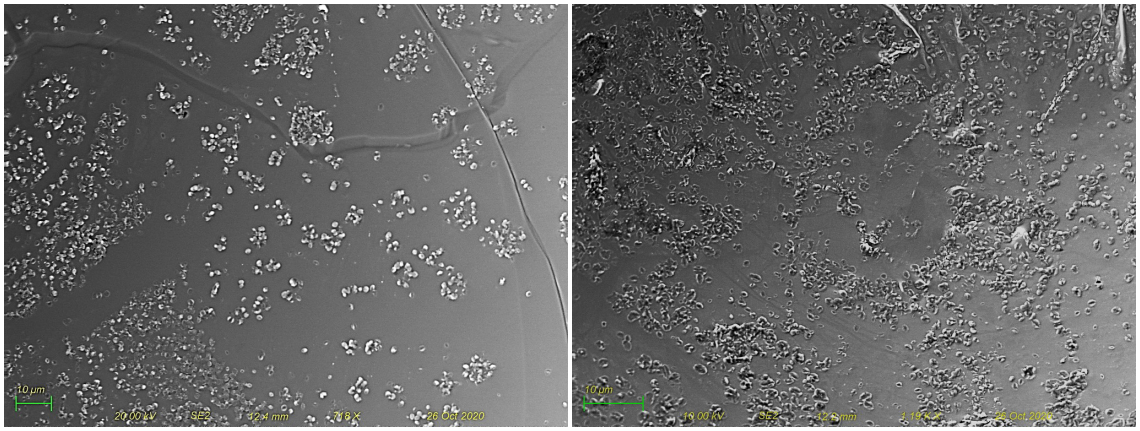

Figure 2.3 SEM images of gallium oxide inclusions found at the cross-section of the gallium sample.

The EDS analysis confirms that those oxide inclusions consist of oxygen and gallium, as shown in figure 2.4. Further, the EDS quantitative analysis from multiple oxide particles reveals that the formula of gallium oxide is Ga_2O_3. The gallium oxide (Ga_2O_3) is produced naturally when gallium is melted in air. Based on our laboratory experiment conditions, the

produced gallium oxide should be the β-Ga_2O_3 [85]. Hereinafter, gallium oxide refers specifically to the β-Ga_2O_3.

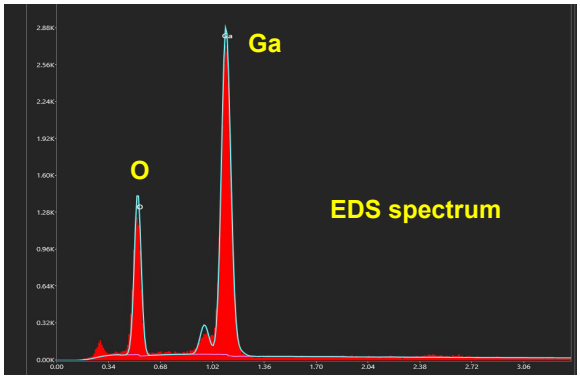

EDS Quant Calculation

Atomic %	**O** element	**Ga** element
Particle-1	59.05	40.95
Particle-2	57.71	42.29
Particle-3	61.84	38.16
Particle-4	61.08	38.92

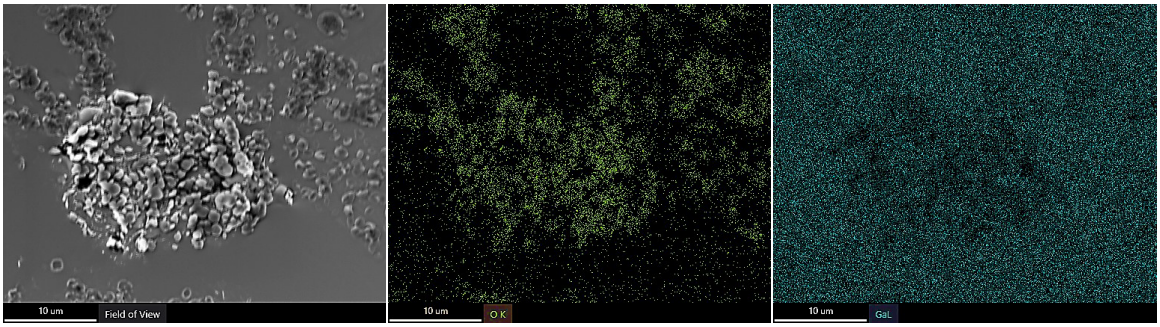

Figure 2.4 EDS analysis of gallium oxide inclusions. From the EDS quantitative analysis results, the atomic percentage of O and Ga reveals that the formula of gallium oxide is Ga_2O_3. In the EDS element maps, green and blue dots represent the locations of oxygen and gallium, respectively.

Besides oxide inclusions, we also found many different kinds of metal impurities from the bottom surface of the gallium sample, as shown in figure 2.5. Those metal impurities might have been introduced into gallium during our experimental procedures or during manufacturing processes (gallium is produced as a by-product in the processing of other metals ores). Notably, when many gallium oxide particles agglomerate together, metal impurities may also be included inside the agglomeration.

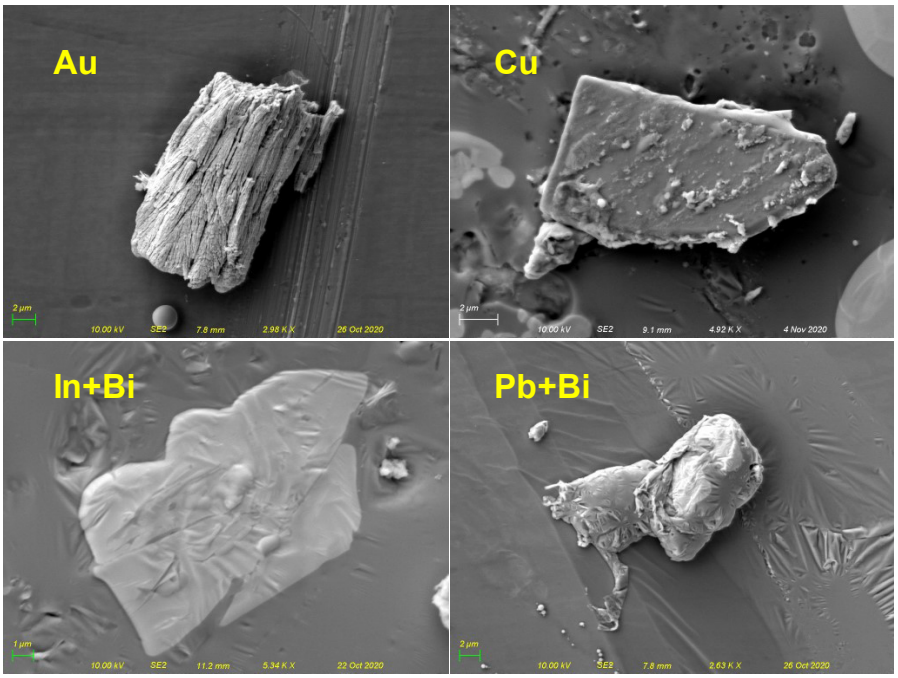

Figure 2.5 SEM images of metal impurities found from the bottom surface of the gallium sample.

Note that for some impurities, such as indium, it is difficult to determine whether they were solid particles suspended in the molten gallium at all times, or they were dissolved in liquid gallium and precipitated out during solidification later. However, most of those impurities, including gallium oxides, cannot be melted under our experiment temperatures (maximum 60°C). Therefore, all those impurities can serve as the echoing objects to scatter ultrasound waves in gallium.

2.3 Detecting moving directions of echoing objects

According to the SEM examination results, all impurities found from the gallium sample could be the potential source of bulk echoes. To find out which type of impurity is the main source or is mainly responsible for providing the bulk echoes, further investigation is

required. The experimental idea is to identify the type of echoing objects by detecting their direction of motion under gravity. If gravity is the only force driving the motion of echoing objects, then the echoing objects composed of impurities with a density less than gallium will rise, whereas the echoing objects composed of impurities with a density higher than gallium will sink.

2.3.1 Validation test in water

Experiment and methods

The above experimental idea was first validated in a water experiment. The experimental configuration is shown in figure 2.6. A vertical vessel made of acrylic was filled with water, where tracer particles with density (1.022 g/cm^3) slightly higher than water (0.998 g/cm^3 at 20°C) were seeded to water for providing ultrasound bulk echoes. We expected that the heavier tracer particles would move downwards under the effect of gravity.

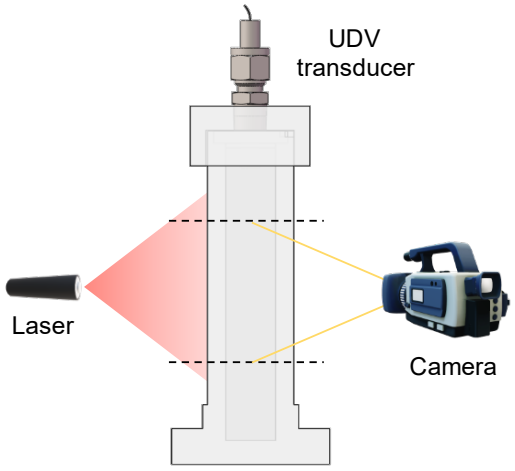

Figure 2.6 Experimental apparatus for measuring particle moving directions by UDV and PTV simultaneously. A UDV transducer was placed on top of a vessel for the UDV measurement. A laser sheet and a camera were used for the PTV measurement.

A UDV transducer with a working frequency of 8 MHz was mounted on top of the vessel by a swage fitting. The transducer probe surface was submerged below the water free surface. The transducer was connected to the DOP3010 Velocimeter and operated in emit/receive mode for data acquisition. This time, DOP3010 was operated in energy-profile mode for measuring the movement of echoing objects. Compared with the traditional ultrasound echo profile, the UDV energy profile measures and records only the echoes caused by objects moving along the ultrasound wave propagation direction (detail introduction for the UDV energy profile is in Appendix B). The echo information measured by the UDV energy profile could also be used to derive the flow velocity, because the echoes from moving objects are exactly what the UDV velocity measurement needs.

For comparison, Particle Tracking velocimetry (PTV) measurements were also performed simultaneously in the water experiment. We made PTV measurements in a region nearly matching the region where UDV measurements were made. We estimated the width of the ultrasound beam based on the transducer diameter and beam divergence to determine the measurement region, and then covered the rest of the camera's field of view with black tape to block PTV measurement in those regions.

Results and discussion

Figure 2.7 (a) and (b) show the measurement results from UDV and PTV, respectively. In the UDV energy profile, bright pixels represent echoing objects detected at different positions and times. The brightness of the pixel represents the echo intensity, which is affected by the size of the echoing objects: larger particles result in stronger echoes. Multiple consecutive pixels from the same object form a trajectory appearing as a streak, whose slope indicates the velocity of that echoing object. From the measured trajectories,

under gravity, tracer particles in the water moved away from the transducer placed on top over time. From the PTV tracking result, arrows indicate the moving direction of tracer particles, which is downward. Both the UDV and PTV measurements agreed well with each other and are also consistent with the fact that the seeded tracer particles have a higher density than water.

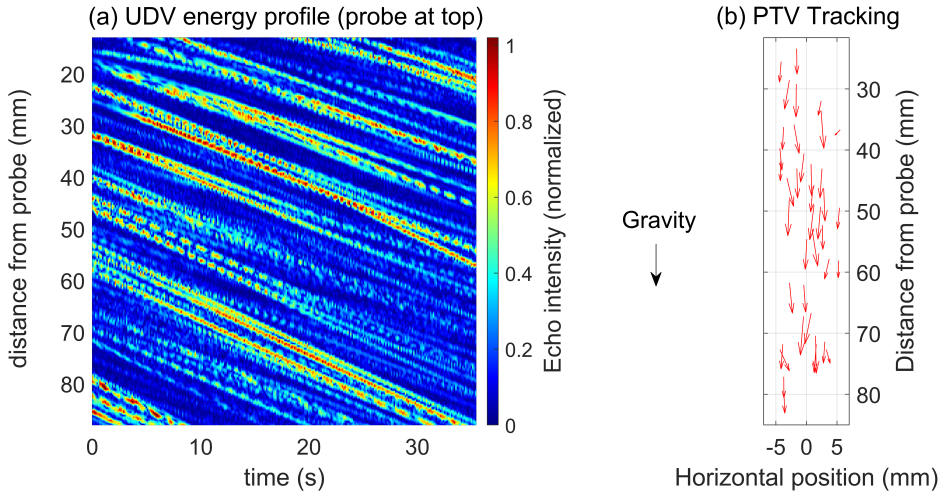

Figure 2.7 (a) UDV energy profile and (b) PTV measurement in the tracer particle water. Both the UDV particle trajectories and PTV tracking arrows indicate the particles are moving downwards.

Besides detecting the direction of motion, the UDV energy profile also allows us to estimate the particle velocity from the slope of its trajectory. Specifically, the velocity is calculated by dividing the displacement by the elapsed time. This is of course only a rough estimation because trajectories have different slopes. Trajectories following louder echoes from larger particles would have steeper slopes (higher velocity) than trajectories following weaker echoes from smaller particles. Also, the number of visible trajectories is determined by the set threshold of echo intensity. From our measurements, a rough estimation averaged from five trajectory streaks gives a velocity of 0.861 mm/s, which roughly matches the mean velocity measured from PTV of 0.742 mm/s. Note that the

tracer particles measured by the UDV may not be the exact same particles measured by the PTV. Regardless of the exact velocity, this water experiment validated our experimental idea: using the UDV energy profile to determine the moving directions of echoing objects under gravity.

2.3.2 The source of bulk echoes in liquid gallium

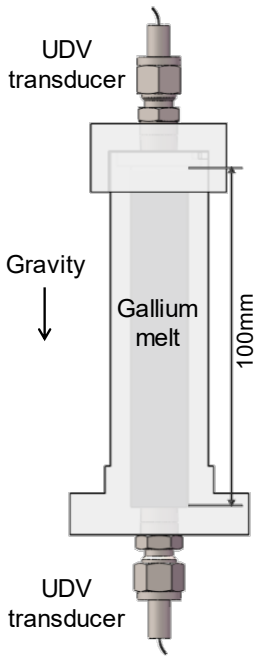

Figure 2.8 Experimental apparatus for measuring the moving direction of echoing objects in gallium by UDV.

After validation with water, we performed similar experiments in liquid gallium. Figure 2.8 shows the experimental setup for gallium. The liquid gallium was first melted in a PTFE crucible at 60°C, and then poured into the vertical vessel. The measurement was started three minutes after pouring, in order to eliminate the flows introduced by the pouring process. Since liquid gallium is not transparent, PTV measurement is unavailable. Instead,

two UDV transducers with a working frequency of 8 MHz were mounted at the top and bottom of the vessel, respectively. Both were connected to the DOP3010 Velocimeter and operated in emit/receive mode for data acquisition. The multiplexer function was used so that the two transducers worked independently: they emitted and received signals in turns and switched after acquiring one profile in sequence.

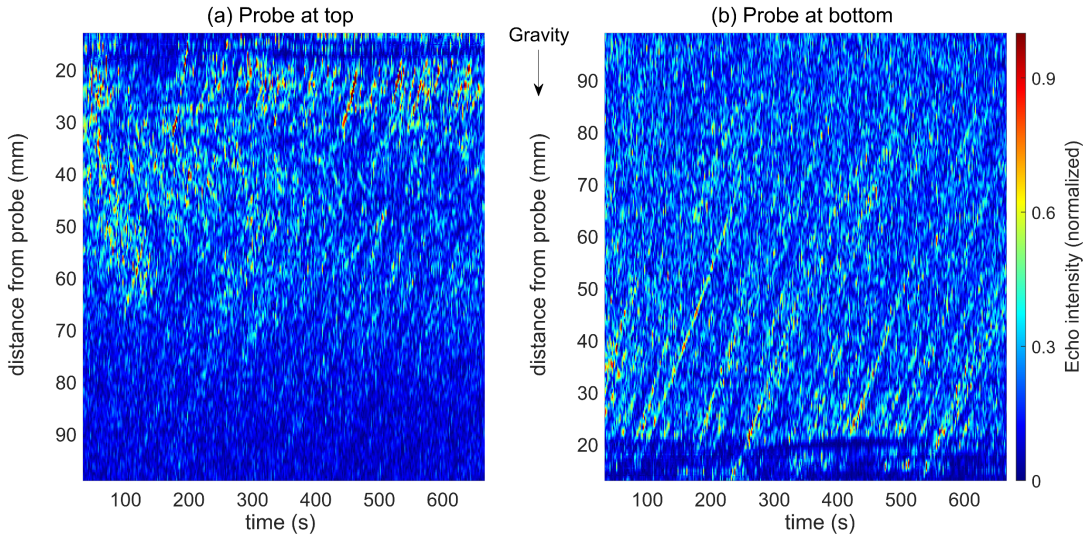

Figure 2.9 UDV energy profiles measured in gallium by transducers placed at the top (a) and bottom (b) of the vessel. The slope of trajectories indicates that the echoing objects are moving upwards in gallium.

Again, UDV energy-profile mode was used to measure the free movement of echoing objects in gallium under gravity. The measured trajectories, as shown in figure 2.9(a) and (b), indicate that most of the echoing objects are moving upwards, suggesting that the density of those echoing objects is smaller than that of liquid gallium. Among all the impurities we found under SEM, only gallium oxide (β-Ga_2O_3, 5.88 g/cm^3) is less dense than liquid gallium (6.058 g/cm^3 at 60°C). Other metal impurities have higher densities, consistent with the fact that they were mainly found at the bottom surface of the gallium

sample. In addition, the amounts of gallium oxide inclusions found from the cross-section and top surface of the sample are much larger than the amounts of metal impurities.

Combining the SEM and UDV measurement results, gallium oxides are likely to be the main source of bulk echoes in liquid gallium. The density of gallium oxide is only slightly less than liquid gallium so that they can closely follow the flow motion of gallium. Small density differences and sufficient quantities allow gallium oxide to provide strong and long-lasting bulk echoes. Metal impurities could also provide echoes. However, due to the large density differences between metal impurities and gallium, the metal impurities would sink quickly so that the echoes would not last long.

2.3.3 Producing and dissolving gallium oxides

When liquid gallium is exposed to air, gallium oxide is produced from the reaction of gallium and atmospheric oxygen, and the reaction of gallium and atmospheric water vapor.

$$3O_{2(g)} + 4Ga_{(L)} \rightarrow 2Ga_2O_{3(s)} \tag{2.1}$$

$$3H_2O_{(g)} + 2Ga_{(L)} \rightarrow 3H_{2(g)} + Ga_2O_{3(s)} \tag{2.2}$$

Therefore, gallium oxide could be artificially produced by mixing water into liquid gallium. Since the melting temperature of gallium oxide (β-Ga_2O_3) is 1725°C, it will always remain solid under our experimental conditions. However, gallium oxide will be dissolved in acid or strong alkali, so it can be removed by HCl treatment of gallium:

$$Ga_2O_{3(s)} + 6HCl_{(aq)} \rightarrow 2GaCl_{3_{(aq)}} + 3H_2O_{(l)} \tag{2.3}$$

Based on the above chemical reactions, we artificially produced or removed gallium oxides in liquid gallium by treating the liquid gallium with water or HCl solution. Specifically, we mixed a thin layer of deionized water with liquid gallium and stirred them to produce gallium

oxides, or we added a thin layer of 1 mol HCl solution to liquid gallium and stirred them to remove gallium oxides. The remaining water or $GaCl_3$ aqueous solution was removed by filtration. The as-treated gallium exhibited significant differences in surface appearance. As shown in figure 2.10, the untreated gallium has a shiny surface with some gallium oxides showing as wrinkled structures on it; the water-treated gallium is covered by a wrinkled matte oxide skin; the HCl-treated gallium has a shiny mirror-like surface with little gallium oxide on it, and the high surface tension due to its high purity results in a curved surface shape.

We also performed ultrasound measurements in the treated gallium. The untreated/treated liquid gallium was poured into the vertical vessel shown in figure 2.8, and a UDV transducer placed at the bottom was used to measure the movement of gallium oxide inclusions with the energy-profile mode. As shown in figure 2.11, the trajectories still indicate that the echoing objects in gallium are moving upwards. However, there are significant differences in the amounts of echoing objects that could be detected under different treatment conditions. For the water-treated gallium, more echoing objects were detected in the UDV energy profile, and their echo intensities were also stronger. For the HCl-treated gallium, fewer echoing objects were detected, and their echo intensities were weak. This experiment confirmed again that gallium oxide is mainly responsible for bulk echoes in gallium, as the addition or removal of gallium oxides directly determines the detected echo signals. In addition, it provides us a way to control the amounts of gallium oxides (although not precisely) in liquid gallium by chemical treatments. The control of gallium oxides is a fruitful topic and is further discussed in section 2.5.

Figure 2.10 Pictures of liquid gallium with different treatments. The treated gallium exhibited significant differences in surface appearance.

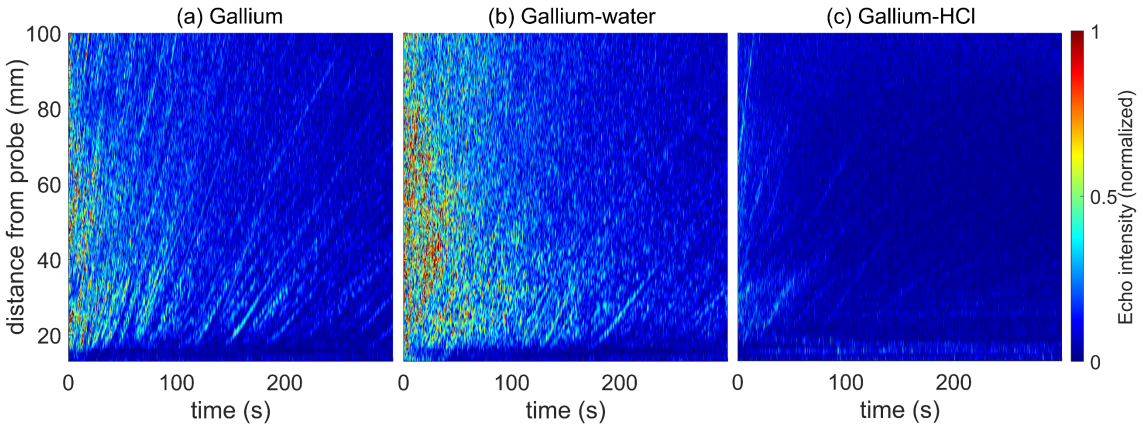

Figure 2.11 UDV energy profiles measured in liquid gallium under different treatments. The amounts of gallium oxides being detected by UDV changed a lot.

2.4 Investigation of scattering mechanisms

Depending on the ratio of the ultrasound wavelength to the echoing object's size, echoes are produced by different mechanisms. When the size of the echoing object is much larger than the ultrasound wavelength, echoes are produced from the specular reflection of ultrasound waves on the object; when the size of the echoing object is much smaller than

the ultrasound wavelength, echoes are caused by the Rayleigh scattering of ultrasound waves on the object; when the size of the echoing object is comparable to the ultrasound wavelength, complicated diffraction would happen, and the Mie scattering is a possible mechanism [79, 86].

The wavelength of an 8 MHz ultrasound in gallium is ~350μm. From the SEM images shown in figure 2.2 and figure 2.3, gallium oxide inclusions could exist as single particles or agglomerates, ranging in size from one to tens of microns. Therefore, the bulk echo signals in gallium are produced from the backscattering of ultrasound waves by oxide inclusions. Further, if bulk echoes mainly come from single-particle oxide inclusions whose size is much smaller than the ultrasound wavelength, then Rayleigh scattering would be the dominant mechanism; if bulk echoes come mainly from agglomerates whose size is comparable to the ultrasound wavelength, then Mie scattering might be the dominant mechanism. Therefore, learning the size of the echoing objects would help us better understand the scattering mechanism in gallium.

2.4.1 Particle size estimation based on terminal velocity

Although we learned the dimensions of gallium oxide inclusions from SEM examinations, we do not know what size inclusions actually produce bulk echoes in gallium. Since the UDV is mainly used to measure velocity, we developed a method to estimate the mean size of echoing objects based on the principle of terminal velocity. For a spherical object falling in a fluid, it will reach its terminal velocity (constant velocity) when the net force acting on it is zero [87], as described by:

$$\frac{4}{3}\pi r^3 g\left(\rho_{object} - \rho_{fluid}\right) = 6\pi\mu r v \tag{2.4}$$

where ρ is the density, g is the gravitational acceleration, r is the radius of the object, and μ is the dynamic viscosity of the fluid. The above formula is obtained by considering the balance among the drag force, buoyancy, and gravity acting on the object. Given the densities and fluid viscosity, the size of the object can be calculated by measuring its terminal velocity.

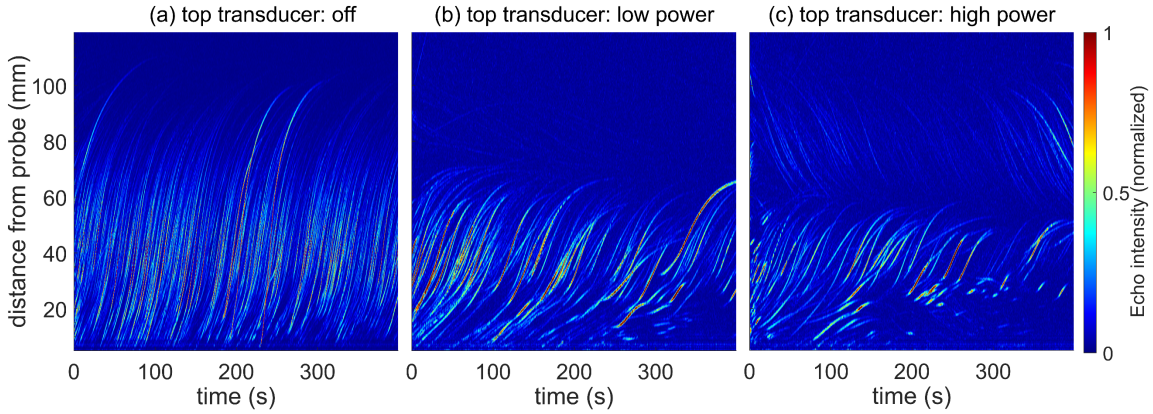

Figure 2.12 UDV energy profiles measured in a tracer particle water. All three profiles were measured by the bottom transducer. The bottom transducer was always operated at high emitting power, while the emitting power of the top transducer was changed between different tests. The acoustic force generated by the bottom transducer caused an acoustic streaming flow in water that pushed the particles near the bottom to move upward. The moving behavior of tracer particles was affected when changing the emitting power of the top transducer.

In ultrasound measurements, however, an acoustic force exerted by the ultrasound transducer also acts on the object. To demonstrate the effect of acoustic force, we filled tracer particle water into the experimental apparatus shown in figure 2.8 and ran UDV measurements with the top and bottom transducers simultaneously under different ultrasound emitting powers. As shown in figure 2.12, although the higher density of tracer particles should cause them to move downward, the acoustic force generated by the

bottom transducer was so strong that it pushed the particles near the bottom to move upward. The motion of tracer particles was also affected by the emitting powers of the top and bottom transducers. When only the bottom transducer emitted ultrasound, particles were pushed further towards the top, as shown in figure 2.12(a). When the top transducer emitted ultrasound, even at low power, the upward movement of the tracer particles caused by the bottom transducer was suppressed, as shown in figure 2.12(b). When the top and bottom transducers operated with the same emitting power level, their acoustic forces were balanced by each other in the middle-height region (around 60 mm), as shown in figure 2.12(c).

Note that in order to highlight the effect of the acoustic force, we set a very high ultrasound burst length value (thus a strong acoustic force) to produce figure 2.12. In real measurements, we only use 4 or 6 burst length values so that the generated acoustic force is not that strong. In addition, we should also note that the downward movement of the tracer particles in water shown in figure 2.7 was caused by a combination of both gravity and acoustic force. The conclusion of figure 2.7 is still valid because the acoustic force produced by the top transducer is in the same direction as gravity. However, we should be aware that although the acoustic force could push the tracer particles away along the wave propagation direction in the water, even against gravity, we have not observed such phenomena in gallium. As shown in figure 2.9, the acoustic force generated by the top transducer did not push the gallium oxide inclusions to move downward. This might be due to the relatively high viscosity of liquid gallium or the relatively weak acoustic force that can be transmitted into gallium. As a result, the acoustic force generated by the top transducer was not strong enough to overcome the effect of gravity in gallium.

No matter what, the acoustic force must be considered in the terminal velocity calculation. In the above water case, the acoustic force generated by the top transducer is in the same direction as gravity, whereas the acoustic force generated by the bottom transducer opposes gravity. We can thus derive two equations from Equation 2.4:

$$F_{acoustic} + \frac{4}{3}\pi r^3 g\left(\rho_{particle} - \rho_{liquid}\right) = 6\pi\mu r v_{top} \tag{2.5}$$

$$F_{acoustic} - \frac{4}{3}\pi r^3 g\left(\rho_{particle} - \rho_{liquid}\right) = 6\pi\mu r v_{bot} \tag{2.6}$$

where $F_{acoustic}$ is the acoustic force, v_{top} and v_{bot} are the velocity measured by the top and bottom transducers, respectively. The magnitude of $F_{acoustic}$ is unknown, and the fact is that the acoustic force produced by different transducers is not the same. To compensate that, instead of using two different ultrasound transducers simultaneously, we used the same transducer to perform two individual UDV measurements: one with the transducer placed on the top, and the other with the transducer placed at the bottom. By doing so, the $F_{acoustic}$ can be eliminated algebraically, and the average size of echoing objects can be estimated from the measured velocities.

Here, we made a few assumptions for this size estimation method. First, we assumed the echoing objects were spherical, though their real shape might be irregular. Second, we neglected the ultrasound attenuation and the near-field effects by choosing a small measurement region far away from the transducer surface (5 mm region around the middle-height). Third, we assumed that the echoing objects were in an equilibrium state within that small measurement region. Fourth, we assumed the objects inside that small measurement region were moving with the same velocity.

Before estimating the size, we also need to verify the accuracy of UDV velocity measurements. As mentioned in section 2.3.1, the slope of a particle's trajectory obtained from the UDV energy profile can only provide a rough estimation of velocity, which is not accurate enough for particle size calculation. More accurate velocity measurements can be obtained from the UDV velocity profile. Again, the UDV velocity measurements have been verified with PTV measurement in tracer particle water, using the experimental apparatus shown in figure 2.6. Table 2.1 shows the particle velocities measured under different ultrasound emitting power levels, in which the UDV velocity values were obtained by first removing the zero values and then averaging velocity data measured by UDV over time and space, and the PTV velocity values were obtained by averaging the velocity data measured by PTV over time and space within the ultrasound beam range. Clearly, the velocity of tracer particles is different under different ultrasound emitting power levels. Overall, the average velocity values measured by UDV and PTV agreed well. Therefore, the UDV velocity measurement is accurate enough for size estimation.

Table 2.1 PTV and UDV velocity measurement results

Emitting power level	PTV (mm/s)	UDV (mm/s)
High power	1.05	1.16
Mid power	0.68	0.71
Low power	0.53	0.52

We first calculated the size of tracer particles in water by the terminal velocity method. Inserting the velocities v_{top} and v_{bot} measured by the top and bottom transducers into Equation (2.5) and (2.6), we calculated the mean diameter of the tracer particles to be 96-140μm. This number closely matches the particles size labeled by the manufacturer (100-

130μm), as well as the size we measured under an optical microscope (108-122μm). The water experiment successfully validated this estimation method.

Then we used the same method to estimate the size of gallium oxides that provide echoes in gallium. By measuring the v_{top} and v_{bot} in liquid gallium, we calculated the mean diameter of oxide inclusions to be 58-64 μm (the range results from multiple repetitive measurements). This size is larger than a single gallium oxide particle (~1 μm), suggesting that bulk echoes in gallium are primarily scattered by oxide agglomerations. One possibility is that the echoes scattered by single oxide particles are too weak to be detected by the UDV transducer. Given the 8 MHz ultrasound wavelength in gallium (~350μm), the size of echoing objects is only one order of magnitude smaller than the ultrasound wavelength. Under this size range, Mie scattering might be the dominant mechanism producing echoes in gallium, but Rayleigh scattering may also play an appreciable role.

2.4.2 Discussion of Rayleigh Scattering

We further explored the scattering mechanism of oxide inclusions via experiments focusing on Rayleigh Scattering. Rayleigh Scattering occurs when the size of scattering particles is much smaller than the ultrasound wavelength (usually for a particle size < 1/10 ultrasound wavelength), in which the ultrasound wave is scattered to all directions with uniform amplitude, and only a few reflections return to the transducer [86]. One feature of Rayleigh Scattering is its strong frequency dependence: the scattering intensity is proportional to the fourth power of the frequency. Based on this feature, we have experimentally tested whether Rayleigh Scattering is the dominant scattering mechanism for ultrasound measurements in gallium.

The experimental apparatus is shown in figure 2.13, in which a 4 MHz transducer and an 8 MHz transducer were placed on the two sides of a container, respectively. Those two transducers were used simultaneously to measure echo intensities in tracer particle water or in liquid gallium. If the Rayleigh Scattering is the dominant mechanism, then we would expect the echo intensity measured by the 8 MHz transducer to be much stronger than that measured by the 4 MHz transducer. Given the ultrasound wavelength in water (185 μm for the 8 MHz ultrasound and 370 μm for the 4 MHz ultrasound), we selected two different sizes of tracer particles based on their size parameters, where the small tracer particle with diameters of 1~5μm is in the Rayleigh Scattering range, and the larger tracer particle with diameters of 50~80μm is out of the Rayleigh Scattering range [88].

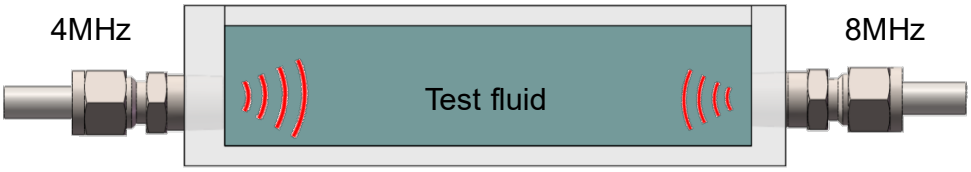

Figure 2.13. Experimental apparatus for investigating Rayleigh Scattering. Two ultrasound transducers with different frequencies were aligned horizontally on the two sides of the container to measure the bulk echo intensities in tracer particle water or liquid gallium.

The time-averaged mean echo intensities measured in tracer particle waters and gallium are shown in figure 2.14. For the small tracer particle water, although the Rayleigh Scattering should dominate, the bulk echo intensities measured by the two transducers were comparable. This is because the difference between the 4 MHz and 8 MHz ultrasound wave properties: the sound fields and beam divergence angle produced by the 8 MHz transducer is smaller than that produced by the 4 MHz transducer, as shown in figure 2.15, and the attenuation rate of 8 MHz ultrasound waves is greater than 4 MHz

ultrasound waves. These factors make a 4 MHz transducer produce/receive stronger echo signals than an 8 MHz transducer. Taking those factors into account, the frequency dependence of Rayleigh Scattering makes the echo intensities measured by the 8 MHz transducer comparable to that measured by the 4 MHz transducer. However, when the tracer particle size was too large to fall in the Rayleigh Scattering range, as shown in figure 2.14(b), the bulk echo intensity measured by the 4 MHz transducer was much stronger than that measured by the 8 MHz transducer. In liquid gallium, the bulk echo intensity measured by the 4 MHz transducer was also much stronger, implying that the Rayleigh Scattering is not the dominant mechanism. This is consistent with our size estimation results that the bulk echoes in gallium are mainly contributed by oxide agglomerations. In that size range, Mie scattering is more likely the dominant scattering mechanism.

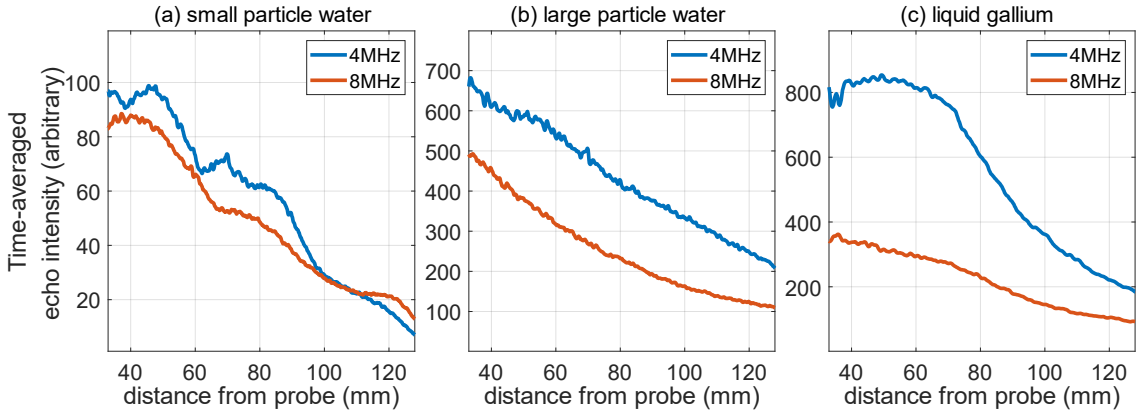

Figure 2.14 Ultrasound echo intensity measurements in tracer particle water and gallium. When the Rayleigh Scattering is dominant (a), the bulk echo intensities measured by the 4 MHz and 8 MHz transducers are comparable. When the Rayleigh Scattering is not dominant (b and c), the bulk echo intensity measured by the 4 MHz transducer is much stronger than that measured by the 8 MHz transducer.

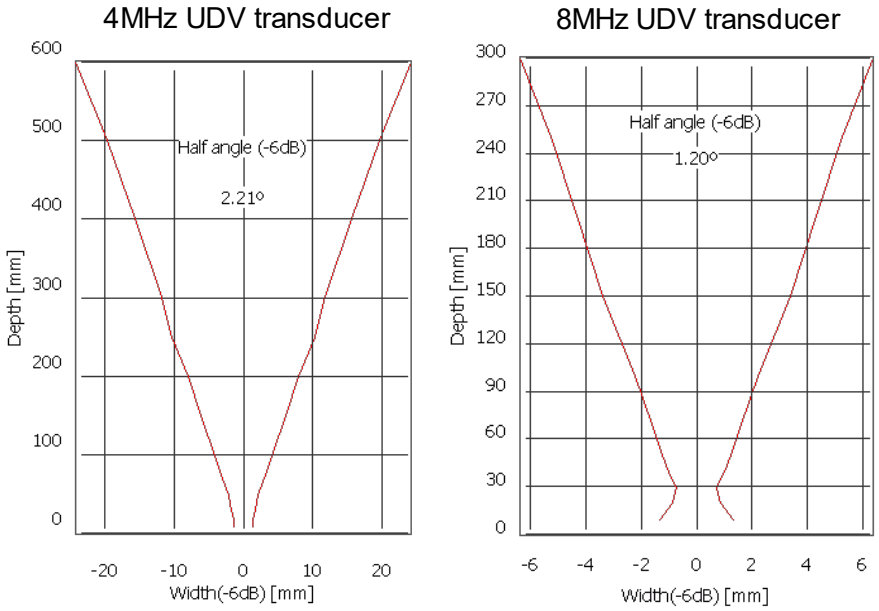

Figure 2.15 Ultrasonic field and divergence angle (half angle) produced by UDV transducers in the water. Both the ultrasonic field and divergence angle of a 4 MHz UDV transducer are larger than those of an 8 MHz UDV transducer. (Credit: https://www.signal-processing.com/trans-select.php)

2.5 Electrochemical control of gallium oxides

Knowing that gallium oxide is the source of bulk echoes, we have performed some preliminary experiments to control the concentration of gallium oxides via electrochemical methods. As shown in figure 2.16, we designed a special vessel in which one current collector made of steel plate is installed at the bottom of the vessel and in contact with the liquid gallium. A NaCl solution (1 M) was used as the electrolyte, placed on top of the gallium, and stratified steadily by density. The other current collector made of steel mesh floated on the top of the NaCl solution. The two current collectors were connected to a battery cycler (ARBIN INSTRUMENTS, USA). This system could be treated as a simple battery, in which the liquid gallium is the anode and air is the actual cathode. We can either

charge this system to remove gallium oxide or discharge the system to intensify the oxidation of gallium based on the reactions below:

$$\boldsymbol{Anode}: 4Ga + 6O^{2-} \rightarrow 2Ga_2O_3 + 12e^- \qquad \boldsymbol{Cathode}: 3O_2 + 12e^- \rightarrow 6O^{2-}$$

$$\boldsymbol{Net\ reaction}: 4Ga + 6O_2 \leftrightarrow 2Ga_2O_3 \tag{2.7}$$

The formation or dissolution of gallium oxides would consequently change the concentration of scattering particles in gallium. A UDV transducer was inserted into the gallium to measure the change of bulk echoes. At the same time, a computer connected to the battery cycler recorded the change in voltage. Figure 2.17 shows the relationship between the measured voltages and bulk echo intensities during the charging and discharging processes. When we charged the system, gallium oxides were dissolved, and the bulk echo intensities decreased. When we discharged the system, gallium oxides were produced, and the bulk echo intensities increased.

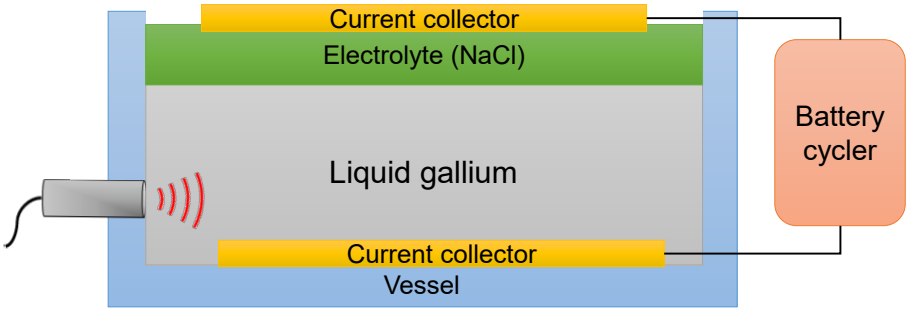

Figure 2.16 Schematic of the apparatus for controlling the concentration of gallium oxides. An ultrasound transducer was used to detect the change of echo intensities in liquid gallium during the charging and discharging processes.

From the experiment results, the overall amplitude of the echo intensity did not change significantly, probably because the formation and dissolution of gallium oxides were restricted to the vicinity of the gallium-NaCl interface, far from the ultrasound beam path.

In addition, the ohmic loss and mass transport also limit the reliability of this method. How to quantitatively correlate the voltage with the oxide concentration and the resulting echo intensity is a challenge. Thus, further experiments and comprehensive studies are required to establish a model for this electrochemical control method.

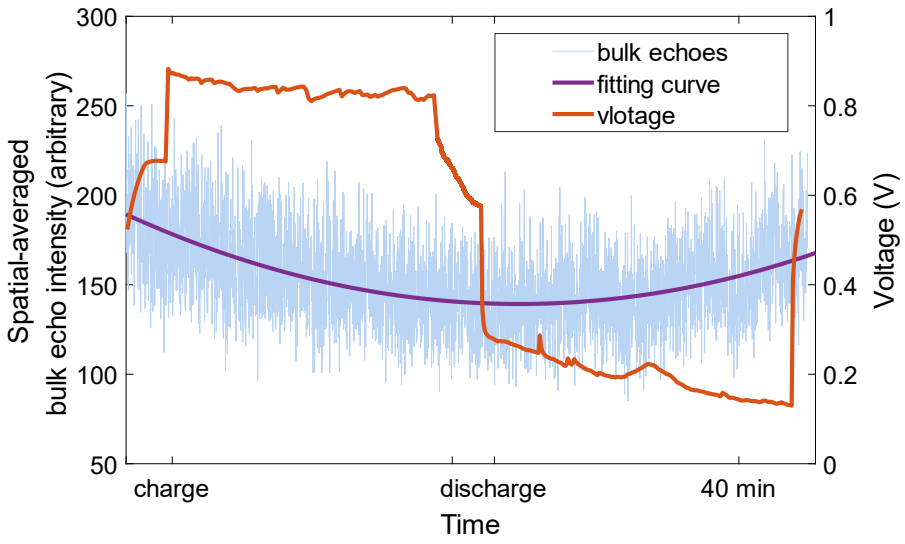

Figure 2.17 Electrochemical control of gallium oxide concentration. The bulk echo intensity curve was obtained by spatial averaging the bulk echoes within the measuring range (excluding the backwall echo). The bulk echo intensity decreased during charging and increased during discharging.

Although chemical methods can also be used to produce or remove oxides, as shown in figure 2.11, electrochemical methods are more promising. The application of electrochemical methods to control the concentration of oxides is not only limited to the UDV measurements. For example, in order to control the surface tension and wetting behaviors of eutectic gallium-indium alloy, Song et al. have built a similar electrochemical system to adjust the concentration of gallium oxides, in which NaOH was used as the electrolyte [89]. Their research also reminds us that the change of surface tension and

wetting properties involved in the electrochemical process might also affect the ultrasound measurements. The effect of wetting on ultrasound measurements in liquid metals will be further discussed in Chapter 3.

2.6 Summary of chapter

In this chapter, we investigated the source of bulk echoes and its corresponding scattering mechanisms during the ultrasound measurements in liquid gallium. Through SEM and EDS examinations, we found that gallium oxide inclusions and various metal impurities present in liquid gallium could be possible sources of bulk echoes. Further, we utilized the UDV energy profile to measure the free rising/sinking behaviors of particles under gravity. The method has been first validated by PTV in tracer particle water. Combining the SEM and UDV measurement results, we determined that gallium oxide inclusions are the main source of bulk echoes in liquid gallium.

We explored the ultrasound scattering mechanisms of oxide inclusions in gallium by estimating the size of gallium oxide inclusions that provide bulk echoes. We developed an estimation method based on terminal velocity measurements, in which the acoustic forces generated by the UDV transducers were also taken into account. This estimation method has been validated in tracer particle water, and it also provides a universal method of size estimation that can be applied to a variety of opaque fluids. We estimated the size of gallium oxide inclusions providing bulk echoes to be 58-64 μm, suggesting that oxide inclusions in the form of agglomerates, rather than single particles, are mainly responsible for bulk echoes. In this size range, although both Mie scattering and Rayleigh scattering might play an appreciable role, we expect the Mie scattering is more likely to dominate.

We further tested the scattering mechanism via analogous experiments in tracer particle waters, through which we confirmed that the Rayleigh scattering is not the dominant mechanism in gallium.

By far, we demonstrated that ultrasound waves in gallium are mainly scattered by gallium oxide inclusions in agglomeration form, and Mie scattering is the dominant mechanism. Since the mean size of oxide agglomerates is still smaller than the ultrasound wavelength, we assume the intensity of Mie scattering is greatest in the direction opposite to the wave propagation direction (backscattering), although the shape of agglomeration is irregular. In summary, UDV utilizes the backscattering echoes from gallium oxides to obtain consecutive bulk echoes and thus enable flow velocity measurements in gallium. The measured bulk echo intensity is directly related to the concentration of gallium oxides, and we have demonstrated that both chemical and electrochemical methods can affect the bulk echoes by changing the concentration of gallium oxides.

The small density difference between gallium oxide and liquid gallium allows gallium oxides to closely follow the motion of liquid gallium in most experiment cases measured by UDV. On the other hand, by knowing the density and mean size of gallium oxide inclusions, one can evaluate whether gallium oxides can be used as a good tracer for their experimental configurations, how many measurement errors will be introduced, and thus determine whether the velocity measured by UDV can reflect the real fluid speed of liquid gallium. However, although the free-rising velocity of gallium oxide inclusion in liquid gallium, measured to be 0.1-0.3 mm/s, is small, its influence on UDV measurement duration is not negligible; this will be further discussed in Chapter 4.

2.7 Acknowledgments

The thesis author was the primary person conducting all experiments and data analysis described in this chapter. The MATLAB script for extracting and demodulating the UDV data from binary files was written by Douglas Kelley. Thanks to URNano of the University of Rochester for the use of SEM and EDS facilities. Thanks to Brian McIntyre for the instruction and help on SEM and EDS examinations. Thanks to James Alkins and Omar Soufan for the instruction and help on designing, machining, and 3D printing some of the vessels and containers. Thanks to Ruy Ibanez for help setting the PTV measurements. Thanks to Rakan Ashour for help designing the electrochemical experiments. Thanks to Jean-Claude Willemetz of Signal Processing for helpful conversations on the UDV transducers and instruments.

—— Chapter 3 ——

Optimal Vessel Materials for Indirect-contact Ultrasound Measurement

In this chapter, we discuss the difference between direct-contact ultrasound measurement and indirect-contact ultrasound measurement. To find the optimal vessel material for indirect-contact ultrasound measurements in water and gallium, we study the effect of vessel wall material, including the material type, thickness, and wetting properties, on UDV measurements. We demonstrate that by carefully choosing the vessel materials, indirect-contact ultrasound measurements can achieve the same or better measurement quality than direct contact.

Part of the results listed in this chapter have been published in [90].

3.1 Introduction

3.1.1 Indirect-contact ultrasound measurement

Ultrasound measurement is noninvasive, but not fully contactless: to transmit ultrasound waves from the ultrasound transducer to the test fluid, a continuous acoustic path is required [10]. The continuous acoustic path can be created by placing the ultrasound transducer surface in contact with the test fluid, which is the so-called direct-contact measurement. However, in some cases, the ultrasound transducer cannot be inserted into the test fluid directly. For example, the test fluid might be stored in a sealed container

where no insertion opening is available for the transducer, such as a pipe flow measurement. If measurements are required from different directions and locations, transducers may need to be moved during the experiments, and opening holes would cause fluid to leak. In some scenarios, the transducer itself might affect the to-be-tested flow structures. Transducer arrays [2] also make direct-contact measurement unavailable. Metal melts as test fluids present particular challenges: first, high temperatures involved in metal melts can damage transducers by destroying the piezoelectric materials used to make them; second, corrosive metal melts might attack transducer casings; third, as a foreign substance, the transducer itself might contaminate the metal melt; fourth, since most of the commercially available ultrasound transducers are designed for water-based fluids, their acoustic coupling to liquid metals is often poor. The fact is that most of the ultrasound studies on liquid metals were performed by using ultrasound transducers designed for water. Acoustic waveguides provide one solution [68, 69], but they reduce signal strength significantly [11], and the restrictions of the experimental setup, mentioned above, persist. An alternative is to place the transducer outside the vessel of the fluid, such that the transducer does not contact the fluid directly but can achieve acoustic coupling through the vessel wall. We call this indirect-contact ultrasound measurement.

Indirect-contact ultrasound measurement has been widely used in previous studies, involving many kinds of fluids, especially liquid metals. In those studies, vessels or containers for the test fluids are made of different materials. For transparent fluids like water, transparent vessel materials such as acrylic (also called Plexiglass or Perspex) are preferred for easy visual observations [41, 91]. For liquid metals, such as liquid gallium and sodium, acrylic [2, 29, 33, 35, 43, 45, 46, 51, 52, 58, 92], glass [38, 67], copper [26, 41, 65, 83], and steel [11, 27, 93] are commonly used to build the vessels.

Compared with direct-contact ultrasound measurements, the ultrasound waves must pass through an additional layer, the vessel wall, when using indirect-contact measurements. Of course, we prefer more acoustic energy to pass through the vessel wall instead of being reflected by the wall. However, acoustic impedance mismatch between the wall material and the test fluid attenuates the ultrasound transmission and thus the performance of ultrasound measurements. Brito et al. observed multiple strong reflections caused by the entrance wall in echo profiles of gallium [26]. Obayashi et al. calculated the sound field passing through an acrylic wall and confirmed the influence of multiple reflections within the wall [92]. Murakawa et al. found that the flow velocities measured near the wall fluctuated due to the overlapping regions between the ultrasound and wall [91]. Vogt et al. reported that about 10% of the measurement range is unavailable due to the strong interface echoes caused by vessel walls [58]. Aubert et al. showed that multiple echoes resulting from the impedance contrast between a copper wall and liquid gallium blind the ultrasound measurement near boundaries [83]. Therefore, the vessel materials used for ultrasound measurements should not be chosen arbitrarily. The transmission behavior of ultrasound waves through the vessel wall needs to be carefully considered.

3.1.2 Ultrasound intensity transmission coefficient

To achieve a continuous, low-loss acoustic path in the indirect-contact ultrasound measurement, an acoustic coupling medium should be used to eliminate air gaps and thus provide enough acoustic coupling between the transducer and the vessel wall. The existence of the vessel wall will introduce two extra interfaces in the ultrasound path: the acoustic coupling medium/vessel wall interface and the vessel wall/test fluid interface. The acoustic coupling condition at each interface depends on the acoustic impedance $Z = c \cdot \rho$,

where *c* is the sound speed in the material and *ρ* is the density of the material. Usually, good acoustic coupling occurs when the impedance mismatch between the two materials is small.

The ultrasound transmission rate through the two interfaces between coupling medium, vessel wall, and test fluid is [14]

$$T_I = \frac{4}{2 + \left(\frac{Z_3}{Z_1} + \frac{Z_1}{Z_3}\right) \times cos^2 \frac{2\pi f L}{c_2} + \left(\frac{Z_1 Z_3}{Z_2^2} + \frac{Z_2^2}{Z_1 Z_3}\right) \times sin^2 \frac{2\pi f L}{c_2}} \times 100\% \qquad (3.1)$$

where T_I is the intensity transmission coefficient, Z_i are the acoustic impedances (i=1: acoustic coupling medium, i=2: vessel material, i=3: test fluid), c_2 is the sound speed in the vessel material, and L is the thickness of vessel wall. When L equals an integer multiple number of half-wavelengths such that $L = (n/2)\,\lambda$ (where n is a positive integer), Equation 3.1 reduces to

$$T_I = \frac{4Z_1 Z_3}{(Z_1 + Z_3)^2} \times 100\% \qquad (3.2)$$

In this case, the wall material is predicted to be irrelevant; the signal strength matches that of a sound wave transmitted from the acoustic coupling medium to the test fluid directly. If the acoustic coupling medium and test fluid are also the same material, 100% transmission is predicted.

When the vessel material's thickness L equals an odd number of quarter wavelengths such that $L = (2n-1)\lambda/4$, Equation 3.1 reduces to

$$T_I = \frac{4Z_1Z_3}{(Z_2 + Z_3\frac{Z_1}{Z_2})^2} \times 100\% \quad (3.3)$$

In this case, if $Z_2 = \sqrt{Z_1Z_3}$, then the intensity transmission coefficient again equals 100%. Thus, a wall material whose acoustic impedance equals the geometric mean of the impedances of the acoustic coupling medium and test fluid is predicted to maximize the acoustic transmission. A wall made from such a material is called a matching layer [14]. Taking liquid gallium as an example, if water is used as the acoustic coupling medium, nylon with a thickness of quarter wavelengths closely matches the above conditions and is predicted to make an excellent matching layer.

For a given test fluid and acoustic coupling medium, Equations 3.1 and 3.2 suggest that the acoustic impedance and thickness of the vessel wall are important as they determine the ultrasound transmission through the wall. Prior ultrasound studies have begun to consider the role of the vessel wall, particularly its thickness. Michaud et al. studied the sound transmission through steel plates of different thicknesses, in which they validated the multiple half-wavelength theory as shown in Equation 3.2 [94]. Takeda and Kikura comprehensively discussed the relationship between wall thickness, ultrasound frequency, and ultrasound pulse width when they conducted ultrasound measurements in mercury through a steel wall; they also set criteria for the wall thickness to optimize the ultrasound measuring volumes [84]. Eckert et al. machined a steel adaptor with a thickness-to-wavelength ratio of 1.5 for maximizing the ultrasound transmission coefficient [27]. Those prior works have demonstrated the importance of the wall for indirect-contact ultrasound measurements. However, most of them only focused on a certain type of vessel material. In this chapter, we systematically investigated the effect of vessel wall material on the

performance of indirect-contact ultrasound measurements, for both water and liquid gallium. We designed a special container that allows us to perform indirect-contact ultrasound measurements through test plates made of different materials and with different thicknesses.

3.1.3 Wetting and contact angle

The sound transmission equations 3.1-3.3 were originally developed for liquids. When an acoustic wave is normally incident on an interface, many solids obey the same equations [79], but other factors should be considered. For example, wetting becomes a key factor determining the physical acoustic coupling: the continuity of the acoustic path. Since most of the commercial ultrasound transducers are designed for water-based liquids, the wetting between the transducer probe surface and water is usually sufficient. However, for indirect-contact measurements, good wetting between the vessel wall and test fluid is not guaranteed. This is especially true when the test fluid is a liquid metal, because molten metals have unusually high surface tension. The high surface tension tends to prevent liquid metal from wetting the vessel wall thoroughly. Instead, it causes some air gaps or pockets left between the liquid metal and vessel wall, disrupting the continuity of the acoustic path. As the acoustic impedance mismatch between gas and liquid is huge, the air gaps would reflect ultrasound waves strongly. Therefore, when the wetting between liquid metal and vessel wall (or transducer surface) is insufficient, part of the ultrasound waves cannot transmit through the solid-liquid interface, resulting in repeated reflections. On the one hand, the amount of acoustic energy transmitted into the test liquid is reduced, which leads to low signal strength. On the other hand, the repeated reflection signals accumulate over the entire echo profile, which disturbs the UDV measurement [25].

The importance of wetting has been realized and discussed in earlier publications: Tasaka et al. selected Pyrex glass as the vessel material since it can be wetted by liquid gallium [38]; further, Cramer et al. found that the oxides formed on the liquid gallium surface improved its wetting to a Perspex wall [29]; Eckert and Gerbeth polished the surface of the steel adapter and chemically removed its oxide layer to achieve good wetting with liquid sodium [27]; Brito and Aubert et al. coated a thin cataphoretic film on a copper container wall to ensure good wetting contact with gallium [26, 83]. Wetting is important, but how to choose a vessel material that has good wetting with the test fluid, or how to evaluate the wetting between them, has barely been mentioned. In our study, we measured the contact angle to evaluate the wetting conditions. The contact angle is often used as the primary data in wettability studies; it indicates the degree of wetting between a liquid and a solid [95]. The contact angle is the angle at the three-phase line on which the liquid, vapor, and solid phases meet. Since the contact angle provides an inverse measure of wettability, a small contact angle indicates good wetting, and a large contact angle indicates poor wetting [96]. As a rule of thumb, a contact angle less than 90° means good wetting, a contact angle larger than 90° means poor wetting, and a contact angle larger than 150° can be considered non-wetting. In this chapter, we would provide substantial results to demonstrate the effect of wetting on the UDV measurements.

3.2 Experiments and methods

3.2.1 Experimental apparatus

To investigate the effect of vessel wall materials on ultrasound measurement, we used test plates of various materials to perform indirect-contact ultrasound measurements in water and gallium. Figure 3.1 shows a schematic diagram of the experimental apparatus, which is designed to measure acoustic transmission through test plates of various materials and thicknesses. The container is machined from an Acetal block. The dimension of the container is 120 mm in length, 50 mm in width, and 40 mm in height, wide enough that the ultrasound measurement will not be affected by the reflection from the side walls. A slot near the front wall of the container allowed the test plate to be inserted. The test plate splits the container into two chambers: a small chamber for placing the acoustic coupling medium, and a large chamber for placing the test fluid. Rubber seals on both sides of the test plate were used to hold the plate in position and prevent leaks. Multiple rubber sealing layers with different thicknesses were available for different test plates. The apparatus also allowed experiments without any test plate in place, i.e., direct-contact measurement. The results from direct-contact measurement are used as a reference for indirect-contact measurements.

Two ultrasound transducers with working frequency of 8 MHz were placed on the two opposite walls of the container and fixed by swage fittings. As shown in figure 3.2, the transducer-1 placed on the front wall was connected to the DOP3010 Velocimeter and operated in emit/receive mode for data acquisition. In indirect-contact measurements, the transducer-1 was inserted into the acoustic coupling medium until gently touching the test plate. The transducer-2 placed on the container’s back wall was connected to an

oscilloscope (Teledyne LeCroy, U.S.A.) and served as a hydrophone for sound pressure measurement.

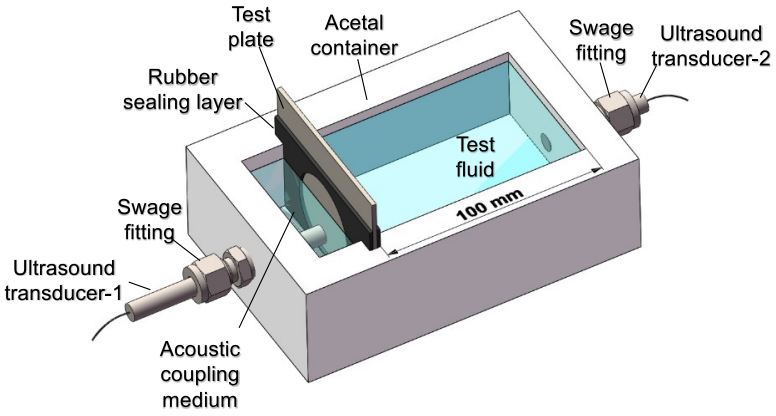

Figure 3.1 Schematic of the container for vessel materials testing. The slot near the front wall of the container positions the test plate and rubber layers.

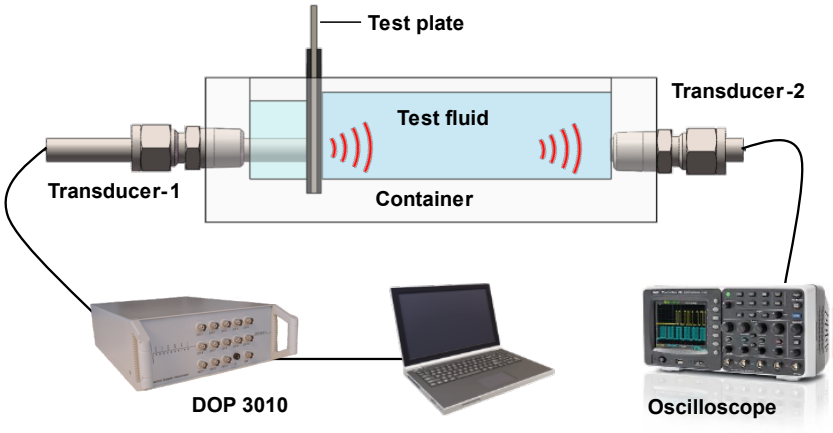

Figure 3.2 Instrumentation for vessel materials testing. Transducer-1 was positioned on the front wall of the container and connected to the ultrasound velocimeter. Transducer-2 was positioned on the back wall and connected to an oscilloscope.

During experiments, the ultrasound transducer-1 emitted a series of ultrasound pulses. The same transducer was also used to receive the reflected signals, which contain information about echo intensity and flow velocity. The ultrasound measuring line is

parallel to the centerline of the container, 5 mm away from the central position. The ultrasound signals were recorded by the UDOP software and displayed on a connected computer in real-time. For each test, 1000 transient echo profiles and velocity profiles were recorded, and their averaged values were used as the final results of echo intensity and flow velocity, respectively. In all measurements, a time gate compensation (TGC) with uniform magnitude was applied to compensate for the sound attenuation occurring when ultrasound propagated through the fluid. After each measurement, we cleaned the container and ultrasound transducer's tip thoroughly before inserting another test plate.

Meanwhile, the transducer-2 was used to measure the acoustic pressure passing through the test plate and reaching the back wall. The position of the transducer-2 was directly facing the transducer-1. The measured waveforms were acquired and stored by an oscilloscope. Since we were only interested in the relative acoustic pressure values transmitted through different test plates, the acoustic pressure was reported in arbitrary units.

3.2.2 Water experiments

First, we used deionized water as the test fluid. To produce bulk echoes, tracer particles (50~80 μm in diameter) were seeded to the deionized water. A rotating flow was produced in water by a magnetic stir bar spun by a stirring plate beneath the container. To avoid measuring the velocity of the stir bar itself, the position of the stir bar was not at the ultrasound wave path. In order to produce a similar flow for all tests, both the position of the container on the stir plate and stirring speed were kept constant. Stirring was slow enough (~85 rpm) that the resulting flow (Reynolds number ~800) was apparently laminar. We observed no oscillations at frequencies other than that of the stir plate. All tests were

carried out with the same ultrasound parameter settings.

The test plate materials we selected for water experiments are listed in Table 3.1. We chose those materials because they are readily available and have been frequently used in previous studies. The thickness of each test plate was measured by an electronic micrometer at the exact region where the ultrasound transducer made contact. The measured thicknesses are listed in Table 3.1. As mentioned above, to achieve the best acoustic transmission and to minimize reflection from the plate itself, the thickness of the test plate should be multiples of its half-wavelengths. The thickness we selected for each test plate is approximately equal to integer multiples of half-wavelengths. All test plates were carefully cleaned by an ultrasonic cleaner and totally dried before ultrasound measurements.

Table 3.1 Test plate materials selected for water

Vessel Materials	Acoustic impedance Z (MRayls)	Thickness (mm)	Number of wavelength	Intensity transmission coefficients	Contact angle (STD)
ABS	2.31	0.138	0.50	99.98%	59º (5.96)
Acrylic	3.26	0.508	1.48	98.74%	76º (4.13)
Rubber	1.47	0.199	1.03	99.97%	85º (5.55)
Aluminum	17.33	0.412	0.51	82.15%	47º (3.35)
Copper	44.6	0.307	0.49	56.22%	74º (5.57)
Steel	45.7	0.366	0.51	78.25%	62º (5.28)

For indirect-contact ultrasound measurement, an acoustic coupling medium must be used surrounding the ultrasound transducer to eliminate the air gaps. The influence of the acoustic coupling medium on ultrasound measurement was investigated by using water or ultrasound transmission gel (Aquasonic 100, PARKER LABORATORIES, Inc., U.S.A.)

as the acoustic coupling medium. The reason for choosing water and ultrasound transmission gel as the acoustic coupling medium is that the UDV transducer was originally designed for water-based applications. Therefore, good wetting and acoustic transmission are achieved when the transducer surface is in contact with water directly. In addition, keeping the acoustic coupling medium the same as the test fluid can eliminate variation due to interactions at the transducer surface. Interfacial conditions between the acoustic coupling medium and test plate necessarily vary when the test plate changes. However, when water is used as both the acoustic coupling medium and the test fluid, interfacial conditions are the same on both sides of the test plate. Each side is presumably responsible for half of the measured variations.

We also explored the effect of test plate thickness on ultrasound transmission. Selected test plates made of the same material but with different thicknesses were used to conduct ultrasound measurements. Still, the select thicknesses were close to the multiples of half-wavelengths.

3.2.3 Gallium experiments

Similar experiments were also conducted in liquid gallium. Deionized water was used as the acoustic coupling medium. We expect the interface between gallium and the test plate to dominate measured signal variations, because water almost always produces better coupling to both the transducer surface and test plates. The liquid gallium was melted from pure solid gallium (99.99% pure) and kept at 60°C for all experiments. The container, test plates, and ultrasound transducers were also preheated before experiments. The gallium oxide layer formed on the top surface of liquid gallium was scraped off before each measurement. After each test, the liquid gallium was left for ten minutes to rebalance. For

the gallium cases, no stir bar was added, and the flow in gallium was induced by a rotating magnetic field generated by the stirring plate beneath the container. To produce a similar flow for all tests, both the position of the container and rotating speed were kept constant. All tests were carried out using the same ultrasound parameter settings. We did not add any artificial tracer particles to gallium, and the gallium oxide inclusions provide bulk echoes.

Table 3.2 lists the test plate materials we selected for liquid gallium, which have been widely used as vessel materials in prior studies. The thickness of each plate was measured and listed in Table 3.2 as well. As in the water experiments, the thicknesses of selected test plates are near-integer multiples of their half-wavelengths, except for nylon. The thickness of the nylon plate was chosen to be an odd number of its quarter-wavelengths, since nylon has approximately the right acoustic impedance to be a matching layer for gallium. All test plate materials were carefully cleaned by an ultrasonic cleaner and totally dried before experiments.

Table 3.2 Test plate materials selected for liquid gallium

Vessel Materials	Acoustic impedance Z (MRayls)	Thickness (mm)	Numbers of wavelength	Intensity transmission coefficients	Contact angle (STD)
Acrylic	3.26	0.508	1.48	30.27%	97º (4.20)
Nylon	4.93	0.808	2.23	95.81%	130º (2.92)
Borosilicate glass	13.1	3.318	4.71	45.23%	109º (8.06)
Copper	44.6	0.307	0.49	29.38%	124º (7.46)
Steel	45.7	0.376	0.52	27.85%	121º (4.71)

To investigate the effect of plate thickness on ultrasound measurement in gallium, test plates made of the same type of material but with different thicknesses were used to

perform indirect-contact ultrasound measurements, and the measured echo intensities were compared.

When comparing the measurement results from different test plate materials, we assumed the condition of the gallium was the same in each test. In fact, the amounts of oxide inclusions and impurities are always changing due to exposure to atmospheric oxygen. However, this change did not affect our final results, which were similar in repeated experiments.

3.2.4 Contact angle measurements

To evaluate the wetting behaviors of water on different test plates, the contact angles of water on each test plate were measured by using the static sessile drop method [97]. A goniometer (AST Products Inc., U.S.A.), the equipment specially designed for contact angle measurements consisting of a syringe, a camera, and a moving stage, was used.

All test plates were carefully cleaned by an ultrasonic cleaner and totally dried prior to measurement. During the measurement, a test plate was placed in the measurement stage of the goniometer, and deionized water droplets were injected through a syringe placed above the test plate. A camera behind the measurement stage recorded the shape of the droplet. From the profile of the droplet, the contact angle could be measured.

For water experiments, the contact angle measurement was repeated five times for each test plate at different positions. Each image provided two contact angle values: the contact angles at the left and right of the droplet. Under ideal conditions, the shape of the droplet is symmetrical, and the left and right contact angle values are the same. In real cases, a successful experiment would produce an almost symmetrical droplet, but there would always be small deviations in the left and right contact angle values due to the uneven

surface topography of the test plate and measurement errors. For each test plate, there are ten contact angle values measured in total, and the average value is shown in table 1.

Switching to gallium, due to its high surface tension and the presence of the oxide layer, the wetting behavior of liquid gallium is much more complicated. The static sessile drop method was used to evaluate the contact angle of gallium on different test plates. The syringe of the goniometer is not suitable for gallium as the needle is too thin to eject gallium. Instead, a syringe pump and a syringe with a thicker needle were used to produce gallium droplets. If the size of the droplet varies too much between tests, it might affect the results. Therefore, the syringe pump was set to push the syringe at a constant speed, and the position and height of the syringe were fixed, so we could keep the size of the droplets similar. The measurement stage and camera of the goniometer were still used for placing the test plates and taking pictures, respectively.

As in the water experiments, all test plates were carefully cleaned by an ultrasonic cleaner and totally dried. The gallium was melted and maintained at 60°C on a hotplate. All test plates and the syringe were preheated on the hotplate as well. The contact angle measurement was repeated six times for each test plate at different positions. The first drop on each test plate was discarded because it had a longer contact time with air and thus more oxidation. In total, ten contact angle values were measured for each test plate, and the average value is listed in Table 1. Since the UDV transducer was not designed for gallium, the contact angle between the liquid gallium and the transducer probe surface was also measured.

3.2.5 Calculation of ultrasound intensity transmission coefficient

We calculated the acoustic intensity transmission coefficients for each test plate in water

and gallium according to Equation 3.1. The sound speed of water used in this study is 1480 m/s, and the sound speed of liquid gallium is 2860 m/s. The sound speeds (bulk speed) and acoustic impedances (bulk characteristic impedance) of all test plate materials used here were taken from the DOP3010 User Manual [78]. The calculated results for water and liquid gallium are listed in Table 3.1 and Table 3.2, respectively. It should be noted that the acoustic intensity transmission coefficients we calculated here are limited to three layers: acoustic coupling medium, test plate, and test fluid. Definitely, there will also be energy loss when ultrasound waves are emitted from the transducer into the acoustic coupling medium. Since the ultrasound transducer was designed for water applications, we assumed that the acoustic transmission from the probe surface to the water-based acoustic coupling medium is lossless.

3.3 Results and discussion

3.3.1 Vessel material for water

The influence of vessel material on ultrasound measurement was inferred from three measurements: the echo intensity profile measured by transducer-1, the acoustic pressure waveform measured by transducer-2, and the flow velocity profile measured by transducer-1. The measured ultrasound echo intensity profiles in water, for test plates of different materials, are plotted in figure 3.3. Each curve shows a relationship between the distance from the transducer and the measured echo intensity amplitude. The echo intensity of direct-contact measurement, without any test plate, is shown for reference. The curves shown in figure 3.3 (a)-(f) were obtained by time-averaging over 1000 transient profiles spanning 168 seconds. All selected test plates allowed detection of the strong

reflection echo from the back wall of the container, evident as the large peak at about 100 mm from the transducer in figure 3.3. This indicates that indirect-contact ultrasound measurement through vessel walls made from any of those six materials would be able to detect large liquid-solid interfaces in water.

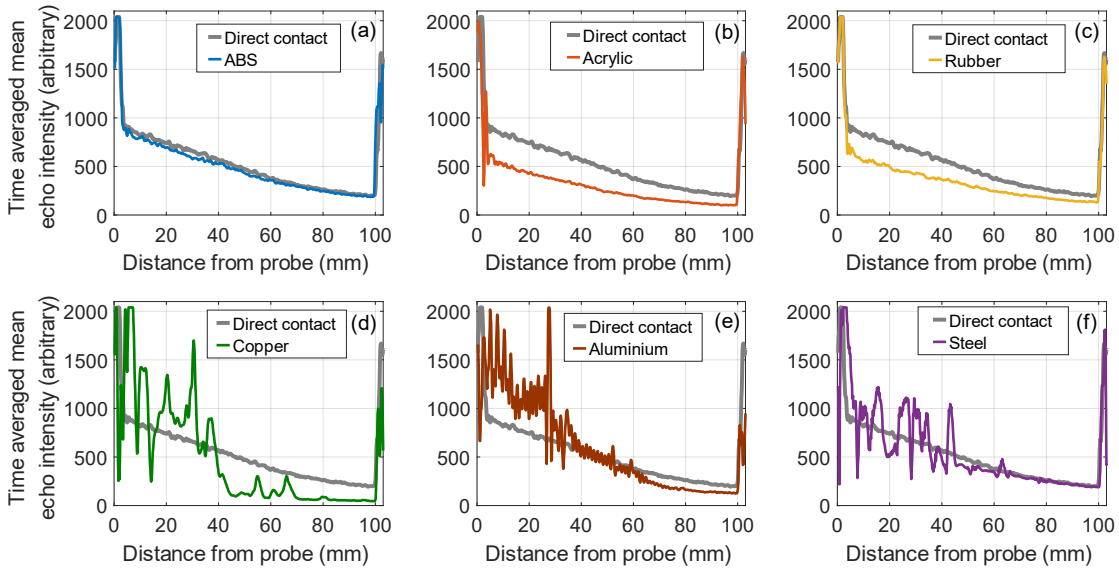

Figure 3.3 Ultrasound echo intensity measurements in water with different test plate materials. Strong echoes are evident near the transducer surface (0 mm) and at the vessel wall (near 100 mm). The echo intensity of direct-contact measurement is shown for reference. Results suggest that plastic materials are better for transmitting sound into water.

In addition to detecting large interfaces, the ability to detect echoes scattered by small tracer particles suspended in the bulk part of the fluid is necessary for velocity measurement. Although the bulk echo intensity is mainly determined by the type, size, and concentration of tracer particles in the fluid, the existence of the vessel wall might affect the measured bulk echo intensities. Figure 3.3 (a)-(c) shows that the measured bulk echo intensities in water are similar between the direct-contact measurement and indirect-contact measurements through test plates made from ABS, acrylic, or rubber. ABS plastic

produces the best acoustic transmission, closest to that of direct contact measurement. Note that bulk echo intensity always declines with distance from the transducer due to sound pressure distribution and attenuation in the fluid, even though time gate compensation was applied.

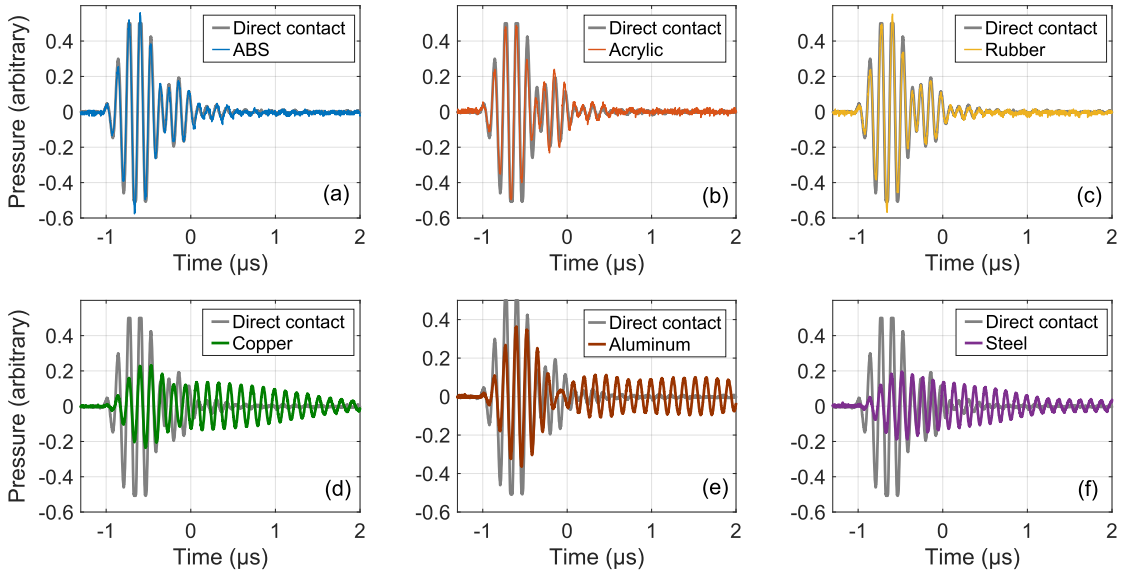

Figure 3.4 Sound pressure measurements in water through different test plates, measured by the transducer-2 located at the container's back wall. Each curve describes a transient pressure waveform in one ultrasound pulse duration. The transient pressure waveforms measured with plastic plates are close to the reference. More reverberation noises appeared within the waveforms of the metal test plates.

Figure 3.4 shows the sound pressure transmitted through different test plates, measured by the transducer-2 located on the back wall. As shown in figure 3.4(a)-(c), the sound pressure transmitted through ABS, acrylic, and rubber is similar, consistent with the calculated transmission coefficients listed in Table 3.1. However, the measured contact angles in Table 3.1 indicate that the three plate materials have different wettability to water. As mentioned above, good wetting improves acoustic coupling, which explains why the

ABS transmits sound better than acrylic or rubber.

Unlike the plastic test plates, the metal test plates exhibited totally different behaviors. As shown in figure 3.3(d)-(f), acoustic transmissions through copper, aluminum, and steel are poor. Those metal plates caused several artificial peaks to appear in the bulk part of the curve, especially at the first 50 mm from the transducer. Those artificial noises mask and interfere with the real echoes of the tracer particles. The artificial peaks could be explained by reverberations occurring when sound waves are reflected repeatedly within the metal plates. Each reflection is strong because of the large acoustic impedance mismatch between the metal plate and water. Many reflections can occur because the metals have small acoustic damping coefficients, so sound waves are attenuated little as they traverse the metal. Reverberation is also evident in the sound pressure waveform from figure 3.4(d)-(f) at times greater than 1.5 ms. Note that in figure 3.4 (d)-(f), the peak-to-peak pressures measured from metal plates are also smaller than that of direct-contact measurement. This reduced sound pressure could be predicted from the calculated transmission coefficients listed in Table 3.1. Sound pressure may also be reduced by the fact that the metal plates are solid, while Equation 3.1 is strictly accurate only when all three layers are liquid. When applying this equation to solid materials, the density and stiffness of the material must be considered. As discussed in prior studies [94], acoustic energy is dissipated in the solid test plate even when Equation 3.1 predicts 100% transmission at the interface. As shown in figure 3.3, all test plates have introduced strong echoes near the transducer surface (0 mm) due to the acoustic impedance mismatch between acoustic coupling medium, test plate, and test fluid. We call these strong echoes front-wall noises. However, when the test plate was plastic, the front-wall noises were weak and only covered about 5 mm measurement regions; when it was metal, front-wall

noises were stronger and covered nearly 40 mm measurement regions, as shown in figure 3.3 (d)-(f). Although some of the front-wall noises could be mitigated by adjusting ultrasound parameters like the emitting power or TGC (discussed in Appendix B), most of the front-wall noises could not be eliminated.

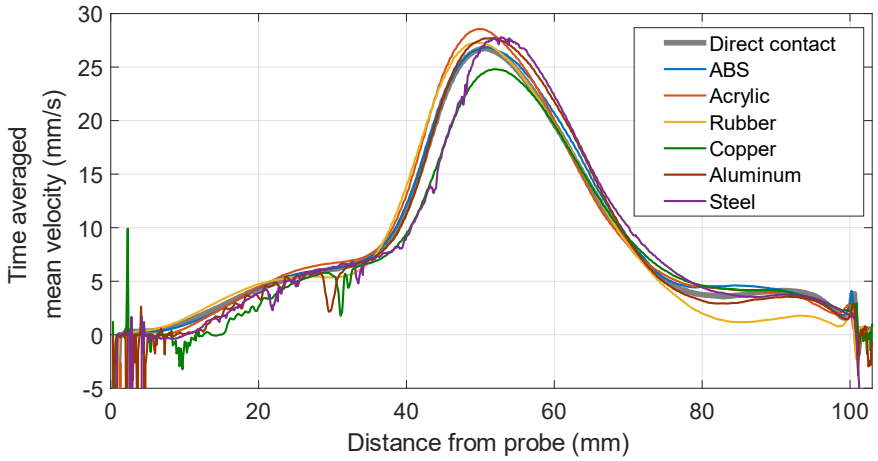

Figure 3.5 Ultrasound velocity measurements in water with different test plates. The velocity profiles were obtained by time-averaging over 1000 transient profiles. The flow structure produced in this experiment could be described by the direct-contact measurement curve. All selected materials allowed ultrasound velocity measurements in water, and the measured mean flow structures are close to the reference curve.

Figure 3.5 shows the measured flow velocity profiles in water with different test plates. Those velocity profiles include only one velocity component along the wave propagation direction. All test plates considered allow ultrasound velocity measurements, and the measured mean flow structures are close to the reference curve. Measurements through copper plate differ most from the reference velocity curve, indicating significantly lower peak velocity. The mismatched velocity correlates with distorted bulk echo intensities, as shown in figure 3.3 (d). Interestingly, it seems like the ultrasound velocity measurement is less sensitive to the choice of vessel material than the echo intensity measurement. Even

for metal vessel materials, which cause multiple noises in the bulk echo measurements, the velocity profiles could still describe the basic flow structure. However, we should also note that, in order to facilitate the comparison between different test plates, the flow generated in the above experiment was a simple rotating flow. In real measurements where more complex flow structures appear, the effect of different test plates on velocity measurements might be huge.

To compare the measured velocity profiles quantitatively, we defined a dimensionless quantity, the normalized root-mean-square velocity mismatch M_{nrmsv}, for each test plate:

$$M_{nrmsv} = \sqrt{\frac{1}{n} \times \sum_{i=1}^{n} \left(\frac{Velocity_i(test\ plate) - Velocity_i(direct\ contact)}{Velocity_i(direct\ contact)}\right)^2} \qquad (3.4)$$

where the summation is over the *n* measurement locations in the bulk (5 mm to 100 mm from the transducer surface). Smaller M_{nrmsv} means that the measured velocity profile is closer to that of the direct-contact measurement. The value of M_{nrmsv} for each test plate is listed in Table 3.3. From the results, plastic test plates show better performance than metallic test plates, and the ABS test plate is the best. That fact is consistent with the close resemblance between the echo profile measured through the ABS plate and that of direct contact (figure 3.3(a)), as well as the close resemblance between the sound pressure measured through the ABS plate and that of direct contact (figure 3.4(a)). It should be noted that the metal test plates also caused significant measurement mismatches for distances less than 5 mm, which would further increase their M_{nrmsv} values if those regions were included in the calculation.

Table 3.3 Normalized root-mean-square velocity mismatch for each test plate in water

Test plate material	Normalized root-mean-square velocity mismatch $\boldsymbol{M_{nrmsv}}$
ABS	0.1073
Acrylic	0.2574
Rubber	0.3059
Copper	0.5813
Aluminum	0.4239
Steel	0.4158

Considering the measured echo intensity and flow velocity results, we would suggest using ABS as the vessel material for performing indirect-contact ultrasound measurements in water. Although prior studies have used steel or copper vessels successfully, ABS is preferable. First, due to the large acoustic impedance mismatch between water and metal, even a small change in vessel thickness would lead to a large difference in transmission coefficients, according to Equation 3.1. Taking the copper test plate as an example, a one-micron change in its thickness will cause an 8% change in the theoretical acoustic intensity transmission coefficients. Therefore, vessels made of metal require more precise control of thickness to achieve a good sound transmission. For plastic and polymer materials with acoustic impedance close to water, more tolerance in thickness can be allowed. Second, metal plates or walls cause strong front-wall noises and reverberations, which interfere with bulk echoes and introduce errors in velocity profiles. Third, due to the higher density and stiffness, metals deviate more than plastics from the prediction given by Equation 3.1. It also causes more sound energy than expected to dissipate inside the metal walls, which might reduce the sensitivity and disturb ultrasound measurements.

Focusing on ABS, we further investigated the effect of test plate thickness on ultrasound

measurement. Figure 3.6(a) shows the echo intensity measured through ABS test plates with two different thicknesses. The calculated transmission coefficients are listed in the caption. Equation 3.1 accurately predicts the relative transmission strength for plates made from the same material with different thicknesses. The velocity profiles in figure 3.6 (b) imply that increasing the thickness affects the flow velocity measurements little.

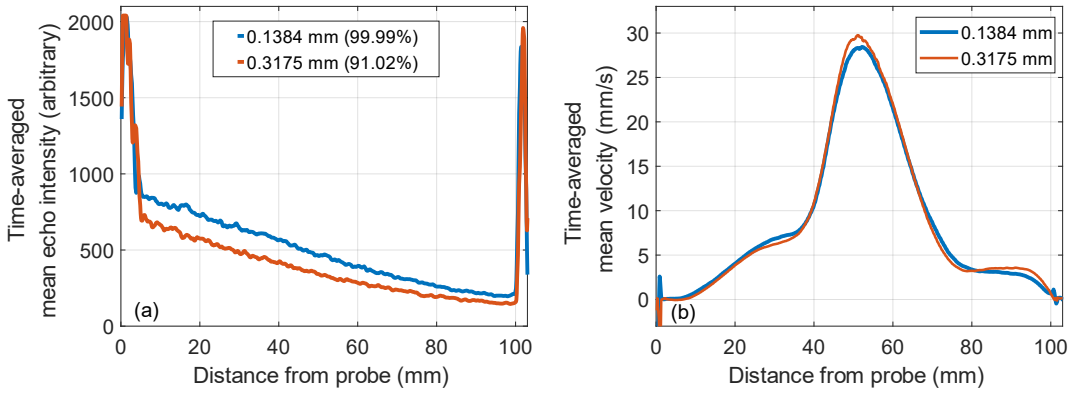

Figure 3.6 Ultrasound measurements in water through ABS test plates with two different thicknesses. (a) echo intensity measurement. (b) velocity measurement. For plates made of the same material but with different thicknesses, the calculated transmission coefficient is a good prediction for their relative transmission strength.

We also studied the effect of acoustic coupling medium on ultrasound transmission. In this experiment, deionized water and ultrasound gel were used as the acoustic coupling medium, and the test plate was ABS. The measured echo intensity and flow velocity are plotted in figure 3.7. The results suggest that water and ultrasound gel performed similarly. This result could be expected because the ultrasound transducer we used was originally designed for water-based applications. Considering the availability and operability, water might be a better choice in room-temperature applications. However, at higher temperatures, bubbles might form in water and appear on the ultrasound transducer surface, which would definitely destroy the ultrasound measurements. No matter which

acoustic coupling medium is used, replenishment is necessary between experiments or every once in a while, to eliminate possible bubbles and consumptions due to evaporation.

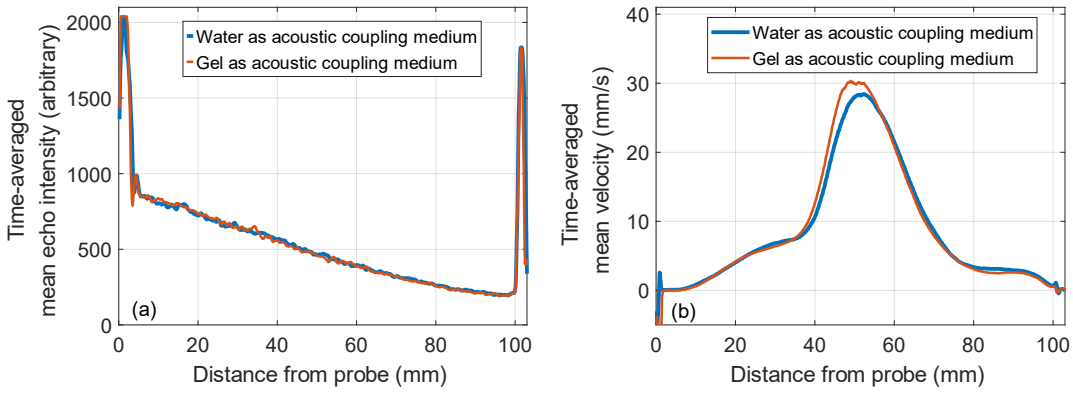

Figure 3.7 Ultrasound measurements in water with different acoustic coupling media (water and ultrasound gel). (a) Echo intensity measurement. (b) Velocity measurement. The test plate was ABS plastic. As an acoustic coupling medium, water and ultrasound gel exhibit similar performance.

3.3.2 Vessel material for gallium

Changing the test fluid from water to liquid gallium, we performed the same ultrasound measurements, with deionized water as the acoustic coupling medium. Figure 3.8 shows the measured echo intensity profiles in liquid gallium for different test plates, which were obtained by time averaging over 1000 transient profiles. All selected test plates allow the detection of back wall reflection signals in gallium. Interestingly, the acrylic test plate transmitted the strongest bulk echo signals, even stronger than that of direct-contact measurement. This phenomenon could be explained by the different wetting behaviors, as shown in figure 3.9. The measured contact angle between the transducer probe surface material (Epotek epoxy) and liquid gallium is 137°, indicating that the wetting in direct-contact measurement is poor. The acrylic test plate wets gallium much better, as indicated by its lower contact angle (97°). During the experiment, we also observed that the gallium

oxide layer formed on the gallium surface is more likely to wet acrylic or glass rather than wet the transducer surface, another reason that acrylic and glass give superior acoustic coupling [29, 98]. On the other hand, although nylon, as the matching layer, is predicted to have the highest transmission coefficient, figure 3.8(b) shows that the bulk echo intensity measured through the nylon test plate was not the strongest. This discrepancy can be explained by wetting as well: the contact angle between nylon and gallium (130°) is poor, as in the direct-contact measurement, so the measured echo intensities are also similar. Thus, wetting seems to be the dominant factor in gallium experiments, which explains why the indirect-contact measurement through acrylic produces stronger echoes than the direct-contact measurement. We will consider the effects and mechanisms of wetting in greater detail below.

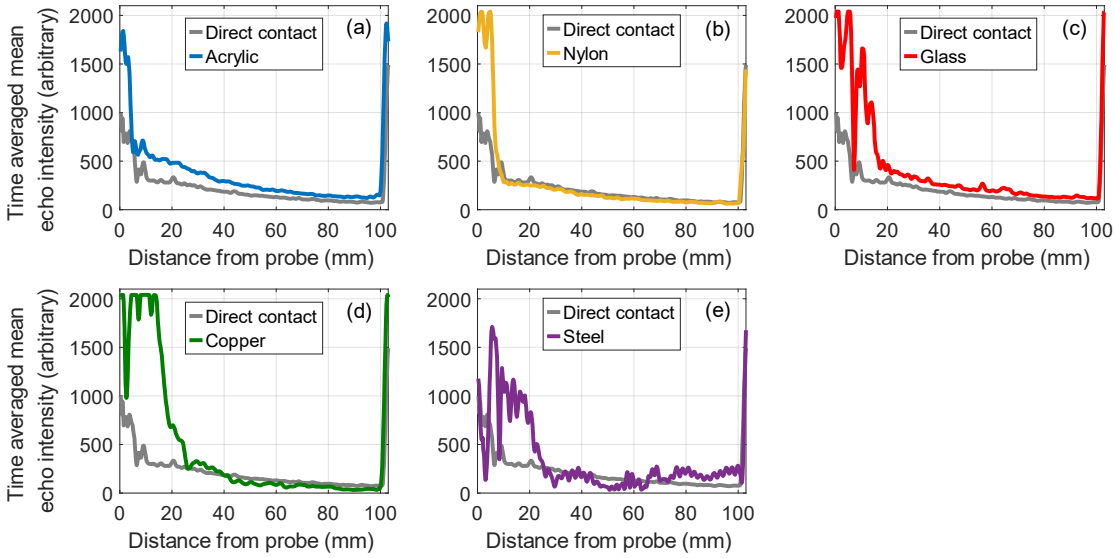

Figure 3.8 Ultrasound echo intensity measurements in liquid gallium with different test plate materials. Strong echoes are evident near the transducer surface (0 mm) and at the vessel back wall (near 100 mm). The echo intensity of direct-contact measurement is shown for reference. Results suggest that acrylic has a better performance in terms of sound transmission into liquid gallium than other vessel materials, even better than the direct-contact measurement.

Figure 3.8(d)-(e) shows that the metal test plates, especially steel, produced many undesirable reverberations when gallium is the test fluid. All test plates have introduced strong front-wall noises near the transducer surface (0 mm) due to the large acoustic impedance mismatch to gallium. Under the same TGC settings, the front-wall noises produced by metal test plates were stronger and covered more measurement regions than those of plastic test plates. For the borosilicate glass test plate, although strong front-wall noises appear in the echo profile, the bulk echo intensity is better than that of direct-contact measurement. This may be explained by the high predicted transmission coefficient and relatively small contact angle between glass and liquid gallium.

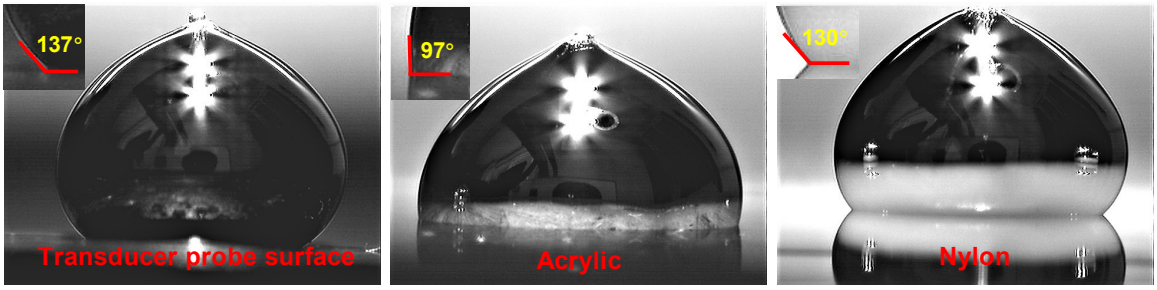

Figure 3.9 Contact angle measurement results for liquid gallium on different substrates. Acrylic shows a smaller contact angle value and thus a better wetting to liquid gallium.

Comparing the echo intensity measurements in water and gallium, as shown in figure 3.3 and figure 3.8, it is clear that the reverberation noises are much stronger in liquid gallium. We attribute this difference to the much higher surface tension of liquid gallium. Comparing the contact angles in Table 3.1 and Table 3.2, for all test plates, wetting with water is easier than wetting with liquid gallium. It is reasonable to assume that some of the reverberations in the gallium cases resulted from repeated reflections of ultrasound waves at the plate-gallium interface due to their poor wetting. Our measurements suggest that wetting plays a more important role in liquid metal cases. As discussed above, the oxide layer could

reduce the surface tension of liquid gallium and thus promote wetting. However, a thicker oxide layer would intensify the reverberation or even degrade the ultrasound signal. The effect of the gallium oxide layer will be further discussed in Chapter 4.

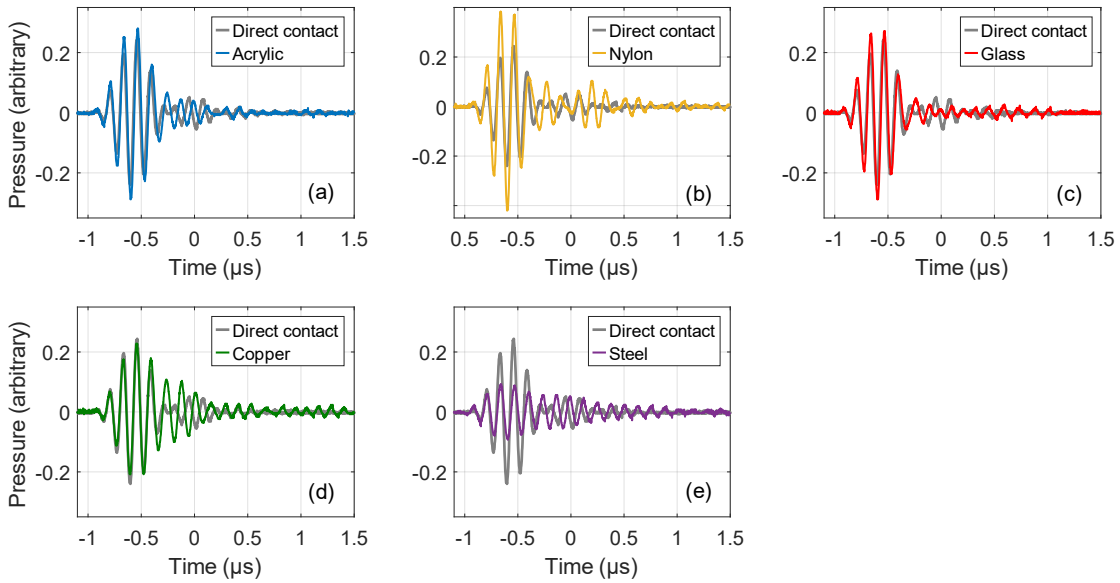

Figure 3.10 Sound pressure measurements in liquid gallium through different test plates, measured by the transducer-2 located at the container's back wall. Each curve describes a transient pressure waveform in one ultrasound pulse duration. More reverberation noises appeared within the waveforms of the metal test plates.

Figure 3.10 shows the sound pressure waveforms measured by transducer-2. Note that even without the influence of wetting, the ultrasound transmission from the transducer to gallium is not 100% in direct-contact measurement, because of their acoustic impedance mismatch. Since nylon causes little attenuation via acoustic mismatch (Equation 3.1 predicts 95% transmission), its peak-to-peak pressure measured by transducer-2 is the highest, as shown in figure 3.10 (b). For copper and steel test plates, figure 3.10(d)-(e) shows strong reverberations appearing in the measured sound pressure waveforms (at

times greater than 2 ms). In addition, figure 3.10(e) clearly shows that the sound pressure amplitude was weakened by the steel test plate.

Figure 3.11 shows the measured flow velocity profiles in liquid gallium with different test plates. All measured flow structures are almost the same as in direct-contact measurement. Again, the normalized root-mean-square velocity mismatch M_{nrmsv} was calculated for each test plate, and the results are listed in Table 3.4. The calculated M_{nrmsv} values are small and close to each other, indicating that all test plates have the ability to basically describe the velocity structure. The acrylic test plate gives the smallest M_{nrmsv} number, consistent with the echo intensity measurement result. The steel plate not only had a high M_{nrmsv}, but also caused such strong reverberation noises that the flow velocity could not be measured within 25 mm from the transducer surface. Comparing Table 3.2 and Table 3.4, we found that ranking the test plates in order of increasing contact angle (acrylic, glass, steel, Cu, nylon) produces a list that closely matches the ranking of test plates in order of increasing velocity mismatch (acrylic, glass, Cu, nylon, steel), whereas ranking in order of decreasing transmission coefficient (nylon, glass, acrylic, Cu, steel) does not match as closely. That is, for gallium experiments, contact angle predicts the fidelity of velocity measurements better than the transmission coefficient does.

Considering the echo intensity and flow velocity measurement results, as well as the machinability of the material itself, we would suggest using acrylic as the vessel material for ultrasound indirect-contact measurements in liquid gallium. Borosilicate glass is a good choice for high-temperature applications. If the purpose is only to detect large interfaces or measure simple flows, stainless steel might also be an option. However, copper is not recommended, since slow corrosion of copper by gallium has been observed in our

experiments and prior works [99].

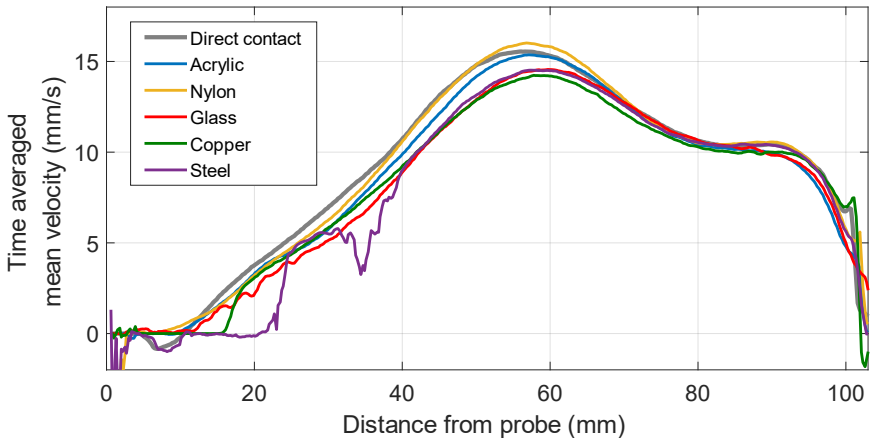

Figure 3.11 Ultrasound velocity measurements in liquid gallium with different test plates. The velocity profiles were obtained by time-averaging over 1000 transient profiles. The flow structure produced in this experiment could be described by the direct-contact measurement curve. All selected materials allowed ultrasound velocity measurements in gallium, and the measured mean flow structures are close to the reference curve.

Table 3.4 Normalized root-mean-square velocity mismatch for each test plate in liquid gallium

Test plate material	Normalized root-mean-square velocity mismatch $\boldsymbol{M_{nrmsv}}$
Acrylic	0.1825
Nylon	0.2901
Glass	0.2427
Copper	0.2485
Steel	0.4064

To study the effect of wall thickness on ultrasound transmission, four acrylic plates with different thicknesses were used for ultrasound measurements. The measured echo

intensities are plotted in figure 3.12 as a function of distance from the transducer. The thickness of each acrylic plate and the calculated intensity transmission coefficients are listed in the caption. Acrylic always shows good acoustic transmission into liquid gallium, even when thick. However, thicker plates caused more noises near the transducer surface. As with measurements in water, Equation 3.1 accurately predicts the relative transmission strength for plates made of the same material; but for much thicker plates, the energy dissipation inside the plate would play a role and should be considered. Note that some previous studies have used simplified ultrasound transmission models in which only two layers, the vessel wall and test fluid, are considered so that the acoustic impedance mismatch becomes the only factor determining the transmission rate. Our results demonstrated that the thickness of the wall affects the ultrasound transmission and thus should be considered.

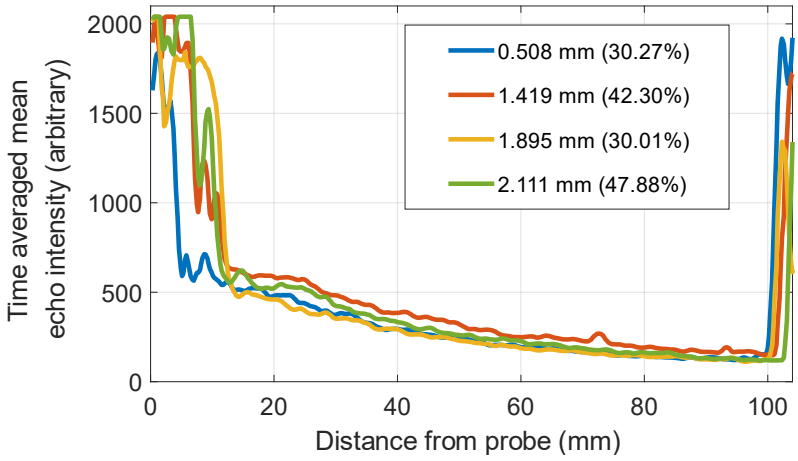

Figure 3.12 Ultrasound echo intensity measurements in liquid gallium through acrylic test plates with varying thickness. The thickness of each acrylic plate and the calculated intensity transmission coefficients are listed in the caption. The calculated transmission coefficients can predict the relative transmission strength for plates made of the same material but with different thicknesses.

3.3.3 The effect of wetting

The results of water and gallium experiments suggest that a large theoretical transmission coefficient cannot guarantee good ultrasound measurement quality. Wetting, which affects the acoustic coupling, is a key factor in indirect-contact ultrasound measurements. We further explored the effect of wetting by conducting indirect-contact ultrasound measurements in water and gallium through two steel plates with different surface treatments.

Both steel plates were cut from the same sheet, so they have the same acoustic impedances. One steel plate (figure 3.13 right) was roughened by grinding with 12-micron alumina suspensions so that its surface was not as smooth as the original one (figure 3.13 left). The surface roughness of these two steel plates was measured by white-light interferometric microscopy (Zygo Corporation, U.S.A.). As shown in figure 3.14, the measured surface roughness value (root-mean-square) for the smooth steel is 0.091 μm, and for the roughened steel is 1.120 μm.

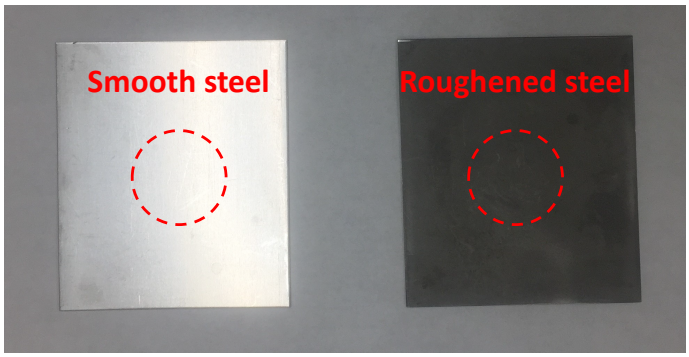

Figure 3.13 Test plates made of steel with a smooth surface (left) and a roughened surface (right). Circles mark the regions where contact angles were measured and ultrasound transducers made contact.

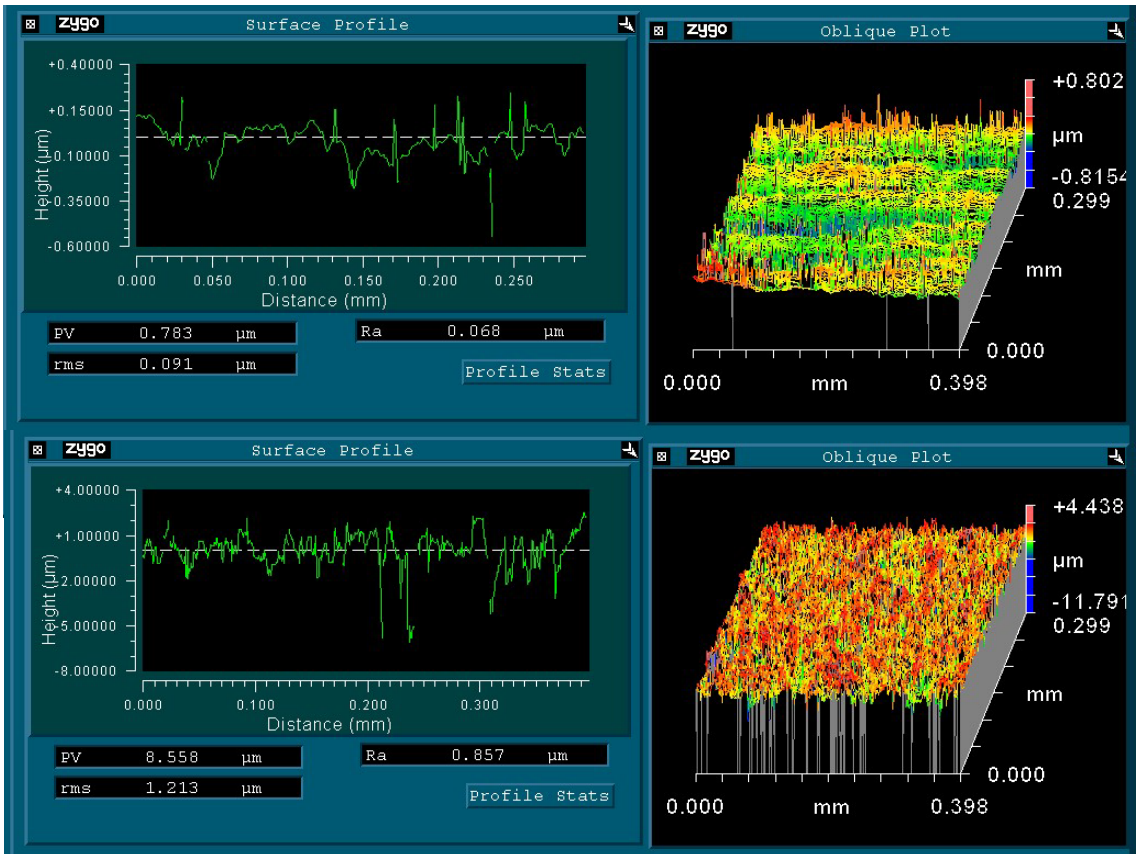

Figure 3.14 Surface roughness measurements for the smooth steel plate (top) and the roughened surface (bottom).

Again, we measured the contact angle to quantify wetting. Figure 3.15 shows the measured contact angles between water and the smooth steel plate and roughened steel plate. The smaller contact angle of roughened steel indicates better wetting with water and therefore predicts better acoustic coupling. Figures 3.16 shows the ultrasound measurement results. From the echo measurements, both steel plates allowed the ultrasound to detect the back-wall signals; however, there are fewer artificial noises produced by the roughened steel than the smooth steel. The two steel plates yield similar velocity measurements, as shown in figure 3.16 (c) and (d).

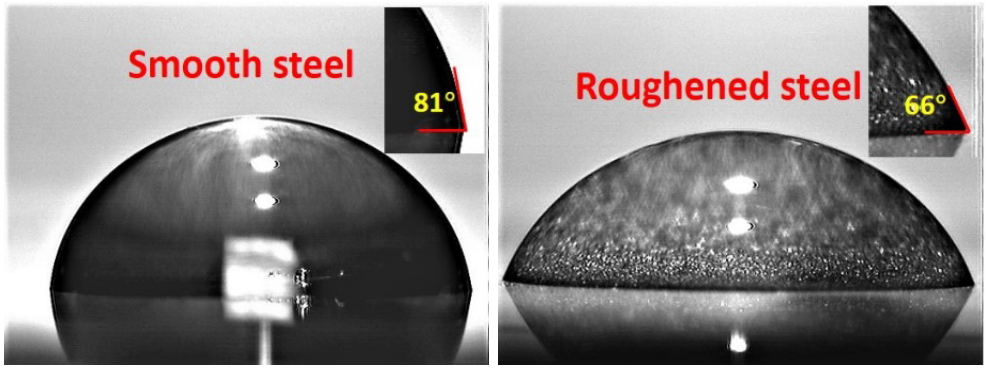

Figure 3.15 Contact angle measurements of water on smooth and roughened steel plates.

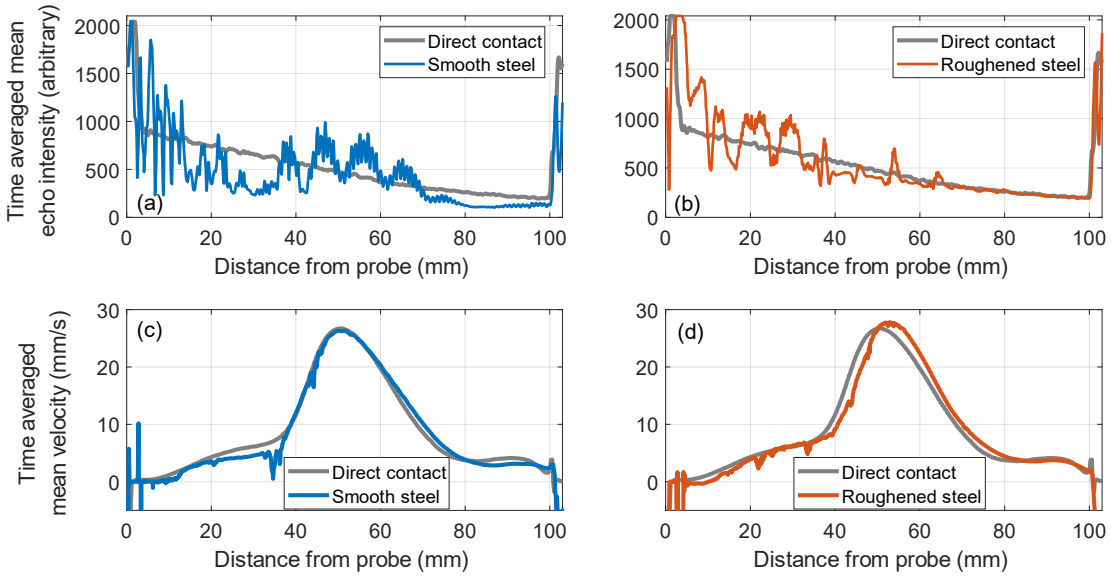

Figure 3.16 Indirect-contact ultrasound measurements in water through smooth and roughened steel plates. (a) and (b) show the measured echo intensity profiles; (c) and (d) show the measured velocity profiles. Gray curves are obtained from the direct-contact measurement for reference.

Figure 3.17 shows the contact angle measurements between liquid gallium and the smooth and roughened steel plates. For gallium, the difference in contact angles between the smooth and roughened steel is much larger than that with water. The contact angle between gallium and the smooth steel is 121°, small enough that the gallium droplet

spreads across the surface somewhat. For the roughened steel, however, the contact angle is so large that the gallium hardly wets the surface at all. During the experiment, we observed that the gallium droplet could roll back and forth on the roughened steel plate without leaving any trace, which implies minimal interaction between gallium and steel molecules. Thus, we would expect better acoustic coupling between gallium and smooth steel than roughened steel. That expectation is confirmed by ultrasound measurements shown in figure 3.18. For the roughened steel plate, little useful information but only noises are contained in the echo intensity profile, even the back-wall signal could not be detected. Consequently, no real velocity was measured, and the ultrasound measurement failed.

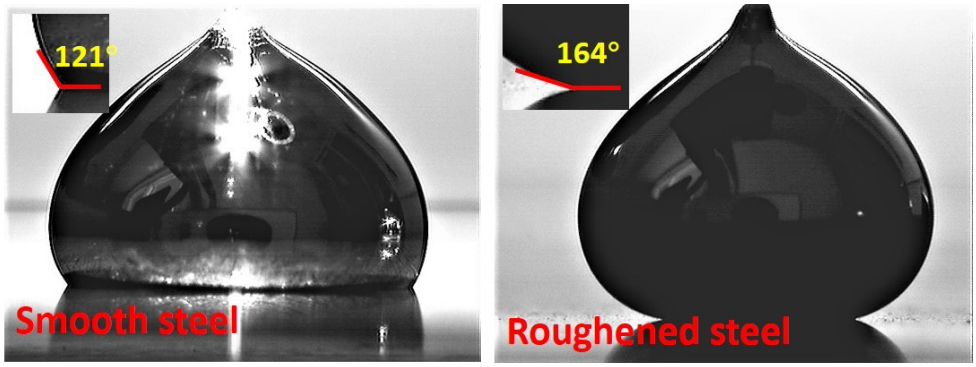

Figure 3.17 Contact angle measurements of liquid gallium on smooth and roughened steel plates.

When we keep the plate's material and thickness unchanged, variations in echo and velocity measurements can be predicted from contact angles. However, contact angles in water and gallium follow opposite trends: roughened steel wets water better, but smooth steel wets gallium better. We explain that fact by considering surface microstructure. Since water and steel have a contact angle less than 90°, it is energetically favorable for water molecules to interact with the steel surface instead of each other. Water droplets on steel are likely in a Wenzel state [95], in which roughness troughs are filled with water. In this

scenario, grinding the steel creates roughness troughs and makes water wetting stronger. However, since liquid gallium and steel have a contact angle greater than 90°, it is energetically favorable for water molecules to interact with each other instead of the steel surface. Gallium droplets on steel are likely in a Cassie-Baxter state [95], in which the droplets rest against local roughness peaks and air gaps remain in roughness troughs. In this case, a smooth surface with less roughness troughs enhances contact. Moreover, because the acoustic impedance mismatch between air and gallium is large, eliminating air gaps could improve ultrasound signal quality substantially.

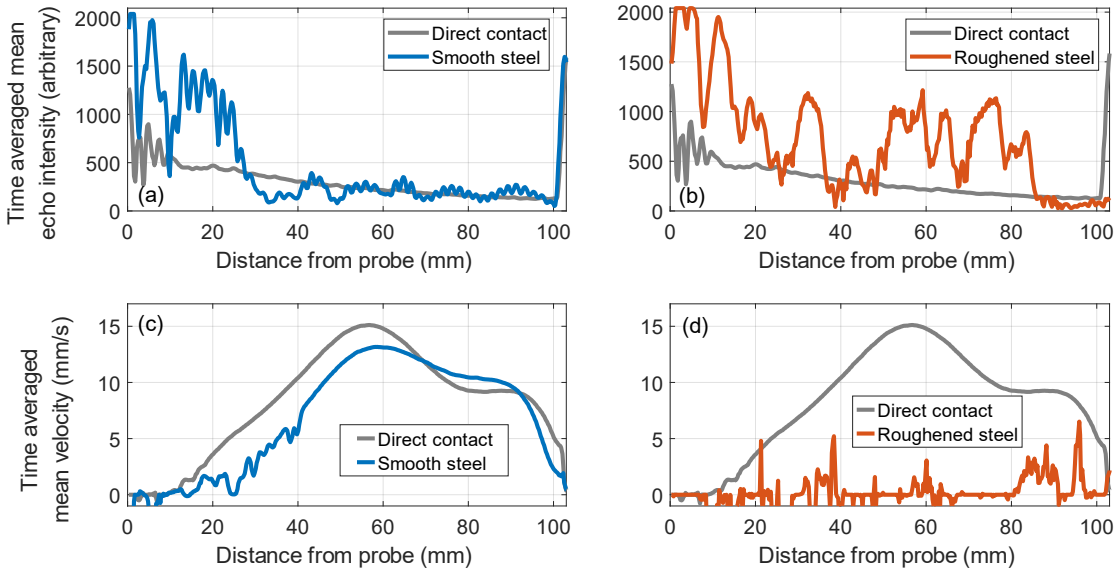

Figure 3.18 Indirect-contact ultrasound measurements in liquid gallium through smooth and roughened steel plates. (a) and (b) show the measured echo intensity profiles; (c) and (d) show the measured velocity profiles. Gray curves are obtained from the direct-contact measurement for reference. Ultrasound measurement in gallium was not feasible through the roughened steel plate.

To test our above analysis, we tried to eliminate air gaps between gallium and the roughened steel plate by wetting the roughened steel with a layer of water. Figure 3.19

shows the contact angle and ultrasound measurements in gallium with the wetted steel plate. Because the gaps left between gallium droplet and roughened steel were filled by water, the contact angle between liquid gallium and steel was reduced to 115°, much smaller than before. In the echo intensity profile, although there are still many reverberation noises present in the bulk region, the back-wall signal could be detected, which means that the ultrasound wave could be transmitted into the gallium successfully. In the measured velocity profile, the basic flow structure could also be roughly described. Therefore, filling the gap caused by poor wetting with another liquid seems to be a good strategy to improve the quality of ultrasound measurements. However, we are still not clear whether there is a thin layer of water existing as an intermediate layer between the liquid gallium and steel surface, or the water only exists in the gaps. It is also possible that liquid gallium reacts with the water and forms a gallium oxide layer, which changes the wettability of gallium.

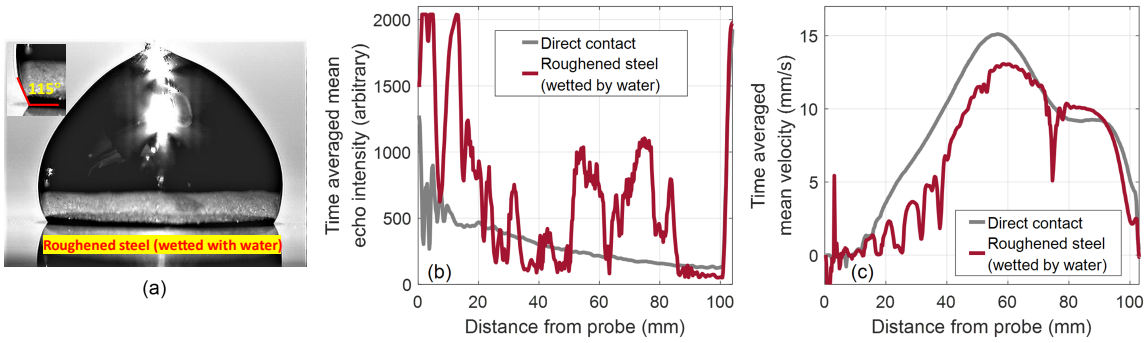

Figure 3.19 Contact angle measurement and indirect-contact ultrasound measurement in gallium for the water-wetted roughened steel plate. (a) the contact angle between liquid gallium and wetted steel plate; (b) echo intensity profiles; (c) flow velocity profiles. Gray curves are obtained from the direct-contact measurement and used as reference. The roughened steel plate could enable indirect-contact ultrasound measurement in gallium after wetting by water.

The above experiments emphasize that the wetting must be considered when performing indirect-contact ultrasound measurements, especially when liquid metal is the test fluid. The contact angle between the vessel material and test fluid could be used to predict and evaluate their wetting conditions and thus the ultrasound measurement performance.

3.4 Summary of chapter

In this chapter, we systematically studied the effect of the vessel material on ultrasound signal quality when conducting indirect-contact ultrasound measurements in water or liquid gallium. We used test plates made of various materials to simulate the vessel wall. By comparing the indirect-contact measurement results with direct-contact measurement, we demonstrated that the type of material and the thickness of the test plate affect the measured echo intensity and flow velocity profiles, especially at the region close to the transducer surface. In water, the ABS test plate showed the best performance that the measured echo intensity and flow velocity are close to the direct-contact measurement. In gallium, acrylic is a good choice as the measured signal strength is even better than the direct-contact measurement. In both water and gallium, plastic test plates always have a better performance than metal test plates, the latter often cause strong front-wall noises and reverberations. We want to emphasize that those noises would cause negative effects not only for velocity measurements, but for other sorts of ultrasound measurements. When applying ultrasound to detect bubbles or track solidification fronts, front-wall noises and reverberations are also undesirable as they might mask the real echo signals.

Through our study, we also found that the calculated intensity transmission coefficients alone cannot predict the measured sound transmission through a wall precisely. The

intensity transmission coefficient is a theoretical value applicable to liquid layers with ideal acoustic coupling. In real ultrasound measurements, especially when the test fluid is a liquid metal, the wetting conditions between the vessel wall and test fluid determine their physical acoustic coupling — the continuity of the acoustic path. The contact angle between the vessel material and test fluid could be used to predict and evaluate their wetting conditions and thus the ultrasound measurement performance. According to our experimental results, indirect-contact ultrasound measurements might fail if the contact angle between the vessel wall and test fluid is greater than 150°. When performing indirect-contact ultrasound measurements in liquid metals other than gallium, the contact angle could be a good index for selecting suitable vessel materials. In addition, surface treatments that change the surface roughness directly affect the wetting and ultrasound measurements. We hypothesize that for combinations of test fluid and vessel material with contact angles less than 90°, increasing roughness would improve the ultrasound signals; and for combinations with contact angles greater than 90°, decreasing roughness would improve the signals. This hypothesis is verified in our liquid metal battery experiments, as shown in Appendix A.

Other than wetting, the thickness of the vessel wall not only affects the sound intensity transmission coefficients, but is also proportional to the acoustic energy dissipation within the vessel wall. Since the vessel wall is solid, its density and stiffness affect acoustic energy dissipation and reverberation noises as well. When choosing the vessel material for a certain type of fluid, all those factors should be taken into account in order to achieve the best ultrasound transmission performance.

3.5 Acknowledgments

The thesis author was the primary person conducting all experiments and data analysis described in this chapter. The MATLAB script for extracting and demodulating the UDV data from binary files was written by Douglas Kelley. Thanks to Prof. Anthamatten's group of the University of Rochester for the use of their goniometer. Thanks to James Alkins for help designing and machining some of the vessels and containers. Thanks to Mike Pomerantz for help grinding the steel test plates and measuring their surface roughness.

—— Chapter 4 ——

Ultrasound Signal Deterioration and Ultrasound-induced Cavitation

The UDV signal deterioration with time is an undesirable phenomenon, which often occurs during UDV measurements in liquid metals. In this chapter, we experimentally study the UDV signal deterioration behavior in liquid gallium. Two distinct mechanisms cause the signal deterioration: the loss of scattering particles from the bulk and the degradation of wetting at the transducer surface. We further investigate the ultrasound-induced cavitation in gallium, a possible underlying mechanism causing the degradation of wetting. In this chapter, some failed experiments are also discussed, which still provide interesting results. The author believes those attempts were meaningful, which have brought us insights and ideas for subsequent research.

Part of the results listed in this chapter have been published in [80, 81].

4.1 Bulk echo decay and UDV signal deterioration

When applying the UDV to liquid metal flows, we expect to obtain long-time continuous flow measurements with high accuracy. However, in practical measurements, we have always observed a deterioration of ultrasound signal quality over time in liquid gallium. Figure 4.1 shows a raw spatial-temporal echo profile measured in liquid gallium. The z-axis and color indicate the echo intensities measured at different times and locations. The

position of the UDV transducer surface corresponds to the 0 mm distance on the x-axis. The strong echo peaks measured at the 110 mm distance are caused by the reflection of ultrasound waves at the container's back wall. As discussed in Chapter 2, the echoes measured in the bulk part of gallium are from the scattering of ultrasound waves by gallium oxide inclusions. A decrease in bulk echo intensity with respect to both time and distance could be observed in the echo profile.

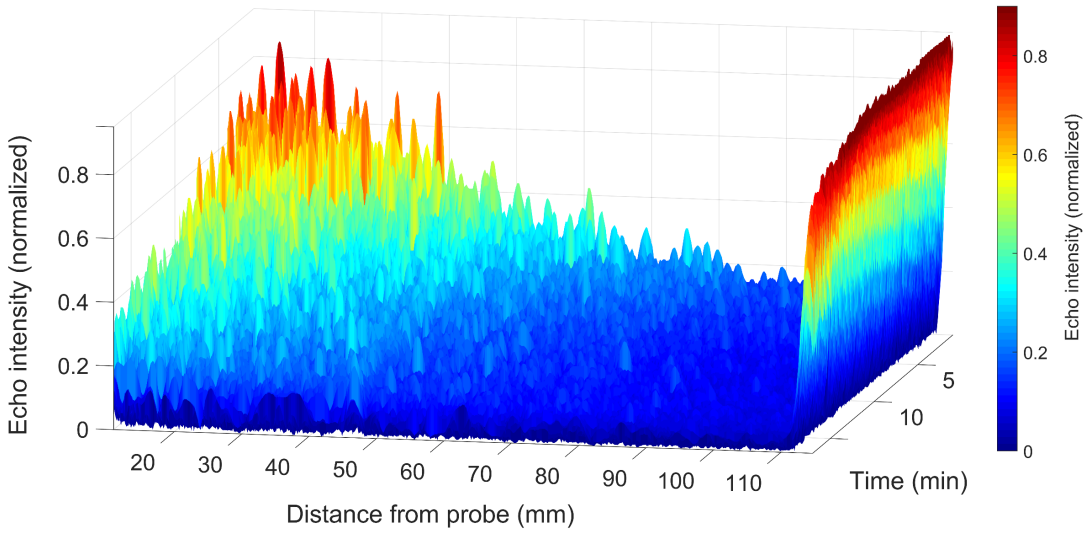

Figure 4.1 UDV spatial-temporal echo intensity profile measured in liquid gallium. The strong echoes at 110 mm are caused by the reflection of ultrasound waves at the container's back wall. Bulk echoes are from the scattering of ultrasound waves by gallium oxide inclusions.

By time-averaging the echo intensities and plotting them as a function of distance, as shown in figure 4.2 (a), we see that the echo intensities decrease monotonically with distance. This phenomenon is mainly caused by the attenuation of ultrasound waves when propagating in a medium. The ultrasound attenuation is inevitable, but the measurements can be compensated to some extent by the TGC control, as discussed in Appendix B. By spatially averaging the bulk echo intensities (20-100 mm) and plotting them as a function

of time, as shown in figure 4.2 (b), we see that the echo intensities also decay over time. This decay of echo intensity over time is absolutely undesirable. Since the velocity measured by the UDV method is derived from information contained in successive echoes, the echo intensity directly determines the quality of velocity measurements. When the echo intensity at a certain measurement position is too weak to be discerned from the surrounding noises, null or spurious velocities appear at that position. When bulk echoes across the whole measurement region decay with time, both the accuracy and reliability of the velocity measurements are reduced.

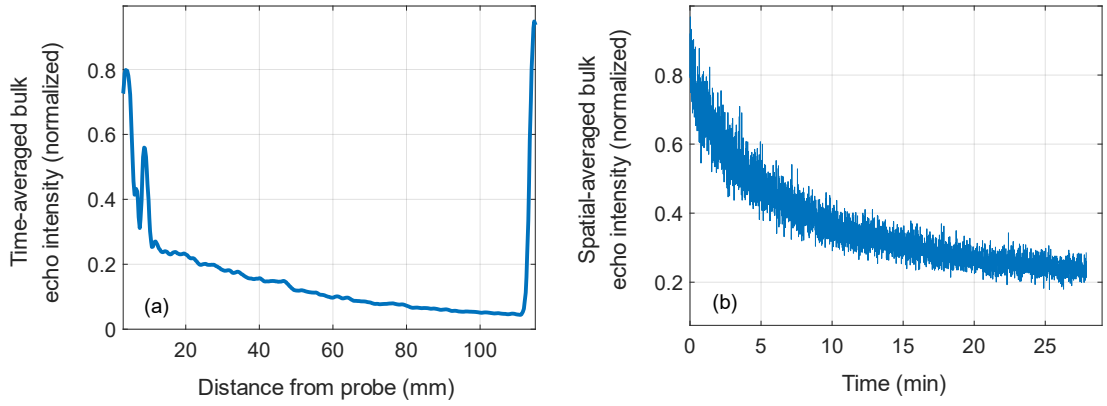

Figure 4.2 (a) Time-averaged bulk echo intensity vs. distance from probe. (b) Spatial-averaged bulk echo intensity vs. time. Bulk echo intensities decrease with respect to both time and distance.

Figure 4.3 clearly shows how the UDV measurement fails after a long time of measurement. Figure 4.3 (a) presents a raw spatial-temporal velocity profile measured in liquid gallium, in which the colors indicate the flow direction: red colors signify flow moving away from the transducer, blue colors signify flow moving towards the transducer, and white signifies zero velocity or null measurement. In that experiment, a steady flow was induced in the liquid gallium. The velocity structures measured in the first 100 minutes appear to be consistent. However, null or spurious velocity measurements started to appear after 150 minutes, manifesting by the increase of white measurement spots. Figure

4.3 (b) plots the corresponding mean velocity profiles obtained by averaging one minute of transient profiles at certain times. At 1 minute, a smooth velocity curve was measured which described the flow structure accurately. At 100 minutes, the same flow structure could still be recognized, but small fluctuations had appeared at distance 50-100 mm from the transducer. As shown in figure 4.1, those regions were exactly where the bulk echoes decay to near zero first. At 150 minutes, the measured velocity magnitude weakened substantially; too many noises appeared, and the measured flow profile could not depict the real flow structure anymore. At 200 minutes, almost no meaningful velocity could be measured.

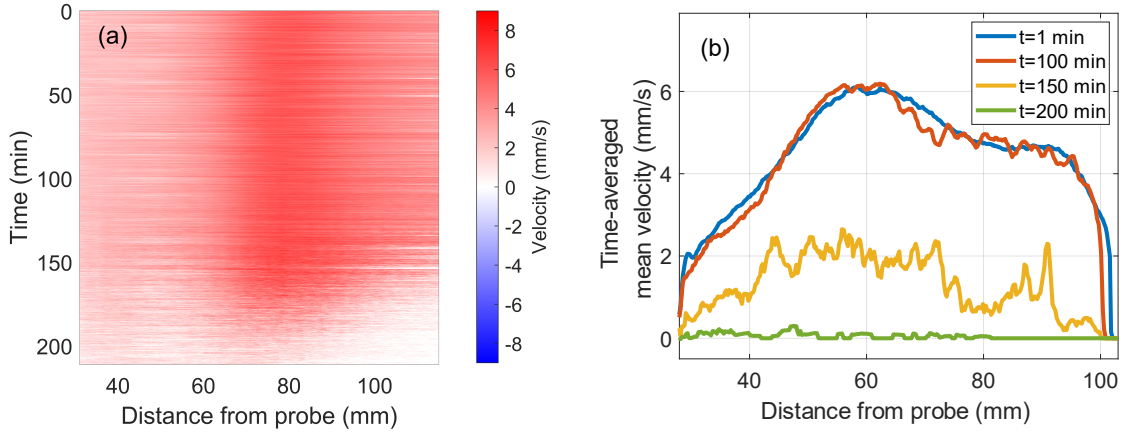

Figure 4.3 UDV velocity measurement failure. (a) Spatial-temporal velocity profile measured in liquid gallium. (b) Corresponding velocity profiles at four different time points. UDV velocity measurement failed after a long time of measurement.

Figures 4.1-4.3 demonstrate how the decay of bulk echoes causes the deterioration and eventual failure of the UDV velocity measurement. Since the deterioration occurs for both bulk echo and velocity, we refer to it as the deterioration of UDV signals. The deterioration of UDV signals has been reported in previous studies. Brito et al. observed that, when applying UDV measurements in gallium, the measured velocity decreased and eventually

was lost completely, starting from the far wall region [26]. Cramer et al. reported that null samples appeared in the velocity profile due to insufficient correlations of the echo signals, and the UDV signals deteriorated with increasing measuring time in InGaSn [29]. Losev et al. pointed out that long-duration UDV measurements became unreliable as the UDV signals were overwhelmed by background noise.

Understanding the mechanisms of bulk echo decay is the key to solving the UDV signal deterioration. The most obvious cause of bulk echo decay in gallium is the loss of scattering particles from the bulk [26, 29, 45]. Due to the density difference between liquid gallium and gallium oxides or any artificially added tracer particles, those particles eventually separate from the gallium bulk, reducing the population of echoing sources. However, prior studies pointed out that the mechanism of bulk echo decay is not that simple. Some studies have discussed decay caused by oxide particles gathering on the vessel walls that attenuate and hinder the ultrasound measurement [26, 67]. To extend measuring time, Brito et al. coated a copper vessel's inner wall with a cataphoretic layer to prevent oxides from sticking to the walls [26]. Cramer et al. claimed that the separating of microbubbles from the fluid, agglomeration of oxides, and adhesion of oxides on the container walls together affected the UDV signal quality [29]. Dadzis et al. conjectured that excessive oxidation of gallium is the cause; they found flushing with argon and periodically removing the oxide layer formed on the gallium surface enabled long UDV measurements [66]. Similarly, Perez and Kelley reported that substantial oxidation of molten PbBi degraded ultrasound signals [44]. Losev et al. found that the change of temperature in gallium eutectic also caused a negative influence on UDV signals; they suggested preheating and maintaining a constant temperature of the liquid metal to improve the stability of UDV measurement [45].

Despite some contradictions, most of the previous views emphasized the critical role of oxides and interfacial conditions. Unfortunately, although empirical advice was proposed by prior studies for prolonging the UDV measurement time, the deterioration cannot be avoided. From Chapter 2 and Chapter 3, we learned the role of gallium oxide and the importance of wetting in UDV measurements of gallium. We believe this knowledge can help us better understand the mechanisms of UDV signal deterioration. In the following section, we experimentally investigated the time evolution of UDV signals in gallium. The underlying mechanisms causing UDV signal deterioration are more complex than we expected and are discussed throughout this chapter.

4.2 The mechanisms of UDV signal deterioration

4.2.1 UDV signal deterioration in direct-contact measurement

Figure 4.4 shows the experimental apparatus for investigating ultrasound signal deterioration in liquid gallium. A rectangular vessel made of Delrin was used to contain the liquid gallium. A rotating flow was induced in the liquid gallium by a rotating magnet of a stirring plate beneath the vessel. The induced flow had a simple vortex structure, which was easy to reproduce and easy for evaluating the accuracy of velocity measurement. To ensure the repeatability of the flow, the position of the vessel relative to the stirring plate was fixed and the stirring speed remained constant.

A UDV transducer with 4 MHz working frequency was connected to the DOP3010 Velocimeter and operated in emit/receive mode for data acquisition. The measuring line was parallel to the centerline of the container with a 5 mm offset; this configuration ensured

that the flow to be measured was always in the same direction. In all measurements, a time gate compensation (TGC) with uniform magnitude was applied in order to compensate for the ultrasound attenuation.

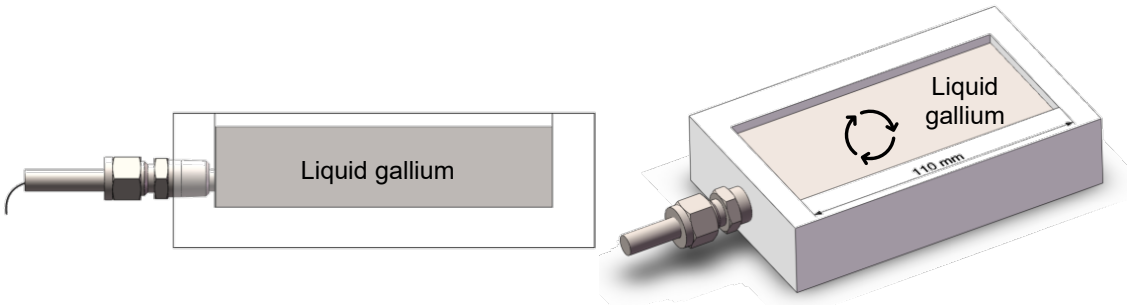

Figure 4.4 Experimental apparatus for investigating the ultrasound signal deterioration in liquid gallium. UDV measurements were conducted in a direct-contact way. Left: side view. Right: top view. A rotating flow was induced in the liquid gallium as shown by the arrows.

To quantitatively evaluate the accuracy of UDV velocity measurement, we define the velocity deviation:

$$Velocity\ deviation = \frac{1}{n} \times \sum_{i=1}^{n} \sqrt{\left(\frac{V_i(t) - V(mean)}{V(mean)}\right)^2} \tag{4.1}$$

where $V_i(t)$ is the transient velocity profile at time t, $V(mean)$ is the mean profile averaged over the first 300 velocity profiles measured in the first 3 minutes. The summation is taken over n measurement locations (in the region 20-100 mm from the transducer). Since the induced rotating flow is laminar, and the UDV measurement usually maintains good accuracy during the first 5-10 minutes, we select the mean profile of the first 3 minutes as the reference. When the velocity deviation value is close to 0, the UDV can produce accurate flow measurements, but when the velocity deviation value approaches 1, the UDV fails to measure the real flow structures. Empirically, when the velocity deviation

value is larger than 0.5, we assume the UDV cannot capture any meaningful flow structure anymore.

We conducted a group of consecutive tests in liquid gallium to characterize the ultrasound signal decay behaviors. Figure 4.5 shows the measurement results, where the top row depicts the variation of the spatially averaged bulk echo intensities with time, and the bottom row displays the temporal evolution of the corresponding velocity deviation calculated using Equation 4.1. In test 1, the vessel was filled with liquid gallium, and UDV measurement was started after one minute (in order to eliminate the flow induced by the pouring process). The measured mean bulk echo intensity exhibited a monotonic, non-linear decay over time. The velocity deviation increased as the echo intensity decayed, indicating that the UDV signals deteriorated and the accuracy of UDV velocity measurement became worse. Assuming the velocity measurement is effective only when velocity deviation is less than 0.5, the effective velocity measurement in test 1 lasted for two hours.

For the cause of echo decay, the first guess coming to mind is the loss of scattering particles from the ultrasound beam path: the density difference between gallium oxide and liquid gallium causes the gallium oxides to move to the top, as discussed in Chapter 2, and thus a decay of bulk echo intensity. If this is the sole mechanism causing the echo decay, then bringing the oxides back should restore the bulk echo intensity. Hence, in test 2, we manually stirred the liquid gallium in the vessel to mix oxide inclusions back into the bulk. However, compared to test 1, stirring the gallium restored less than 1/3 of the initial echo intensity, and the echo intensity then decayed quickly. The velocity deviation then increased so quickly that effective velocity measurement only lasted for 40 minutes. In test 3, we stirred the gallium again, but the subsequent echo and velocity measurements

deteriorated even faster, and the effective measurement time was less than 15 minutes. Tests 1-3 suggest that the loss of scattering particles from the ultrasound beam path is not the only reason causing UDV signal deterioration.

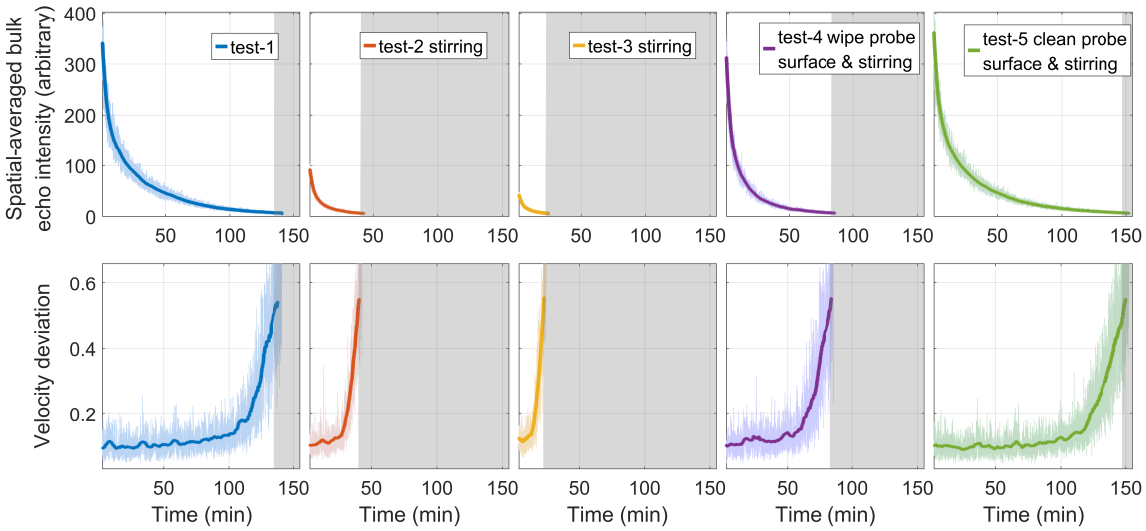

Figure 4.5 Temporal evolution of UDV signals in direct-contact measurement: (top) bulk echo intensity and (bottom) velocity deviation. The bulk echo intensities were obtained by spatially averaging over the region 20-100 mm from the transducer. Regions with velocity deviation greater than 0.5 were shaded. For each test, UDV signals deteriorated with time, manifesting by the decay of bulk echo intensity and increase of velocity deviation. Stirring (tests 2 and 3) alone only restored the UDV signals slightly. Wiping or cleaning the transducer surface (tests 4 and 5) improved signals substantially.

We hypothesized that the deterioration of UDV signals might be also related to changes occurring on the UDV transducer surface. Thus, in test 4, we wiped the transducer surface with a cotton swab in-situ and then manually stirred the gallium. This time, the measured echo intensity was restored a lot, and the effective measurement time lasted much longer than test 2 and test 3. In test 5, we poured the gallium out of the vessel, cleaned the ultrasound transducer surface, and then refilled the gallium to start the UDV measurement.

In other words, we reset the experimental conditions to be the same as test 1. As shown, the measured echo intensity, velocity deviation, and effective measurement time closely match test 1. Test 4 and test 5 verified our hypothesis that the surface processes of the transducer contribute to the UDV signal deterioration.

When pouring gallium out, we have observed a thin layer of gallium oxide covering the transducer surface as well as vessel walls. When oxide inclusions circulate in the gallium, they are thermodynamically favored to accumulate on the transducer surface as it is a heterogeneous spot. We believe the UDV signal deterioration is related to this oxide layer. As a more rigid layer, the oxide layer may degrade the UDV signal in two distinct ways. First, the oxide layer itself can act as an intermediate layer to dampen the ultrasound waves or even block the ultrasound waves when the layer gets thick enough. Second, the oxide layer can degrade the UDV signal by changing the acoustic coupling and wetting between the transducer surface and liquid gallium. The importance of wetting on ultrasound signals has already been discussed in Chapter 3. The contact angle between the transducer surface and gallium is about 130°, which means the wetting is adequate but weak. Although moderate oxidation of gallium lowers its surface tension and improves wetting, the appearance of a thick oxide layer or large oxide agglomerations on the transducer surface would weaken the wetting by contaminating the interface between the transducer and gallium. In real cases, those two mechanisms might work together to weaken the emitted ultrasound signals as well as the received echo signals. Consequently, although stirring can bring scattering particles back to the ultrasound beam path, the degradation of the wetting conditions at the transducer surface still degrades the UDV signals.

4.2.2 UDV signal deterioration in indirect-contact measurement

To eliminate the effect of the transducer/gallium interface, we performed indirect-contact UDV measurements in gallium through an acrylic plate, as shown in figure 4.6. We selected acrylic (with thickness close to a half-integer multiple of its ultrasound wavelength) because acrylic wets gallium better and transmits the strongest ultrasound signals, as demonstrated in Chapter 3. As before, a steady rotating flow was induced in the liquid gallium by a stirring plate beneath the vessel. A 4 MHz UDV transducer was used for data acquisition, which was inserted into acoustic gel until gently touching the acrylic plate. All ultrasound parameters were kept the same as the direct-contact measurements.

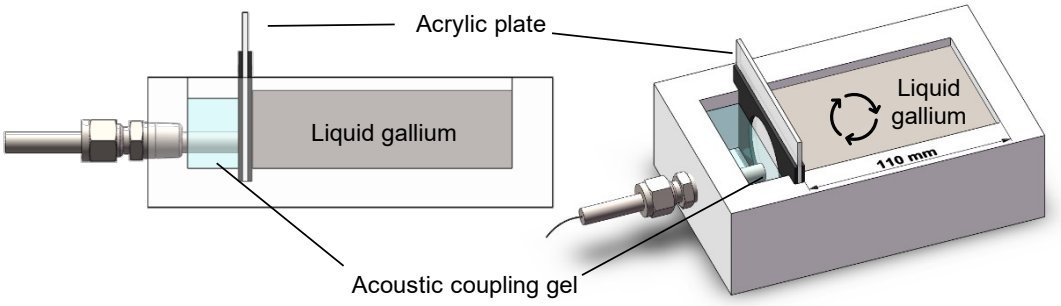

Figure 4.6 Experimental apparatus for investigating the ultrasound signal deterioration in liquid gallium. UDV measurements were conducted through an acrylic plate. Left: side view. Right: top view. A rotating flow was induced in the liquid gallium as shown by the arrows.

The same tests were conducted in gallium with the same steps. Figure 4.7 shows the measured mean bulk echo intensity and the velocity deviation. In test 1, the bulk echo intensity showed a monotonic decay as in the direct-contact case. In test 2 and test 3, unlike in the direct-contact measurements, stirring the gallium restored the initial echo intensity almost completely. Although the effective measurement times of test 2 and test 3 were shorter than test 1, they were much better than in the direct-contact cases. In test

4, wiping the acrylic surface produced a similar result as test 2 and test 3, suggesting that the surface condition of acrylic had no effect, and stirring was the essential step. In test 5, cleaning and refilling completely restored the UDV signals.

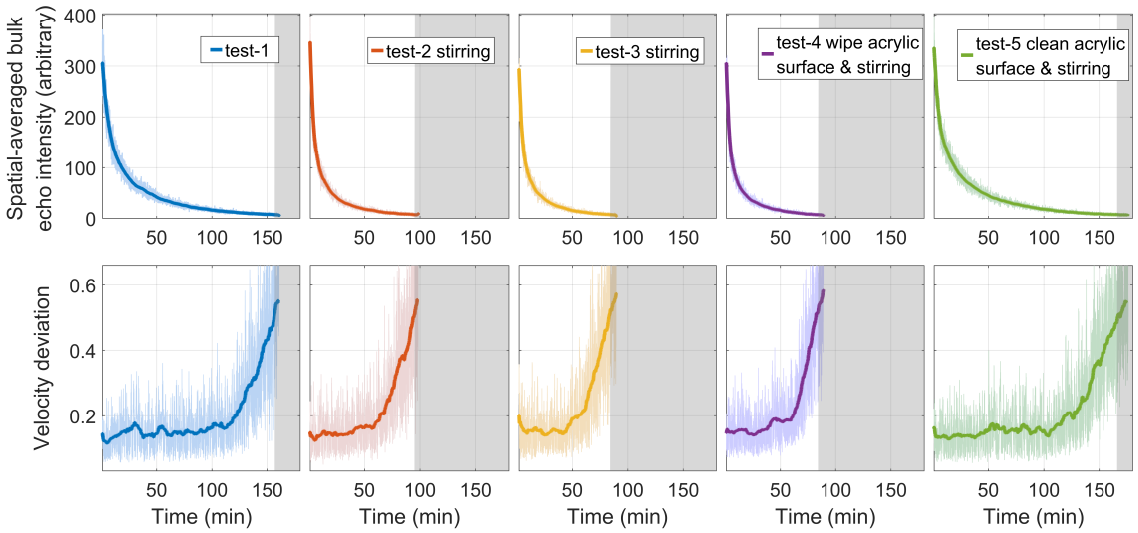

Figure 4.7 Temporal evolution of UDV signals in indirect-contact measurement: (top) bulk echo intensity and (bottom) velocity deviation. The bulk echo intensities were obtained by spatially averaging over the region 20-100 mm from the transducer. Regions with velocity deviation greater than 0.5 were shaded. With the acrylic plate in middle, stirring the gallium (tests 2 and 3) restored most of the UDV signals. Wiping the acrylic surface caused no obvious changes.

The tests from indirect-contact measurements emphasize the role of transducer surface conditions. Since the UDV transducer was not in direct contact with gallium, the wetting and acoustic coupling conditions at the transducer surface were set by the transducer/acoustic gel interface. Therefore, good wetting and acoustic coupling were maintained at the transducer surface, and the ultrasound waves could be transmitted from the transducer to the acrylic plate successfully. In addition, acrylic wets liquid gallium better than the UDV transducer surface. Although we also observed some gallium oxides sticking

to the acrylic plate, they did not affect the ultrasound signals, as wiping the acrylic surface caused no obvious change in the measured echo intensity or velocity deviation. As shown in figure 4.8, gallium oxides accumulated randomly on the acrylic surface rather than being concentrated only in the transducer contact region. In this scenario, the loss of scattering particles is the dominant factor causing the echo decay, so stirring the gallium alone can restore most of the bulk echo intensity. We speculate that stirring cannot mix oxide particles back to the bulk of gallium as effectively as refilling, so the measured bulk echo intensities and measurement last time of tests 2-4 were not as good as test 1 or test 5.

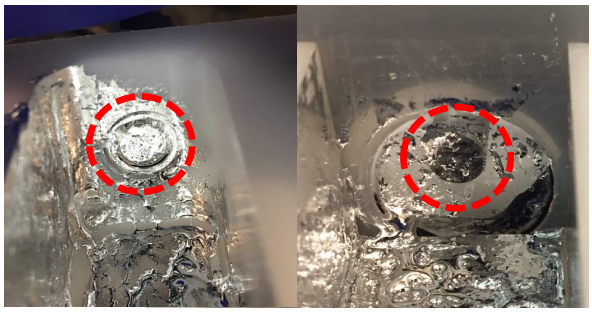

Figure 4.8 Pictures of transducer surface (left) and acrylic surface (right) after pouring gallium out. For direct-contact measurement (left), oxides and gallium residues accumulated preferentially on the transducer surface. For indirect-contact measurement (right), oxides and gallium residues were randomly distributed on the acrylic surface rather than concentrated in the transducer contact area.

Besides the bulk echo intensity, the echo intensity measured at the back wall of the vessel also demonstrates the importance of the transducer surface conditions. Figure 4.9 shows the temporal evolution of back-wall echo intensity from direct-contact and indirect-contact measurements. Theoretically, since the back-wall echo is reflected from the gallium/vessel interface, its intensity is determined solely by the acoustic impedance mismatch between the gallium and Delrin vessel and thus should remain constant. Taking into account the loss of scattering particles from the bulk, we would expect the back-wall echo intensity to

increase slightly over time as more acoustic energy can reach the back wall. However, in the direct-contact measurements, we observed the opposite: after a small increase at the beginning, the back-wall echo intensity decayed with time for each test. From test 1 to test 3, the back-wall echo intensity decreased monotonically, indicating a continuous degradation in the transducer surface condition. Wiping or cleaning the transducer surface restored the back-wall echo signals, confirming again that the surface processes are one of the main factors causing the UDV signal deterioration. For the indirect-contact measurements, on the other hand, since the transducer surface was not subject to oxide accumulation or wetting degradation, the measured back-wall echo intensities remained almost constant in each test and changed little between tests.

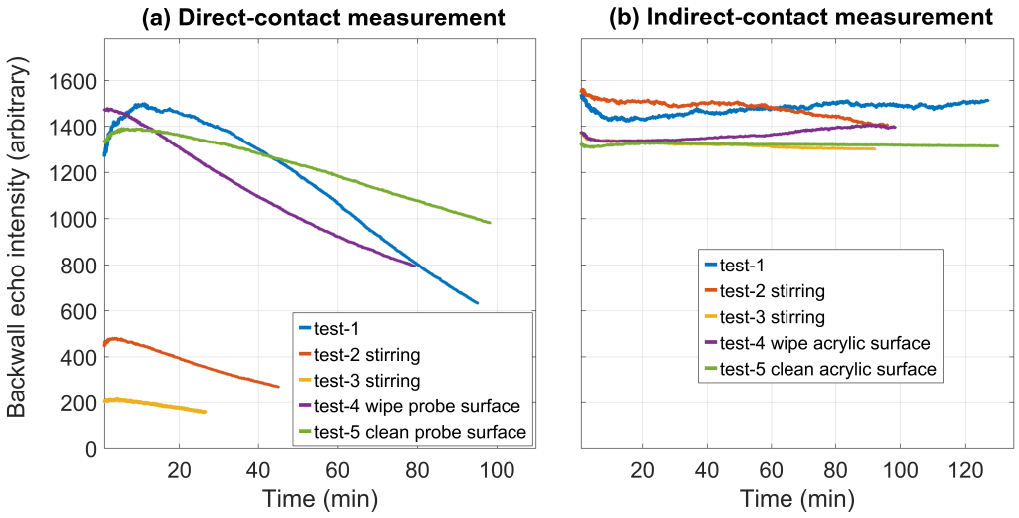

Figure 4.9 Temporal evolution of back-wall echo intensity in direct-contact and indirect-contact measurements. For the direct-contact measurements, back-wall echo intensities decreased with time during each test. Wiping or cleaning the transducer surface restored the signals. For the indirect-contact measurements, back-wall echo intensities remained almost constant in all tests.

The results of bulk echo measurements and back-wall echo measurements agreed well with each other. From those results, we summarized that the UDV signal deterioration in

gallium results from two independent mechanisms: the loss of scattering particles and the degradation of transducer surface conditions. The loss of scattering particles is due to the density difference between liquid gallium and gallium oxide, which can be mitigated by stirring or introducing vigorous flows to bring the oxides back to the bulk. The degradation of transducer surface conditions might be caused by the oxide layer at the transducer surface, which blocks ultrasound waves and/or degrades the wetting. Indirect-contact measurement through a material that wets gallium well, such as acrylic, can be a solution to eliminate the effect of surface degradation.

Since oxide accumulation at the transducer surface is the main cause of ultrasound signal deterioration, whether by blocking ultrasound waves or by degrading wetting, techniques to remove oxides or reduce the oxidation rate in liquid metals may improve UDV signal quality. Prior studies suggested that flushing with inert argon gas could help to preserve UDV signal quality in liquid metals [57, 66, 67]. Acid treatments such as adding a thin hydrochloric acid layer were also frequently used to avoid undesirable oxidation of liquid metals [26, 43, 57, 58]. Tasaka et al. set an experimental procedure: they treated the gallium with a 10% hydrochloric acid-ethanol solution, and also evacuated the vessel before UDV measurements [38]. However, it should be noted that the presence of oxides is a double-edged sword: moderate oxidation lowers the surface tension of liquid metals, whereas excessive oxides hinder ultrasound measurements. In addition, since gallium oxides are the main source of bulk echoes in gallium, excessive deoxidation of gallium would result in bulk echoes too weak to be measured, unless tracer particles were added.

4.2.3 UDV signal deterioration and ultrasound emission

How the oxides adhere and accumulate to the transducer surface is also an unknown process. It is plausible that the gallium oxides adhere and accumulate to the transducer surface naturally as they circulate inside the gallium. Interestingly, we found that the ultrasound signal deterioration caused by the surface process (oxide layer and wetting) only happens when the UDV transducer is emitting ultrasound waves.

Figure 4.10 shows the temporal evolution of bulk echo intensities and velocity deviations from three UDV tests in gallium. The UDV measurements were performed with the transducer surface in contact with liquid gallium, as shown in figure 4.4. In test 1, we filled the vessel with liquid gallium and performed UDV measurement. Continuing to test 2, we manually stirred the gallium without cleaning the transducer surface. The results of test 1 and test 2 were similar to what we observed in previous experiments: the loss of scattering particles caused the monotonic decay of bulk echoes in each test, and the degradation of surface conditions resulted in an even worse signal in test 2. In test 3, we cleaned the transducer surface and then refilled the gallium, but did not start the ultrasound measurement immediately, that is, the transducer surface was immersed in liquid gallium without ultrasound emission. After three hours, we manually stirred the gallium and then restarted the UDV measurement. Interestingly, although the idle transducer had been placed in the liquid gallium for three hours, the measured echo intensity and velocity deviation were still similar to test 1.

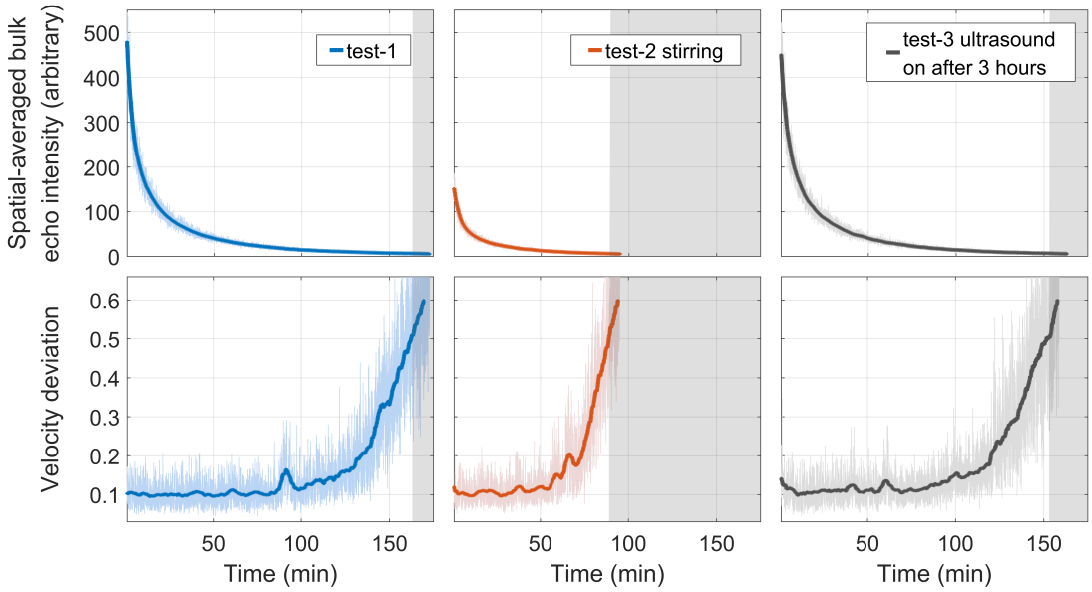

Figure 4.10 Temporal evolution of UDV signals in direct contact measurement: (top) bulk echo intensity and (bottom) velocity deviation. The bulk echo intensities were obtained by spatially averaging over the region 20-100 mm from the transducer. Regions with velocity deviation greater than 0.5 were shaded. The ultrasound signal deterioration caused by surface processes is related to the ultrasound emission activity.

Comparing test 2 and test 3, for both cases the transducer had been immersed in gallium for three hours prior to the test; the only difference is that for test 2, the ultrasound transducer remained working (i.e., test 1) during those three hours, whereas for test 3, there was no ultrasound emission in those three hours. We should also note that during the three-hour “pause” time prior to test 3, the rotating flow was still driven in liquid gallium such that the oxides were still circulating inside the gallium. If gallium oxides still adhere and accumulate to the transducer surface due to their circulation, then the oxide layer itself may not be the direct reason causing UDV signals degradation. If oxides no longer accumulate on the transducer surface, then the oxide accumulation may be related to the ultrasound emission activity. It is not an easy task to determine whether an oxide layer is

present or not: because of the lack of an in-situ imaging technique, we need to first pour the gallium out, then check the transducer surface conditions. From our experimental observation, if we ignore the effects of pouring, oxides still accumulate on the transducer surface even when there is no ultrasound emission. Therefore, the direct influence of the oxide layer itself on the UDV signals can be excluded, which means that the surface processes occurring on the transducer are more likely attributed to the degradation of the wetting conditions. The above experiment implies that the degradation of wetting is correlated to the ultrasound emission activities.

One possible mechanism related to ultrasound emission activities is ultrasound-induced cavitation. Taking gallium as an example, ultrasound-induced cavitation happens when ultrasound waves reduce the local pressure below the vapor pressure of liquid gallium, and bubbles are produced during this process. If ultrasound-induced cavitation happens on or near the transducer probe surface, due to the presence of the oxide layer on the transducer probe surface, the resulting cavitation bubbles could cause micro-gaps between the probe surface and the oxide layer. Those micro-gaps and/or micro-bubbles remaining on the probe surface would significantly degrade the wetting conditions, block ultrasound waves, and consequently deteriorate UDV signals. In the following sections, we discuss the principle of ultrasound-induced cavitation in liquid metals and investigate whether the cavitation occurs in liquid gallium under our experimental conditions.

4.3 Ultrasound-induced cavitation in liquid metals

When ultrasound waves propagate in a liquid, the mechanical vibration causes local pressure fluctuations; if the local static pressure of the liquid is reduced to below its vapor pressure, ultrasound-induced cavitation could happen [100, 101]. During this process, the formation, growth, pulsation, and collapse of micro-bubbles occur under the influence of ultrasound waves: bubbles grow during the rarefaction phase and collapse during the compression phase [102]. The collapse of cavitation bubbles can generate high-speed liquid jets, high temperatures, and high pressures in a small region and for a short period of time, as well as many physical effects such as shock waves or acoustic streaming [101-106]. Due to those features, ultrasound-induced cavitation has been widely applied to cleaning, dispersion, sonochemistry, biomedical treatment, etc. [16, 107-109].

The studies of ultrasound-induced cavitation in liquid metals or metal melts have been started decades ago. Most are devoted to ultrasonic melt treatment processing. In the ultrasonic melt treatment, high-power ultrasound waves are used to treat the metal melts in order to improve their microstructures after solidification, and its mechanism is based on ultrasound-induced cavitation [101]. For example, the formation and pulsation of cavitation bubbles can extract dissolved gases, which are undesirable, from the surrounding melt and release them to the atmosphere as the bubbles float to the melt surface; the collapse of bubbles and acoustic streaming generated during the cavitation process can refine the grain structures after solidification [108].

For an ideal pure liquid, a cavitation threshold exists, which is the theoretical critical pressure to induce cavitation. To induce cavitation in liquid metals, an acoustic pressure higher than the cavitation threshold is required [102]. Thus, high-intensity ultrasound,

usually generated by a sonotrode submerged into the melt, is used in ultrasonic melt treatment to produce sufficient acoustic pressure [101, 106, 108]. The intensity of ultrasound waves used in the UDV is much lower than that used in the ultrasonic treatment, so it is difficult to induce cavitation in liquid metals by the UDV ultrasound waves solely. However, the presence of oxide inclusions, dissolved gas, and other impurities in liquid metals could significantly lower the cavitation threshold by serving as cavitation nucleation sites [101, 102]. Therefore, to study ultrasound-induced cavitation in the UDV measurement of gallium, we first need to investigate what kind of impurities and dissolved gases are present in liquid gallium.

We have already learned that gallium oxide inclusions are widespread in liquid gallium. For dissolved gases, different liquid metals have different dissolved gases, where oxygen and hydrogen are the most common dissolved gases. In gallium, hydrogen is the main dissolved gas, which is similar to the case of aluminum [101]. The hydrogen mainly comes from atmospheric moisture: liquid gallium reacts with water vapor in the air to produce gallium oxide and hydrogen. Since hydrogen does not react with gallium spontaneously, the resulting hydrogen would dissolve in liquid gallium. One of our collaborators, Andrew Caldwell, theoretically studied the solubility of hydrogen and oxygen in liquid metals [110], For gallium, the solubility of oxygen ($X_{O,sat} \approx 10^{-23}$) is 16 orders of magnitude less than the solubility of hydrogen ($X_{H,sat} \approx 10^{-7}$), and since the oxygen easily reacts with liquid gallium to form gallium oxide, thus the hydrogen, instead of oxygen, is the main dissolved gas in liquid gallium [81].

Given the presence of oxide inclusions and dissolved hydrogen, it is theoretically possible that ultrasound-induced cavitation occurs in liquid gallium at pressures much lower than the threshold. Figure 4.11(a) shows a schematic illustration of the formation of cavitation

bubbles on oxide nuclei. However, even if cavitation occurs in UDV measurement, the cavitation intensity is unlikely as strong as that in ultrasonic melt treatment (in which we can hear or see the collapse of cavitation bubbles directly from the melt surface). Therefore, characterizing the weak cavitation in liquid gallium is a challenge. We investigated the cavitation events in liquid gallium from two aspects: numerical analyzing the possibility of cavitation occurring in gallium and experimentally detecting the cavitation activity in gallium.

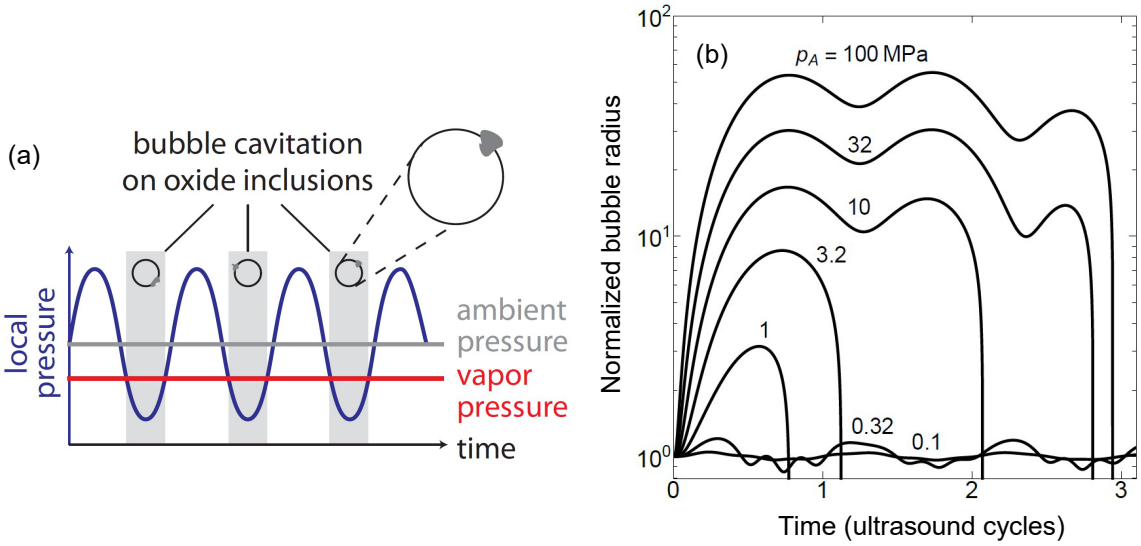

Figure 4.11 Ultrasound-induced cavitation in metal melts. (a) schematic illustration of the formation of cavitation bubbles in metal melts: when an incoming ultrasound wave lowers the local pressure below the vapor pressure, a bubble forms on an oxide inclusion. (b) Model of bubble growth dynamics in liquid gallium (credit: A. Caldwell [81]). The bubble size varies with ultrasound cycles under different acoustic pressures P_a at a hydrogen concentration $x_H = 1.6*10^{-7}$. Collapse is marked by the sudden decrease in bubble size. This model is built by using the Nolting-Neppiras approximation to the Rayleigh-Plesset equation, following the treatment by Eskin [101].

4.3.1 Bubble growth dynamic model and acoustic pressure in gallium

We first numerically analyzed the possibility of cavitation occurring in gallium by comparing the cavitation threshold pressure in gallium and the acoustic pressure amplitude generated by the UDV transducer. Andrew Caldwell built a bubble growth dynamic model in gallium according to our real experimental conditions. The model is shown in figure 4.11(b), where the bubble radius (normalized by the initial cavitation nucleus radius, here 1 μm) is plotted as a function of ultrasound cycles. The model is built for liquid gallium with a concentration of dissolved hydrogen x_H = 1.6*10^{-7} in mole fraction (this is a reasonable concentration of dissolved hydrogen in gallium at 80°C under our laboratory environment), under 8 MHz ultrasound waves with acoustic pressure amplitude p_A from 10^5 to 10^8 Pa [81]. Cavitation is marked by the sudden decrease in bubble size, i.e., bubble collapse. From the model, cavitation bubbles start to grow/shrink at acoustic pressure above 0.32 MPa, and significant cavitation activities occur at acoustic pressure above 1 MPa.

Next, we calculated the amplitude of the acoustic pressure produced by the UDV transducer in gallium. Instead of a specific pressure value, we calculated a pressure range that could be produced in gallium. We first calculated the maximum or the upper-limit acoustic pressure in gallium, via Equation 4.1 and Equation 4.2 [101].

$$I = \frac{emitting\ power}{transducer\ surface\ area} = \frac{35\ W}{\pi * r^2} \tag{4.1}$$

$$P_A = \sqrt{2 * I * \rho * c} = 7.9\ MPa \tag{4.2}$$

I is the ultrasound intensity; the ultrasound emitting power is given fixed for the DOP device, which is 35 W; r is the radius of the piezo element on the transducer probe surface; P_A is the acoustic pressure, ρ and c are the density and sound speed in liquid gallium,

respectively. Note that this calculation assumes a 100% electro-acoustic conversion rate for the UDV transducer. That is definitely not true in practice. Eskin mentioned that only 25% of the electrical power could be converted to useful acoustic power [101]. The conversion rate also depends on the specific transducer used and is affected by the wetting condition between the probe surface and liquid gallium. In addition, this calculation ignores the energy loss due to ultrasound attenuation in gallium. Therefore, the calculated pressure 7.9 MPa is the upper-limit acoustic pressure that could never be achieved in practice. If we assume a 25% electro-acoustic conversion rate, then the upper-limit acoustic pressure becomes 2 MPa.

We then calculated the lower-limit acoustic pressure in gallium. We placed a hydrophone 100 mm from the UDV transducer surface (along the ultrasound measuring line) to measure the acoustic pressure generated in gallium. The hydrophone was connected to an oscilloscope. Since the hydrophone has not been calibrated, the acoustic pressure value was derived from the measured voltage waveform through Equation 4.1-4.3:

$$W = \frac{U_{measured}^2}{R} \tag{4.3}$$

where W is the power, U is the measured peak-to-peak voltage, and R is the resistance of the hydrophone. The resulted W is then substituted into Equation 4.1 and 4.2. By doing so, an acoustic pressure of 0.3 MPa is calculated. This acoustic pressure amplitude is the minimum value produced by the UDV transducer in gallium: first, since the hydrophone was placed 100 mm from the UDV transducer, there is ultrasound energy loss during propagation; second, this method takes into account the energy loss from electro-acoustic conversion twice (one for the UDV transducer and one for the hydrophone). Therefore, the real acoustic pressure produced by the UDV transducer should be larger than the

calculated value 0.3 MPa. Even though, 0.3 MPa is enough to cause small changes in bubbles size, as shown in the bubble growth model in figure 4.11.

It should be also noted that the bubble growth model only took into account the dissolved hydrogen in gallium, whereas the effect of oxide inclusions or other impurities has not been considered, since their concentration in gallium is variable and hard to estimate. No doubt the presence of oxide inclusions and other impurities would further reduce the cavitation threshold pressure.

By comparing the calculated acoustic pressure range and the bubble growth dynamics model, the acoustic pressure produced by the UDV transducer meets the theoretical criteria to induce cavitation in gallium. To determine whether cavitation occurs in liquid gallium during the UDV measurements, more direct evidence is needed.

4.3.2 Detection of cavitation noises in gallium

Next, we experimentally detected the cavitation events in gallium. Although there are various optical methods, for example sonoluminescence [111], to characterize the cavitation in transparent liquids, cavitation activity in liquid metals is hard to detect due to opacity. In ultrasonic melt treatment, the effect of cavitation is usually assessed by the refinement of microstructures of the metal or alloy after solidification [108]. Even if cavitation occurs in UDV measurements, its intensity is not strong enough to cause microstructure refinement. Therefore, an in-situ method is required to detect whether there is cavitation activity in gallium.

One of the in-situ methods to characterize cavitation in opaque liquid metals is to detect the cavitation noises by measuring the acoustic spectra. A feature of cavitation is the generation of characteristic acoustic emissions resulting from the interactions between

cavitation bubbles and ultrasound waves [102, 112]. Generally, for cavitation induced by ultrasound with a fundamental frequency of f_0, the typical frequency spectra would include harmonic frequency peaks (nf_0), sub-harmonic and ultra-harmonic frequency peaks ($nf_0/2$), and broadband noises (white noise) [101, 106, 107, 112-114]. The appearance of harmonic signals is usually associated with the linear pulsation of bubbles, while the sub-harmonic and ultra-harmonic signals and broadband noises are associated with the nonlinear pulsation, resonance, and collapse of bubbles [104, 107, 112-114]. Therefore, detecting the cavitation noises at different frequencies can locate the cavitation zone and monitor the development of cavitation activities [113, 114].

Detecting acoustic emissions of cavitation in metal melts faces some practical restrictions and challenges: the high temperature involved in metal melts and the compatibility between the measurement device and metal melts. In previous studies, a specially designed hydrophone, named the high-temperature cavitometer, was developed for measuring the acoustic emissions of cavitation in molten aluminum [107, 114, 115]. In our study, since we only measure the acoustic spectra in liquid gallium at temperatures below 80°C, a commercial Passive Cavitation Detector (PCD) (Precision Acoustics, UK) was used to detect the cavitation noises. The working principle of PCD is just like a hydrophone: it measures the acoustic emission from its focal zone and provides an optimum signal-to-noise ratio for detecting cavitation-associated signals.

The experimental apparatus for cavitation detection is shown in figure 4.12. A UDV transducer with a working frequency of 4 MHz was used to perform the direct-contact UDV measurement in liquid gallium. The PCD was installed in a con-focal arrangement with a focal length of 20 mm from the central line of the UDV measuring line. The PCD could be moved parallel along the UDV measurement line. An oscilloscope was connected to the

PCD to acquire and display the measured acoustic waveforms. Although high temperature was not involved, the inadequate compatibility between the PCD and gallium, especially the poor wetting between the PCD probe surface and gallium, significantly reduced the sensitivity of the PCD. To compensate, a signal amplifier (Precision Acoustics, UK) was used to amplify the measured acoustic signals.

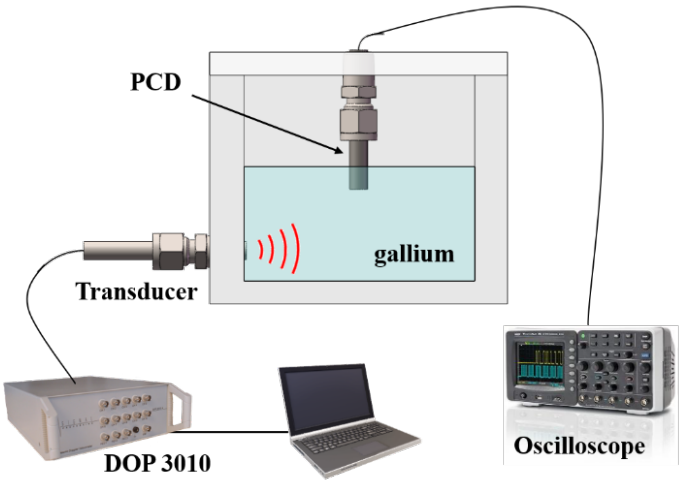

Figure 4.12 Experimental apparatus for cavitation measurements. The UDV emitting frequency was 4 MHz. The Passive Cavitation Detector (PCD) was installed in a con-focal arrangement and connected to an oscilloscope. The PCD could be moved along the UDV measuring line.

To measure cavitation at the UDV transducer surface, the PCD was placed right above the transducer surface. The measured waveform and the corresponding frequency spectrum obtained by fast Fourier transform (FFT) are plotted in figure 4.13. From the frequency spectrum, a strong peak corresponding to the ultrasound emitting frequency of 4 MHz was measured. Besides that, weak peaks also appeared at the sub-harmonic frequency (2 MHz), ultra-harmonic frequency (6MHz), and integer harmonic frequency (8 MHz, 12 MHz, etc.) positions. Therefore, we believe that weak cavitation activities might occur near the UDV transducer surface. Since there is no broadband noise appearing in

the spectrum, the ultrasound might only cause the linear or non-linear pulsation of bubbles, but is not strong enough to cause the collapse of bubbles. The formation and pulsation of cavitation bubbles on the UDV transducer surface, combined with the accumulation of oxide layer on the transducer surface, seems to be a reasonable explanation for the UDV signal deterioration over time that occurs only when ultrasound is emitted.

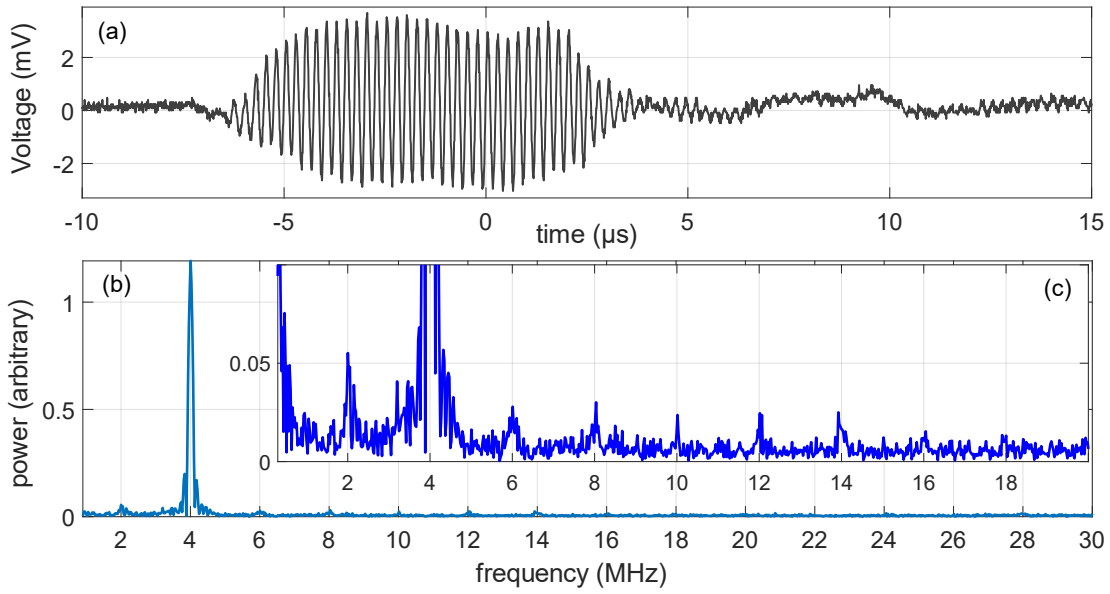

Figure 4.13 Cavitation measurement near the UDV transducer surface. (a) Transient acoustic waveform recorded by the oscilloscope, and the corresponding frequency spectrum (b and c). The inset panel (c) is an enlarged view of (b). Weak sub-harmonic (2 MHz) and ultra-harmonic (6 MHz) peaks, and integer harmonic peaks (8 MHz, 12 MHz, etc.) were detected. Thus, weak cavitation might occur near the transducer surface.

Compared to the strongest peak corresponding to the ultrasound emitting frequency, other peaks associated with cavitation noises are very weak. There are three possible reasons for this phenomenon. First, the cavitation intensity induced by the UDV ultrasound wave is very weak, as predicted from the bubble growth dynamic model. Second, the linear

pulsation of bubbles would also contribute to an increase in the fundamental frequency [107]. Third, the inadequate compatibility and the poor wetting between the PCD probe and liquid gallium significantly reduced the sensitivity of the PCD. When testing the PCD in water and gallium, the acoustic signal measured in water was 100 times stronger than that measured in gallium. The difference in the performance of UDV transducers in water and gallium is not as great. Thus, the compatibility and wettability of the PCD probe to liquid gallium are even worse than that of the UDV transducer. This is not surprising, because firstly, the PCD probe surface is made of stainless steel that has very poor wetting properties to gallium, as discussed in Chapter 2; secondly, the PCD itself is a signal-sensitive device, so a too weak signal affects its performance dramatically. When applying the PCD to liquid gallium, even the fundamental frequency is barely detectable without the signal amplifier. Therefore, there is the possibility that the cavitation intensity at the UDV transducer surface is stronger than what we measured. To compensate for the poor wetting, we also tried adding a layer of water on top of the liquid gallium so that the PCD surface was surrounded by water. Although the wetting between PCD and water is better, the additional water-gallium interface obstructed the acoustic signals from gallium and instead increased the complexity of measurement.

No matter what, using a specialized cavitation detector with better compatibility and wettability to liquid metals is a better way to investigate the ultrasound-induced cavitation in gallium. Another more intuitive way to study the UDV signal deterioration caused by the surface processes is to use in-situ imaging techniques, such as synchrotron radiation X-ray imaging [116], to directly observe the changes occurring at the transducer surface while running UDV measurement.

4.3.3 Cavitation on transducer surface and UDV signal deterioration

Since PCD measurements alone could not provide convincing evidence for the occurrence of cavitation at the UDV transducer surface, two additional experiments were performed to verify the relationship between UDV signal deterioration and cavitation activity at the transducer surface. In this section, UDV signal deterioration refers specifically to the deterioration caused by the surface processes, i.e., the degradation of wetting.

In the first experiment, we investigated the effect of ultrasound frequency on ultrasound signal deterioration. The experiment setup was the same as the one shown in figure 2.13, in which a 4 MHz UDV transducer and an 8 MHz UDV transducer were aligned horizontally on the two sides of a container. Three consecutive UDV measurements were conducted: in test-1 we performed UDV measurements in gallium using both transducers simultaneously; then we manually stirred the gallium to bring the scattering particles back to bulk and conducted test-2; after that, we stirred the gallium again and conducted test-3. The transducers' surfaces were not cleaned between any of the tests.

The echo decay behaviors measured by the 4 MHz and 8 MHz transducers are compared with each other, as shown in figure 4.14. From the results, the measured echo decay behaviors, especially the initial echo intensity, were very different between the 4 MHz and 8 MHz transducers. Apparently, the UDV signal deterioration measured by the 4 MHz transducer was worse than that of the 8 MHz transducer. For the 4 MHz transducer, the degradation of wetting at the transducer surface had started during test-1 (20 minutes of ultrasound emission). For the 8MHz transducer, the degradation of wetting was not obvious, as stirring could still restore most of the echo intensities.

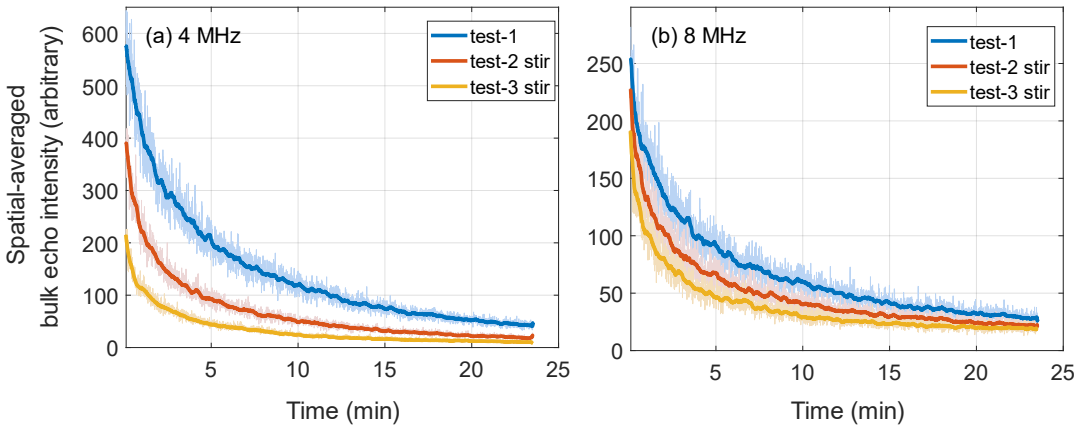

Figure 4.14 Echo decay behaviors in gallium, measured by (a) 4 MHz UDV transducer and (b) 8 MHz UDV transducer. The bulk echo intensities were obtained by spatially averaging over the region 30-120 mm from the transducer. The UDV signal deterioration of the 4 MHz transducer is worse than the 8 MHz transducer.

It is known that ultrasound-induced cavitation has a lower threshold at lower ultrasound emitting frequencies [101, 117]. In other words, ultrasound with lower frequencies induces cavitation more easily. Thus, the ultrasound frequencies used in ultrasonic melt treatment are typically between hundreds of kHz to 1MHz [108, 113, 114]. Accordingly, 4 MHz ultrasound should induce cavitation in gallium more easily than 8 MHz ultrasound. This fact supports our hypothesis: since more intense cavitation occurred at the 4 MHz transducer surface, the degradation of wetting was faster and more severe, resulting in the more significant deterioration of UDV signals measured by the 4 MHz transducer.

In the second experiment, we transferred the UDV measurements to an argon glovebox. As discussed above, the cavitation in liquid gallium might result from the interactions among ultrasound waves, oxide inclusions, and dissolved hydrogen. In that case, the presence of oxide inclusions and dissolved hydrogen would be essential for cavitation. In this experiment, we tried to diminish or eliminate cavitation by reducing the amounts of

oxide inclusions and dissolved hydrogen in gallium. The gallium was melted and stored inside a glovebox filled with argon for a few days, in order to reduce the already existing dissolved hydrogen and oxides.

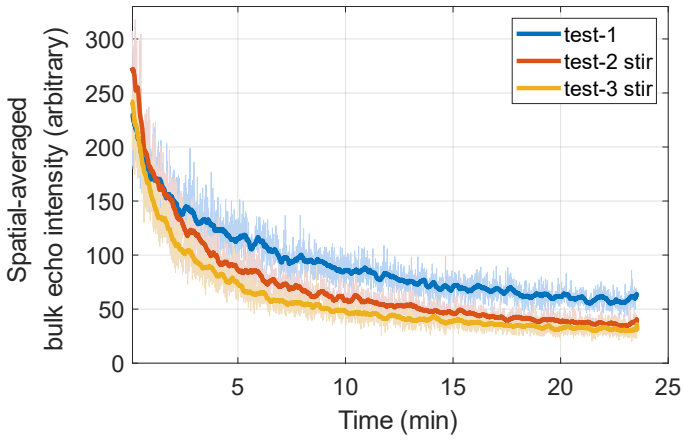

Figure 4.15 Echo decay behaviors in gallium inside an argon glovebox. The bulk echo intensities were obtained by spatially averaging over the region 30-120 mm from the transducer. The UDV signal deterioration caused by the surface processes was mitigated under an argon atmosphere.

We conducted the same consecutive tests in the cleaned gallium with a 4 MHz UDV transducer. The time evolution of the bulk echo intensity is plotted in figure 4.15. Compared to the echoes measured in air (figure 4.14(a)), the overall echo intensity measured in the argon glovebox was much weaker. This is simply because the pretreatment of gallium inside the glovebox reduced the population of oxide inclusions in the gallium. Interestingly, the echo decay behaviors among the three tests were different from those measured in air with the 4 MHz transducer, but more similar to those measured in air with the 8 MHz transducer: the initial echo intensities of the three tests were almost the same, and stirring could recover most echo signals. The result demonstrates that a lower concentration of dissolved hydrogen and oxides can mitigate the degradation of

wetting on the transducer surface. This experiment again supports our hypothesis that cavitation occurring on the UDV transducer surface caused the degradation of wetting.

According to the results of the above two experiments and PCD measurements, we believe that weak cavitation activity might have occurred on/near the UDV transducer surface. The cavitation bubbles formed at the transducer surface, together with the accumulated oxide layer, degraded the wetting conditions between the transducer surface and gallium, destroyed the continuity of the acoustic path from the transducer to gallium, and thus deteriorated the UDV signals in gallium. In theory, cavitation should be more intense with 4 MHz ultrasound waves than with 8 MHz ultrasound waves, which is consistent with our experiment results, as shown by the more significant deterioration of echo signals measured by the 4 MHz transducer. The cavitation in liquid gallium might be induced by the interactions among ultrasound waves, oxide inclusions, and dissolved hydrogen. After transferring to the argon glovebox, because of the lower concentration of dissolved hydrogen and lower amounts of oxide inclusions, cavitation in gallium was weakened or eliminated; consequently, the UDV signal deterioration caused by surface processes was mitigated by the argon atmosphere.

4.3.4 Cavitation in the bulk part and the effect of dissolved gases

One of our hypotheses in the early stage of this study was that the strong bulk echoes measured in liquid metals are caused by the bubbles originating from ultrasound-induced cavitation. Actually, many of our early experiments were conducted based on this preliminary hypothesis. Although our later studies demonstrated that the bulk echoes in gallium are from the scattering of ultrasound waves by gallium oxide inclusions, we have not completely excluded that hypothesis: there is a possibility that the bulk echoes are

scattered by the cavitation bubbles formed on the oxide nuclei rather than by the oxide inclusions themselves.

In our hypothesis, the interactions among ultrasound, oxide inclusions, and dissolved gas produce cavitation bubbles throughout the melt, and the cavitation bubbles provide the bulk echoes in UDV measurements. If the hypothesis is true, the changes in the amount of oxide inclusions or dissolved gas would result in changes in bulk echo intensity. Thus, a good way to test that hypothesis is to study the relationship between dissolved gas and echo signals. However, for a liquid metal whose dissolved gas is oxygen, oxide inclusions are also introduced if dissolved oxygen is present, so the role of dissolved gas could not be investigated separately from oxide inclusions. Since the dissolved gas in liquid gallium is hydrogen, the effect of dissolved gas can be investigated independently, which makes gallium an ideal candidate for investigating the role of dissolved gas in UDV measurements. That is also one of the reasons why we selected gallium as the liquid metal for our UDV studies.

We experimentally studied the effect of dissolved hydrogen on echo signals in liquid gallium. If cavitation occurs in the bulk part of liquid gallium such that the cavitation bubbles produce bulk echoes, and if the concentration of dissolved hydrogen affects the formation and growth of cavitation bubbles, then we should expect bulk echo intensity to increase with increasing concentration of dissolved hydrogen. According to Sieverts' Law [118], we controlled the concentration of dissolved hydrogen in gallium by adjusting the hydrogen partial pressure above the liquid gallium. We designed a special vessel to control the gas atmosphere above the liquid gallium, as shown in figure 4.16. Three gases with different hydrogen partial pressure were injected into the vessel through plastic or copper tubes. Before the experiment, gallium was melted and stored in an argon glovebox to reduce the

pre-existing dissolved hydrogen and oxides. During the experiment, we ran UDV measurements in liquid gallium to observe how the bulk echo signals change under the three different gas atmospheres.

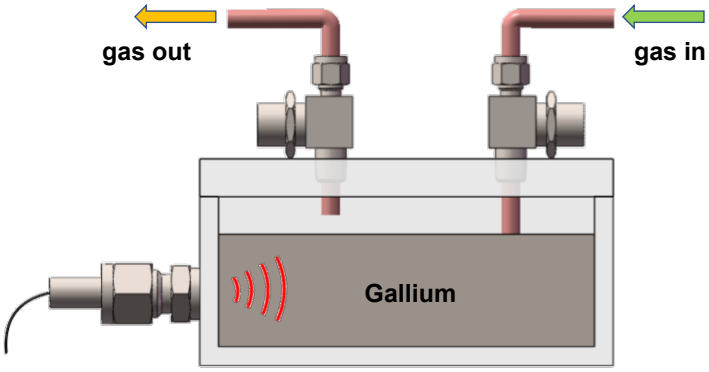

Inject gas	Partial pressure of H (atm)
Pure argon	0
Air (50% relative humidity)	0.005
1% H_2 balanced argon	0.01

Figure 4.16 Experimental apparatus for investigating the effect of dissolved hydrogen on UDV signals. Two threaded ball valves were mounted on the lid to control the gas inlet and outlet. Three gases used in experiments and their hydrogen partial pressures are listed in the table.

At first, we used plastic tubes for the gas inlet and outlet. Argon, 1% H_2 balanced argon, and air were injected into the vessel successively, and UDV measurements were conducted for one hour under each gas atmosphere. The measured echo intensity is shown in figure 4.17. Figure 4.17(a) plots the time-averaged echo intensity as a function of distance from the UDV transducer. When only pure argon was above the gallium, there was almost no dissolved gas inside the gallium, and since the population of oxide inclusions was also low, the bulk echo intensity was very weak. When the 1% H_2 balanced argon was injected into the vessel, an increase in bulk echo intensity could be observed clearly, suggesting that the bulk echo intensity might increase with hydrogen partial pressure. When there was air above liquid gallium, the echo showed the highest intensity; in this case, the introduction of oxygen and oxides might contribute to the bulk echo

intensity. Figure 4.17(b) plots the time evolution of the bulk echo intensity right before and after the increase of hydrogen partial pressure. Pure argon was above the liquid gallium at the beginning, and the 1% H_2 balanced argon gas was injected after the ultrasound signals became stable under the argon atmosphere. A significant increase in echo intensity appeared when the 1% H_2 balanced argon was injected; the echo intensity then reached a plateau after a few minutes of injection.

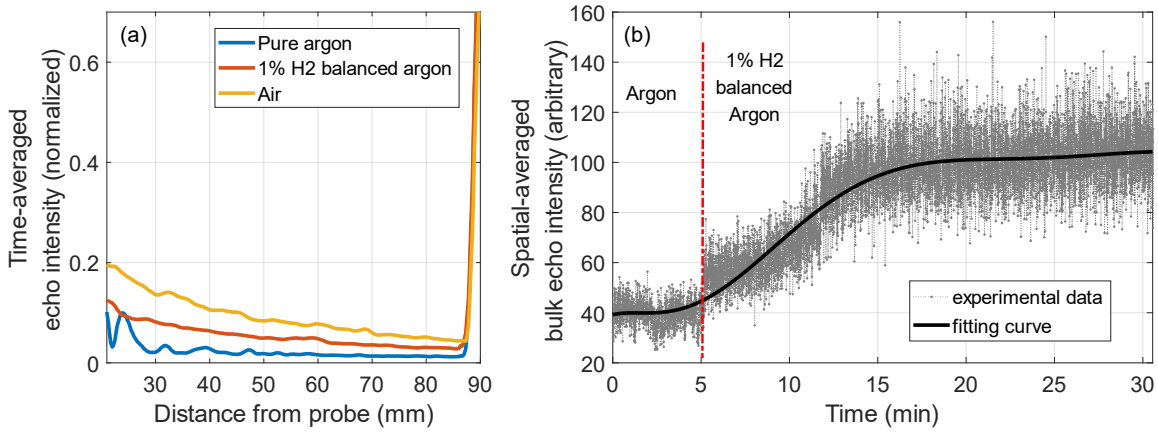

Figure 4.17 UDV measurements under three different gas atmospheres; gases were injected into the vessel through plastic tubes. (a) Time-averaged echo intensity vs. distance. The echo intensity was highest under air atmosphere and lowest under argon atmosphere. (b) Time evolution of the spatial-averaged bulk echo intensity (averaged over the region 30-80 mm from the transducer) before and after the injection of 1% H_2 balanced argon gas. The red dashed line indicates the time when the 1% H_2 balanced argon gas injection started. The echo intensity increased when 1% H_2 balanced argon was injected.

The experimental results seem to imply that the concentration of dissolved hydrogen could affect the bulk echoes in liquid gallium, which means that cavitation occurred in the bulk part of liquid gallium during UDV measurements. However, we have noticed that the plastic tubes used for gas injection did not guarantee an ideal seal, because oxygen in the

air can diffuse into the plastic tube and thus enter the vessel. Therefore, the changes in echo intensity observed in the above experiment were very likely due to the introduction of oxygen and oxides into the gallium.

In later experiments, we replaced the plastic tubes with copper tubes and added a moisture/oxygen trap filter (Restek, USA) in the gas inlet. This configuration provided better control of the gas above the liquid gallium, so that only the hydrogen partial pressure varied between different atmospheres. We performed the same experiment in this better-sealed setup. Three UDV measurements were conducted under the three gas atmospheres, respectively. Figure 4.18 shows the ultrasound measurement results. This time, the measured echo intensities were similar among the three gas atmospheres, as shown in figure 4.18(a). In another measurement, we induced a rotating flow in the liquid gallium by a stirring plate beneath the vessel, in order to observe the echo decay behaviors under different gas atmospheres. As shown in figure 4.18(b), the bulk echoes of gallium showed similar decay behaviors among the three gas atmospheres. The results suggest that the concentration of dissolved hydrogen has little effect on the bulk echo intensity of gallium. This conclusion is opposite to the previous one, which is mainly attributed to better control of the gas atmosphere. Through multiple repeated experiments, we confirmed that the introduction of oxygen/oxides has a strong effect on the bulk echo signals, whereas the concentration of dissolved hydrogen has little effect on the bulk echo signals in liquid gallium. Therefore, cavitation might not occur in the bulk part of liquid gallium during UDV measurements.

One concern was that the oxide layer formed on the liquid gallium free surface might restrict the gas from dissolving into liquid gallium. In an alternative experimental setup, the inlet tube was submerged beneath the liquid gallium free surface so that the gas was

injected into liquid gallium directly. Unfortunately, due to the poor pressure control of the inlet gas flow, the direct injection of gases caused strong bubbling inside the liquid gallium, which destroyed the UDV measurements.

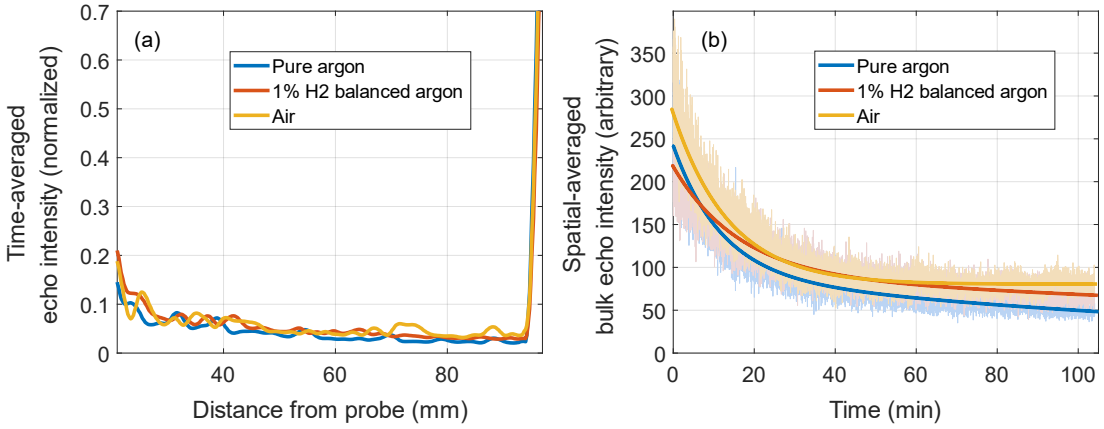

Figure 4.18 UDV measurements under three different gas atmospheres; gases were injected into the vessel through copper tubes. (a) Time-averaged echo intensity vs. distance. The measured echo intensities were similar among the three different gas atmospheres. (b) Spatially averaged bulk echo intensity (averaged over the region 30-80 mm from the transducer) vs. time. The bulk echoes showed similar decay behaviors among the three different gas atmospheres.

Another more direct way to test the cavitation hypothesis was to use the PCD to detect the acoustic emissions from the bulk part of liquid gallium (20-100 mm from the transducer surface). The experimental apparatus was the same as the one shown in figure 4.12. The measured acoustic waveform and the corresponding frequency spectrum are shown in figure 4.19. Different from the spectrum measured near the UDV transducer surface (figure 4.13), the spectrum measured from the bulk part of liquid gallium detected only one frequency peak corresponding to the ultrasound emitting frequency; no cavitation noise was detected. The result suggests that cavitation is unlikely to occur in the bulk part of liquid gallium under the UDV ultrasound intensity. Note that this result does not contradict

our previous conclusions, because the ultrasound has the strongest energy near the transducer surface; the ultrasound energy decreases continuously with the propagation distance due to ultrasound attenuation (absorption and scattering).

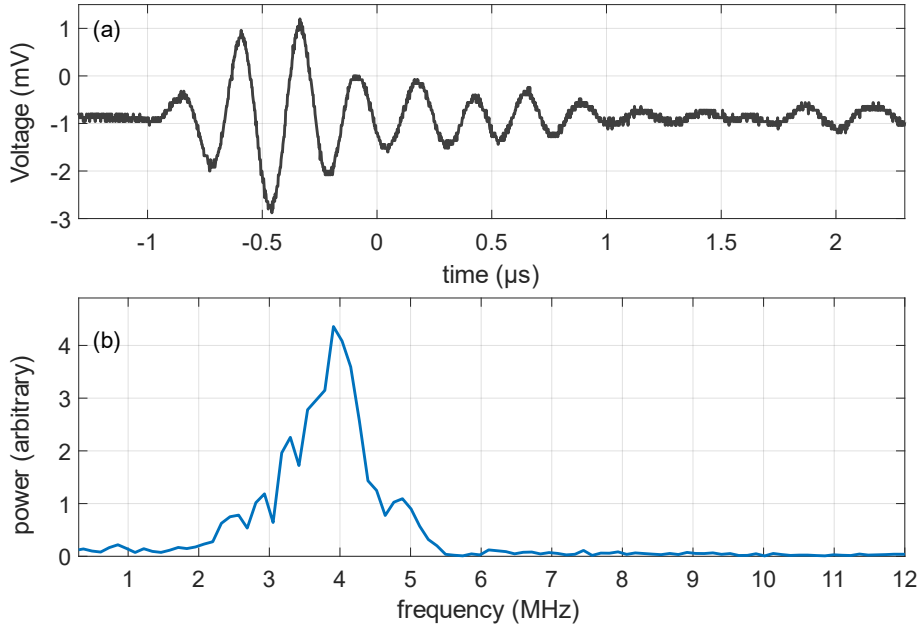

Figure 4.19 Cavitation measurement from the bulk part of liquid gallium. (a) Acoustic waveform recorded by the oscilloscope. (b) The corresponding frequency spectrum. The PCD measurement focal point was 80 mm from the UDV transducer surface. Only the UDV emitting frequency was detected, implying that cavitation did not occur in the bulk part of liquid gallium.

Combining the results of the PCD measurements and dissolved gas experiments, we believe that the ultrasound intensity used in the UDV measurement is unlikely to induce cavitation in the bulk part of liquid gallium under our experimental conditions. The bulk echoes in liquid gallium are mainly scattered by the gallium oxide inclusion itself, not the cavitation bubble forming on it.

4.4 Summary of chapter

In this chapter, we studied an undesirable phenomenon occurring in UDV measurements of liquid gallium, namely the UDV signal deterioration. The UDV signal deterioration is manifested as the flow velocity measurements gradually becoming inaccurate and eventually failing. The direct cause of the UDV signal deterioration is the decay of the bulk echo intensity over time: when the bulk echo is too weak to be detected by the transducer, there is not enough information available to determine the flow velocity. By comparing the echo decay behavior between direct-contact measurements and indirect-contact measurements, we found that the UDV signal deterioration in liquid gallium is caused by two distinct mechanisms: the loss of scattering particles from the bulk and the degradation of wetting between the transducer surface and liquid gallium.

The main source of bulk echoes in liquid gallium is gallium oxide inclusions distributed throughout the liquid gallium. Since the gallium oxide has a density different from liquid gallium, buoyancy would cause oxide inclusions to rise out of the bulk. Consequently, the decrease in the population of oxide inclusions inside the ultrasound beam path causes the decay of bulk echo intensity. We experimentally demonstrated that vigorous stirring, refilling, or introducing vigorous flows in gallium can mitigate the deterioration caused by this mechanism.

For the direct-contact UDV measurement of gallium, the wetting conditions between the transducer surface and liquid gallium also degrade with time, resulting in a deterioration of ultrasound signals that cannot be restored by stirring. This wetting degradation appears to be related to the oxide layer accumulated at the transducer surface, but the underlying mechanism is more complex. We found that wetting degrades only when ultrasound is

emitted. Based on the results of both theoretical and experimental studies, we suspect that the wetting degradation is caused by ultrasound-induced cavitation occurring on/near the UDV transducer surface. The cavitation in liquid gallium might be induced by the interactions among ultrasound waves, oxide inclusions, and dissolved hydrogen. A possible mechanism is that the bubbles generated from cavitation create micro-gaps between the UDV transducer surface and the accumulated oxide layer. Those gaps would then degrade the wetting at the transducer surface by destroying the continuity of the acoustic path from the transducer to liquid gallium. That is why the UDV signal deterioration caused by this mechanism occurs only when there is an ultrasound emission.

Through cavitation noise detection and control experiments, we demonstrated that cavitation only occurred in the vicinity of the transducer surface but not in the bulk part of liquid gallium. The higher acoustic pressure near the transducer surface and the oxide layer accumulated on the transducer surface might promote cavitation. Performing indirect-contact ultrasound measurements, maintaining an inert atmosphere, or using higher frequency ultrasound could mitigate or eliminate the UDV signal deterioration caused by the wetting degradation. Indirect-contact ultrasound measurements help maintain good wetting conditions on the transducer surface. Conducting UDV measurements with higher frequency ultrasound or under an inert gas atmosphere can increase the cavitation threshold, thereby mitigating cavitation near the transducer surface.

Our investigation of cavitation is still at a preliminary stage. The cavitation we discussed here mainly refers to the formation of cavitation bubbles, which is sufficient to degrade the wetting conditions at the UDV transducer surface. The pulsation and collapse of the bubbles, if any, would certainly introduce more complex interactions near the transducer surface, especially in the presence of a gallium oxide layer, but we did not delve into these

interactions. In fact, the intensity of cavitation occurring in the vicinity of the UDV transducer surface was very weak, and we could only probe it through some circumstantial evidence. To fully understand the role of cavitation, more quantitative studies are needed.

4.5 Acknowledgments

The thesis author was the primary person conducting all experiments and data analysis. The MATLAB script for extracting and demodulating the UDV data from binary files was written by Douglas Kelley. Thanks to Prof. Allanore and Andrew Caldwell of Massachusetts Institute of Technology for their collaboration on studying the dissolved gas and ultrasound-induced cavitation in gallium. Thanks to Andrew Caldwell for building the bubble growth dynamic models.

—— Chapter 5 ——

Conclusions and Future Directions

5.1 Summary of work and implications

The ultrasound Doppler velocimetry method is one of the few techniques allowing us to characterize metals or alloys in the liquid state. In our lab, we have successfully enabled real-time imaging and flow measurements in liquid metals such as gallium and PbBi via the UDV method. However, the application of the UDV in liquid metals/metal melts is not completely reliable: practical challenges and poorly understood phenomena are involved in ultrasound measurements. The goal of this work was to establish the UDV measurement as a reliable technique for the study of liquid metals, especially with respect to flow measurements. In this thesis, I have attempted to study the ultrasound measurement in liquid gallium through three research aspects: 1) determining the source of bulk echoes in liquid gallium and the corresponding scattering mechanisms; 2) improving the UDV measurement performance via indirect-contact measurements and demonstrating the effect of wetting on ultrasound measurements; 3) investigating the ultrasound signal deterioration in liquid gallium and exploring strategies to mitigate it.

In Chapter 2, I mainly investigated the source of bulk echoes in liquid gallium and its corresponding scattering mechanisms. Through SEM and EDS examinations, I found gallium oxide inclusions distributed throughout the gallium as isolated particles or agglomerates, which could be the possible source of bulk echoes. I utilized the UDV energy profile to identify the type of echoing objects by detecting their direction of motion

under gravity. The method has been first validated in water then applied to liquid gallium. The results confirmed that gallium oxide inclusions are the main source of bulk echoes in liquid gallium. Then, the ultrasound scattering mechanism in liquid gallium was studied by estimating the size of gallium oxide inclusions. A novel estimation method was developed based on terminal velocity measurements, which also took into account the acoustic forces generated by the UDV transducers. The mean size of oxide inclusions that provide the bulk echoes was estimated to be 58-64 μm, suggesting that the oxide inclusions in the form of agglomerates, rather than single particles, are mainly responsible for the bulk echoes. By comparing that size with the ultrasound wavelength in gallium, together with analogous experiments in water, Mie scattering was found to be the dominant mechanism. Therefore, I concluded that ultrasound waves in liquid gallium are mainly scattered by gallium oxide inclusions in agglomerate form, and Mie scattering is the dominant mechanism. UDV utilizes the echoes scattering by gallium oxides to enable the flow measurement in liquid gallium.

Studying the source of bulk echoes not only helps us better understand the mechanism of UDV measurements in liquid metals, but also has important implications for the practical application of UDV methods. For example, when applying UDV to measure the flows in liquid metal battery experiments, we have exploited the reactions between water and gallium to generate sufficient gallium oxide, and thus obtained strong bulk echo signals in liquid gallium. In addition, the methodology developed in this work for evaluating the kinds and sizes of effective particles for the measurement applies to all opaque fluids. By learning the density and mean size of scattering particles, one can assess whether the velocity measured by UDV can reflect the real fluid flow in their experiments.

In Chapter 3, I attempted to find the optimal vessel material to apply indirect-contact ultrasound measurements in water and liquid gallium. To better understand the ultrasound transmission behavior through a vessel wall, I systematically studied the effect of vessel material type and wall thickness on ultrasound signals. By comparing with direct-contact ultrasound measurement, I demonstrated that the material type and thickness of the vessel wall affect both the measured echo intensity and flow velocity profiles, especially at the region close to the transducer surface. In water, ABS is a good choice for the vessel material because the measured echo intensity and flow velocity are close to the direct-contact measurement. In gallium, acrylic is a good choice for the vessel material, because the measured signal strength is even better than the direct-contact measurement. Overall, plastic vessel materials showed better performance than metallic vessel materials. Our experimental results also revealed that when the test fluid is a liquid metal, the intensity transmission coefficient—calculated from the acoustic impedances of the acoustic coupling medium, vessel material, and test fluid—cannot predict the measured sound transmission through a wall precisely. The wetting conditions between the vessel wall and test fluid determine their physical acoustic coupling — the continuity of the acoustic path. The contact angle between the vessel material and the test fluid was shown to be useful for predicting their wetting conditions and thus the ultrasound measurement performance. We suggest that the contact angle could be used as a good index to select suitable vessel materials for indirect-contact ultrasound measurements.

Our work also demonstrated that surface treatment of the vessel wall could directly affect the ultrasound measurements. Finding appropriate surface treatment methods to improve the acoustic coupling and thus the quality of ultrasound measurements will be a fruitful topic for future study. In practical applications, the comprehensive study of vessel material

enabled us to obtain high-quality ultrasound signals and clear velocity measurements in liquid metal battery experiments. In that study, we conducted indirect-contact ultrasound measurements through a Delrin wall to measure the flow structures of a liquid metal battery layer. We have given appropriate surface treatments to the Delrin wall and successfully improved the ultrasound measurement performance.

In Chapter 4, I studied the ultrasound signal deterioration phenomenon occurring during UDV measurements of liquid gallium. Specifically, the decay of echo over time results in the eventual failure of UDV measurements. By comparing the echo decay behavior between direct-contact measurements and indirect-contact measurements, I found that the ultrasound signal deterioration in liquid gallium is caused by two distinct mechanisms: the loss of scattering particles from the bulk and the degradation of wetting at the transducer surface. Since gallium oxide inclusions distributed throughout the melt are mainly responsible for the bulk echoes, the density difference between gallium oxide and liquid gallium would cause a decrease in the population of oxide inclusions inside the ultrasound beam path, thereby causing the decay of the bulk echo intensity. The degradation of wetting was shown to occur only when ultrasound is emitted. Based on the results of both theoretical and experimental investigations, we suspected that weak cavitation occurring on/near the UDV transducer surface caused the wetting degradation. We hypothesized that cavitation in liquid gallium is induced by the interactions among ultrasound waves, oxide inclusions, and dissolved hydrogen. A possible mechanism is that cavitation bubbles and the oxide layer on the transducer surface degrade the wetting by destroying the continuity of the acoustic path from the transducer to liquid gallium.

A better understanding of the mechanisms of UDV signal deterioration in gallium inspired us to seek ways to extend the ultrasound measurement time and improve the

measurement quality. I showed evidence that the ultrasound signal deterioration caused by the first mechanism could be mitigated by vigorous stirring or by introducing vigorous flows; the signal deterioration caused by the second mechanism could be mitigated by performing indirect-contact ultrasound measurements, maintaining an inert atmosphere, or using higher frequency ultrasound. Armed with this knowledge, we have optimized the UDV measurement when applying it to the flow structure measurement of liquid metal batteries. For more information about our research on liquid metal batteries, please refer to [119-121]. More technical detail of UDV measurements with respect to liquid metal battery experiments and some challenges encountered are discussed in Appendix A.

In summary, this thesis work mainly focused on studying the UDV measurement in liquid gallium. I determined that gallium oxide inclusions are the main source of bulk echoes. Ultrasound waves in liquid gallium are mainly scattered by gallium oxide inclusions in agglomeration form, primarily via Mie scattering. Acrylic proved to be the optimal vessel material for conducting indirect-contact ultrasound measurement in gallium; due to good wetting, the measured signal was even better than direct-contact measurement. In addition, I found that the ultrasound signal deterioration in gallium is caused by two distinct mechanisms: the loss of echoing objects from the bulk due to density difference, and the degradation of wetting at the UDV transducer surface that occurs with ultrasound emission. I demonstrated that indirect-contact ultrasound measurements through a material that wets the melt well could not only improve the accuracy and quality of ultrasound measurements, but also mitigate the ultrasound signal deterioration caused by the degradation of wetting.

5.2 Future Directions

Although the work discussed in this thesis work only focused on UDV measurements of liquid gallium, the research in our lab also involved other metals, such as PbBi alloy and GaInSn alloy. What is the source of bulk echoes in those melts? Does the ultrasound obey the same scattering mechanisms in those melts? Could the methodology developed in this work also be applied to the ultrasound study of other melts? Those questions are worth investigating in the future. GaInSn is common in UDV research, and its active part—the scattering particles—is assumed to be gallium oxides. However, that assumption has not been verified yet. There is no doubt that gallium oxides play a role in providing bulk echoes, but the role of indium oxides or tin oxides needs to be identified as well. In addition, since GaInSn is an alloy, the segregation resulting from localized deviations in eutectic compositions is also a possible source of bulk echoes [39, 51]. One potential approach is to investigate the ultrasound measurements in GaInSn with varying compositions. Note that the change in composition can also lead to changes in melting temperature and surface tension of the melt, and the resulting wetting variation would bring additional challenges. In PbBi, we have found that lead oxides (PbO) are extensively present in the bulk part, which might be the possible source of bulk echoes. Since different phases are formed during the solidification of alloys, identifying oxide inclusions in alloys is much more difficult than in single metals. From our preliminary experiments, ultrasound signals exhibited a more intensive deterioration behavior in liquid PbBi. This might result from the large density difference between PbBi (10.08 g/cm^3) and PbO (9.53 g/cm^3) and/or more intensive surface processes occurring at the UDV transducer surface, or other unknown causes. Due to the higher melting temperature of PbBi (125°C), more challenges are

involved in experiments and UDV measurements; the performance of the UDV transducer might be an important factor.

We focused on liquid gallium not only because gallium is one of the most amazing representatives of liquid metal, but also because the study of gallium has the most practical significance. Many researchers have pointed out that there is a lack of quantitative study focusing on the dependence of ultrasound signal properties on parameters of scattering particles, such as their concentration, morphology, and acoustic properties [10, 29]. As shown in this work, the presence of oxide inclusions is necessary for obtaining ultrasound signals; however, too many oxide inclusions are undesired since they degrade wetting. Therefore, optimizing ultrasound signals by controlling the concentration of oxide inclusions will be a fruitful research direction. We have discussed in Chapter 2 that both chemical and electrochemical methods could be used to adjust the concentration of gallium oxides. However, those experiments were limited to qualitative studies. Electrochemical methods such as building a redox battery with precise current/voltage control might be a potential approach. In addition, changes in the concentration of oxide inclusions would also cause changes in surface tension and wettability of liquid gallium. That is to say, electrochemical methods also have the potential capability to modulate the wetting conditions between the UDV transducer surface and liquid metal. Distinguishing the effect of oxides with respect to the bulk and the surface will become a big challenge. One idea is to quantitatively analyze the echo decay behaviors from direct-contact measurements and indirect-contact measurements. For example, the echo decay curve could be fit to a two-factor exponential equation. Comparing the bulk echo decay curves between direct-contact measurements and indirect-contact measurements can provide information on the surface effects, while comparing the decay

curves between bulk echo and back-wall echo in direct-contact measurements can provide information on the volume effects. To do so, numerous repeated experiments are required so that one can extract statistical information to describe the echo decay curves.

Another research direction with great potential is ultrasound-induced cavitation. Honestly, the study of cavitation in this work is still in its preliminary stage. Characterizing cavitation in liquid metals is not an easy task, especially when the cavitation intensity is weak. It would be desirable if the acoustic pressure produced by the UDV transducer in liquid gallium could be measured quantitatively. One possibility is to buy a well-calibrated hydrophone for water and use it to calibrate a UDV transducer in water first, then use the calibrated UDV transducer as a hydrophone to measure the acoustic pressure produced by another UDV transducer in liquid metal. A more straightforward but expensive approach is to use the synchrotron radiation X-ray imaging technique to observe the cavitation bubbles directly.

Now let us turn to the ultrasonic melt treatment. Although numerical simulation is a well-established method to investigate cavitation in metal melts, experimental studies are indispensable. Almost all current experimental studies on ultrasonic melt treatment use high-power ultrasound to induce cavitation in high-temperature metal melts. Such experiments usually require costly equipment and often involve difficulties and challenges with respect to practical operation. If intense cavitation can be achieved in low-temperature metals, such as gallium, with low-intensity ultrasound techniques, such as UDV, then it will become a promising laboratory model for studying ultrasonic melt treatment. One possible approach is to reduce the cavitation threshold by increasing the concentration of dissolved gas and impurities in the melt. For instance, when performing UDV measurements, we can inject hydrogen gas and seed or produce gallium oxide particles

into liquid gallium until we can detect significant cavitation noises from the bulk. We can also introduce another component, such as indium, to alloy with gallium, which would allow oxygen to dissolve in the melt. For this research purpose, the bubble growth dynamics model is going to play a more important role.

Of course, as a measurement tool, the most important research direction of UDV measurement is to apply it to various research fields related to liquid metals and metal melts. Its capability for real-time imaging and flow measurements in liquid metal has been demonstrated throughout this work. I wish that through this work, the UDV measurement can be better used for various applications.

Bibliography

1. DeGarmo, E.P., *Materials and processes in manufacturing*. 9th ed. 2003, Hoboken, N.J.: Wiley. xiv, 1154 p.

2. Timmel, K., S. Eckert, and G. Gerbeth, *Experimental Investigation of the Flow in a Continuous-Casting Mold under the Influence of a Transverse, Direct Current Magnetic Field.* Metallurgical and Materials Transactions B, 2011. **42**(1): p. 68-80.

3. Yuan, B., et al., *Lightweight Liquid Metal Entity.* Advanced functional materials, 2020. **30**(14): p. 1910709-n/a.

4. Kazys, R., et al. *Investigation of ultrasonic properties of a liquid metal used as a coolant in accelerator driven reactors*. in *2002 IEEE Ultrasonics Symposium*. 2002. Munich, Germany: IEEE.

5. Kelley, D.H. and D.R. Sadoway, *Mixing in a liquid metal electrode.* Physics of Fluids, 2014. **26**(5): p. 57102.

6. Kelley, D.H. and T. Weier, *Fluid Mechanics of Liquid Metal Batteries.* 2017.

7. Kelley, D.H., et al., *Inertial waves driven by differential rotation in a planetary geometry.* Geophysical and astrophysical fluid dynamics, 2007. **101**(5-6): p. 469-487.

8. Adams, M.M., et al., *Liquid sodium models of the Earth's core.* Progress in earth and planetary science, 2015. **2**(1): p. 1-18.

9. Sisan, D.R., et al., *Experimental observation and characterization of the magnetorotational instability.* Physical review letters, 2004. **93**(11): p. 114502.1-114502.4.

10. Eckert, S., A. Cramer, and G. Gerbeth, *Velocity Measurement Techniques for Liquid Metal Flows*, in *Magnetohydrodynamics: Historical Evolution and Trends*, S. Molokov, R. Moreau, and K. Moffatt, Editors. 2007, Springer Netherlands: Dordrecht. p. 275-294.

11. Eckert, S., et al., *Some Recent Developments in the Field of Measuring Techniques and Instrumentation for Liquid Metal Flows.* Journal of Nuclear Science and Technology, 2011. **48**(4): p. 490-498.

12. Szekely, J., C.W. Chang, and R.E. Ryan, *The measurement and prediction of the melt velocities in aturbulent,electromagnetically driven recirculating low melting alloy system.* Metallurgical Transactions B, 1977. **8**(1): p. 333-338.

13. Koster, J.N., T. Seidel, and R. Derebail, *A radioscopic technique to study convective fluid dynamics in opaque liquid metals.* Journal of fluid mechanics, 1997. **343**: p. 29-41.

14. Kinsler, L.E., *Fundamentals of acoustics*. 4th ed. 2000, New York: Wiley.

15. Cobbold, R.S.C., *Foundations of biomedical ultrasound / Richard S.C. Cobbold*. 2007, Oxford ;: Oxford University Press.

16. Dalecki, D., et al., *Bioeffects of positive and negative acoustic pressures in mice infused with microbubbles.* Ultrasound in medicine & biology, 2000. **26**(8): p. 1327-1332.

17. Murai, Y., et al., *Ultrasonic detection of moving interfaces in gas–liquid two-phase flow.* Flow Measurement and Instrumentation, 2010. **21**(3): p. 356-366.

18. Fan, J. and F. Wang, *Review of ultrasonic measurement methods for two-phase flow.* Review of Scientific Instruments, 2021. **92**(9): p. 91502-091502.

19. Krautkrämer, J. and H. Krautkrämer, *Ultrasonic Testing of Materials by Josef Krautkrämer, Herbert Krautkrämer*. 4th ed. 1990. ed. 1990, Berlin, Heidelberg: Springer Berlin Heidelberg.

20. Eskin, D.G., *Ultrasonic processing of molten and solidifying aluminium alloys: overview and outlook.* Materials Science and Technology, 2017. **33**(6): p. 636-645.

21. Andruszkiewicz, A., et al., *Gas bubble detection in liquid metals by means of the ultrasound transit-time-technique.* The European Physical Journal Special Topics, 2013. **220**(1): p. 53-62.

22. Atkinson, P. and J.P. Woodcock, *Doppler ultrasound and its use in clinical measurement / Peter Atkinson and John P. Woodcock*. Medical physics series. 1982, London: Academic Press.

23. Takeda, Y., *Velocity profile measurement by ultrasound Doppler shift method.* International Journal of Heat and Fluid Flow, 1986. **7**(4): p. 313-318.

24. Takeda, Y., *Measurement of Velocity Profile of Mercury Flow by Ultrasound Doppler Shift Method.* Nuclear Technology, 1987. **79**(1): p. 120-124.

25. Takeda, Y., *Ultrasonic doppler velocity profiler for fluid flow / Yasuhi Takeda, editor*. Fluid mechanics and its applications, v. 101. 2012, Tokyo ;: Springer.

26. Brito, D., et al., *Ultrasonic Doppler velocimetry in liquid gallium.* Experiments in Fluids, 2001. **31**(6): p. 653-663.

27. Eckert, S. and G. Gerbeth, *Velocity measurements in liquid sodium by means of ultrasound Doppler velocimetry.* Experiments in Fluids, 2002. **32**(5): p. 542-546.

28. Kazys, R., et al. *Investigation of ultrasonic properties of a liquid metal used as a coolant in accelerator driven reactors*. in *2002 IEEE Ultrasonics Symposium, 2002. Proceedings.* 2002.

29. Cramer, A., C. Zhang, and S. Eckert, *Local flow structures in liquid metals measured by ultrasonic Doppler velocimetry.* Flow Measurement and Instrumentation, 2004. **15**(3): p. 145-153.

30. Takeda, Y., *Velocity profile measurement by ultrasonic doppler method.* Experimental Thermal and Fluid Science, 1995. **10**(4): p. 444-453.

31. Takeda, Y., *Ultrasonic Doppler method for velocity profile measurement in fluid dynamics and fluid engineering.* Experiments in Fluids, 1999. **26**(3): p. 177-178.

32. Eckert, S. and G. Gerbeth. *Velocity measurements in liquid metal flows using the Ultrasonic Doppler Method : examples and perspectives*. 2010.

33. Timmel, K., et al., *Experimental Modeling of the Continuous Casting Process of Steel Using Low Melting Point Metal Alloys-the LIMMCAST Program.* ISIJ International, 2010. **50**(8): p. 1134-1141.

34. Schurmann, D., et al., *Experimental Study of the Mold Flow Induced by a Swirling Flow Nozzle and Electromagnetic Stirring for Continuous Casting of Round Blooms.* Metallurgical and Materials Transactions B, 2019. **50**(2): p. 716-731.

35. Gerbeth, G., et al., *Recent LIMMCAST Results on the Modeling of Steel Casting.* Journal for Manufacturing Science and Production, 2015. **15**(1): p. 131.

36. Schurmann, D., et al., *Impact of the Electromagnetic Brake Position on the Flow Structure in a Slab Continuous Casting Mold: An Experimental Parameter Study.* Metallurgical and Materials Transactions B, 2020. **51**(1): p. 61-78.

37. Chaudhary, R., et al., *Transient Turbulent Flow in a Liquid-Metal Model of Continuous Casting, Including Comparison of Six Different Methods.* Metallurgical and materials transactions. B, Process metallurgy and materials processing science, 2011. **42**(5): p. 987-1007.

38. Tasaka, Y., Y. Takeda, and T. Yanagisawa, *Ultrasonic visualization of thermal convective motion in a liquid gallium layer.* Flow Measurement and Instrumentation, 2008. **19**(3): p. 131-137.

39. Starace, M., et al., *Ultrasound Doppler flow measurements in a liquid column under the influence of a strong axial current.* Magnetohydrodynamics, 2015. **51**: p. 249-256.

40. Eckert, S., et al., *Efficient Melt Stirring Using Pulse Sequences of a Rotating Magnetic Field: Part I. Flow Field in a Liquid Metal Column.* Metallurgical and Materials Transactions B, 2008. **39**(2): p. 374-386.

41. Gillet, N., et al., *Experimental and numerical studies of convection in a rapidly rotating spherical shell.* Journal of fluid mechanics, 2007. **580**: p. 83-121.

42. Gillet, N., et al., *Experimental and numerical studies of magnetoconvection in a rapidly rotating spherical shell.* Journal of fluid mechanics, 2007. **580**: p. 123-143.

43. Zhang, C., et al., *Intermittent Behavior Caused by Surface Oxidation in a Liquid Metal Flow Driven by a Rotating Magnetic Field.* Metallurgical and Materials Transactions B, 2011. **42**(6): p. 1188-1200.

44. Perez, A. and D.H. Kelley, *Ultrasound velocity measurement in a liquid metal electrode.* Journal of Visualized Experiments, 2015. **2015**(102): p. 1-12.

45. Losev, G., R. Khalilov, and I. Kolesnichenko, *UDV study of a liquid metal vortex flow.* IOP Conference Series: Materials Science and Engineering, 2017. **208**: p. 12022.

46. Zürner, T., et al., *Local Lorentz force and ultrasound Doppler velocimetry in a vertical convection liquid metal flow.* Experiments in Fluids, 2017. **59**(1): p. 3.

47. Zürner, T., et al., *Combined measurement of velocity and temperature in liquid metal convection.* Journal of fluid mechanics, 2019. **876**: p. 1108-1128.

48. Zürner, T., et al., *Flow regimes of Rayleigh–Bénard convection in a vertical magnetic field.* Journal of fluid mechanics, 2020. **894**.

49. Vogt, T., et al., *Jump rope vortex in liquid metal convection.* Proceedings of the National Academy of Sciences - PNAS, 2018. **115**(50): p. 12674-12679.

50. Akashi, M., et al., *Jump rope vortex flow in liquid metal Rayleigh-B\'enard convection in a cuboid container of aspect ratio five.* 2021.

51. Franke, S., et al., *Ultrasound Doppler system for two-dimensional flow mapping in liquid metals.* Flow Measurement and Instrumentation, 2010. **21**(3): p. 402-409.

52. Franke, S., et al., *Investigations of electrically driven liquid metal flows using an ultrasound Doppler flow mapping system.* Flow Measurement and Instrumentation, 2016. **48**: p. 64-73.

53. Büttner, L., et al., *Dual-plane ultrasound flow measurements in liquid metals.* Measurement Science and Technology, 2013. **24**(5): p. 055302.

54. Nauber, R., et al., *Novel ultrasound array measurement system for flow mapping of complex liquid metal flows.* The European Physical Journal Special Topics, 2013. **220**(1): p. 43-52.

55. Nauber, R., et al. *Modular ultrasound velocimeter for adaptive flow mapping in liquid metals*. in *2016 IEEE International Ultrasonics Symposium (IUS)*. 2016.

56. Mader, K., et al., *Phased Array Ultrasound System for Planar Flow Mapping in Liquid Metals.* IEEE Transactions on Ultrasonics, Ferroelectrics, and Frequency Control, 2017. **PP**: p. 1-1.

57. Vogt, T., et al., *Mixing Enhancement in Gas-Stirred Melts by Rotating Magnetic Fields.* Metallurgical and Materials Transactions B, 2012. **43**(6): p. 1454-1464.

58. Vogt, T., et al., *Detection of gas entrainment into liquid metals.* Nuclear Engineering and Design, 2015. **294**: p. 16-23.

59. Wang, Z.H., et al., *UDV measurements of single bubble rising in a liquid metal Galinstan with a transverse magnetic field.* International Journal of Multiphase Flow, 2017. **94**: p. 201-208.

60. Smith, D.D., et al., *Practical Use of the Metal Vision Ultrasonic Inclusion Analyzer*, in *Light Metals 2015*. 2015. p. 937-942.

61. Gökelma, M., D. Latacz, and B. Friedrich, *A Review on Prerequisites of a Set-Up for Particle Detection by Ultrasonic Waves in Aluminium Melts.* Open Journal of Metal, 2016. **06**: p. 13-24.

62. Achard, J.-L., et al. *An Innovative Ultrasonic Technology for the Continuous Quality Monitoring of Liquid Aluminum on Casting Lines*. in *Light Metals 2018*. 2018. Cham: Springer International Publishing.

63. Achard, J.L., P. Jarry, and F. Taina. *Ultrasonic Doppler Velocimetry in Liquid Aluminum*. 2018.

64. Zhang, H., et al., *Numerical and Experimental Investigation of Melting in the Presence of a Magnetic Field: Simulation of Low-Gravity Environment.* Journal of Heat Transfer, 2006. **129**(4): p. 568-576.

65. Oborin, P. and I. Kolesnichenko, *Application of the ultrasonic doppler velocimeter to study the flow and solidification processes in an electrically conducting fluid.* Magnetohydrodynamics, 2013. **49**(1-2): p. 231-236.

66. Dadzis, K., et al., *Directional melting and solidification of gallium in a traveling magnetic field as a model experiment for silicon processes.* Journal of Crystal Growth, 2016. **445**: p. 90-100.

67. Thieme, N., et al., *Ultrasound Flow Mapping for the Investigation of Crystal Growth.* IEEE Transactions on Ultrasonics, Ferroelectrics, and Frequency Control, 2017. **64**(4): p. 725-735.

68. Eckert, S., G. Gerbeth, and V. Melnikov, *Velocity measurements at high temperatures by ultrasound Doppler velocimetry using an acoustic wave guide.* Experiments in Fluids, 2003. **35**: p. 381-388.

69. Kazys, R., et al., *High temperature ultrasonic transducers for imaging and measurements in a liquid Pb/Bi eutectic alloy.* IEEE Transactions on Ultrasonics, Ferroelectrics, and Frequency Control, 2005. **52**(4): p. 525-537.

70. Assael, M.J., et al., *Reference Data for the Density and Viscosity of Liquid Cadmium, Cobalt, Gallium, Indium, Mercury, Silicon, Thallium, and Zinc.* Journal of physical and chemical reference data, 2012. **41**(3): p. 33101.

71. Morley, N.B., et al., *GaInSn usage in the research laboratory.* Review of scientific instruments, 2008. **79**(5): p. 056107-056107-3.

72. Hardy, S.C., *The surface tension of liquid gallium.* Journal of Crystal Growth, 1985. **71**(3): p. 602-606.

73. Ayrinhac, S., et al., *Thermodynamic properties of liquid gallium from picosecond acoustic velocity measurements.* Journal of physics. Condensed matter, 2015. **27**(27): p. 275103-275103.

74. Hunter, J.L. and K.S. Hovan, *Ultrasonic Absorption in Liquid Gallium.* The Journal of chemical physics, 1964. **41**(12): p. 4013-4014.

75. Edwards, D.F., *- Beta-Gallium Oxide (β-Ga2O3)*, in *Handbook of Optical Constants of Solids*, E.D. Palik, Editor. 1997, Academic Press: Burlington. p. 753-760.

76. Stepanov, S.I., et al. *GALLIUM OXIDE: PROPERTIES AND APPLICA 498> A REVIEW*. 2016.

77. Greenwood, N.N. and A. Earnshaw, *Chemistry of the elements N.N. Greenwood and A. Earnshaw*. 2nd ed. ed. 1997, Oxford ;: Butterworth-Heinemann.

78. *Ultrasonic Doppler Velocimeter DOP3010*. Available from: https://www.signal-processing.com/download/dop3010-brochure.pdf.

79. Kinsler, L.E., et al., *Fundamentals of Acoustics, 4th Edition*. Fundamentals of Acoustics. 1999. 560.

80. Wang, B. and D.H. Kelley, *Microscale mechanisms of ultrasound velocity measurement in metal melts.* Flow Measurement and Instrumentation, 2021. **81**: p. 102010.

81. Wang, B., et al. *Investigation of Echo Source and Signal Deterioration in Ultrasound Measurement of Metal Melt*. in *TMS 2022 151st Annual Meeting & Exhibition Supplemental Proceedings*. 2022. Cham: Springer International Publishing.

82. Takeda, Y., *Development of an ultrasound velocity profile monitor.* Nuclear Engineering and Design, 1991. **126**(2): p. 277-284.

83. Aubert, J., et al., *A systematic experimental study of rapidly rotating spherical convection in water and liquid gallium.* Physics of the earth and planetary interiors, 2001. **128**(1): p. 51-74.

84. Takeda, Y. and H. Kikura, *Flow mapping of the mercury flow.* Experiments in fluids, 2002. **32**(2): p. 161-169.

85. Bailar, J.C. and A.F. Trotman-Dickenson, *Comprehensive inorganic chemistry*. 1973, [Oxford: Pergamon Press; distributed by Compendium Publishers [Elmsford, N.Y.].

86. Lockwood, D.J., *Rayleigh and Mie Scattering*, in *Encyclopedia of Color Science and Technology*, M.R. Luo, Editor. 2016, Springer New York: New York, NY. p. 1097-1107.

87. Kundu, P.K., I.M. Cohen, and D.R. Dowling, *Fluid mechanics*. 5th ed. 2012, Waltham, MA: Academic Press.

88. Boucher, O., *Interactions of Radiation with Matter and Atmospheric Radiative Transfer*, in *Atmospheric Aerosols: Properties and Climate Impacts*, O. Boucher, Editor. 2015, Springer Netherlands: Dordrecht. p. 83-127.

89. Song, M., et al., *Overcoming Rayleigh–Plateau instabilities: Stabilizing and destabilizing liquid-metal streams via electrochemical oxidation.* Proceedings of the National Academy of Sciences, 2020. **117**(32): p. 19026.

90. Wang, B. and D.H. Kelley. *Optimal Vessel Materials for Indirect-contact Ultrasound Measurements*. in *13th International Symposium on Ultrasonic Doppler Methods for Fluid Mechanics and Fluid Engineering*. 2021. Zürich, Switzerland.

91. Murakawa, H., H. Kikura, and M. Aritomi, *Application of ultrasonic doppler method for bubbly flow measurement using two ultrasonic frequencies.* Experimental Thermal and Fluid Science, 2005. **29**(7): p. 843-850.

92. Obayashi, H., et al., *Velocity vector profile measurement using multiple ultrasonic transducers.* Flow Measurement and Instrumentation, 2008. **19**(3): p. 189-195.

93. Brito, D., et al., *Zonal shear and super-rotation in a magnetized spherical Couette-flow experiment.* Physical review. E, Statistical, nonlinear, and soft matter physics, 2011. **83**(6): p. 066310-066310.

94. Michaud, M., et al., *Design parameters of stainless steel plates for maximizing high frequency ultrasound wave transmission.* Ultrasonics - Sonochemistry, 2015. **26**: p. 56-63.

95. Yuan, Y. and T.R. Lee, *Contact angle and wetting properties*, in *Surface science techniques*. 2013, Springer. p. 3-34.

96. Zisman, W.A., *Relation of the Equilibrium Contact Angle to Liquid and Solid Constitution*, in *Contact Angle, Wettability, and Adhesion*. 1964, AMERICAN CHEMICAL SOCIETY. p. 1-51.

97. Clegg, C., *Contact Angle Made Easy*. 2013, Carl Clegg: Netcong, NJ. p. 4-10.

98. Liu, T., P. Sen, and C.-J. Kim, *Characterization of Nontoxic Liquid-Metal Alloy Galinstan for Applications in Microdevices.* Journal of Microelectromechanical Systems, 2012. **21**(2): p. 443-450.

99. Ancharov, A.I., et al., *Interaction between copper and gallium.* Russian Metallurgy (Metally), 2008. **2008**(6): p. 475-479.

100. Flynn, H.G., *GENERATION OF TRANSIENT CAVITIES IN LIQUIDS BY MICROSECOND PULSES OF ULTRASOUND.* The Journal of the Acoustical Society of America, 1982. **72**(6): p. 1926-1932.

101. Georgy I. Eskin, D.G.E., *Fundamentals of ultrasonic melt processing*, in *Ultrasonic treatment of light alloy melts*. 2015, CRC Press.

102. Brennen, C.E., *Cavitation and Bubble Dynamics*. 2013, New York: Cambridge University Press.

103. Tzanakis, I., et al., *Incubation pit analysis and calculation of the hydrodynamic impact pressure from the implosion of an acoustic cavitation bubble.* Ultrasonics Sonochemistry, 2014. **21**(2): p. 866-878.

104. Tzanakis, I., et al., *Characterisation of the ultrasonic acoustic spectrum and pressure field in aluminium melt with an advanced cavitometer.* Journal of Materials Processing Technology, 2016. **229**: p. 582-586.

105. Flannigan, D.J. and K.S. Suslick, *Plasma formation and temperature measurement during single-bubble cavitation.* Nature, 2005. **434**(7029): p. 52-55.

106. Komarov, S., et al., *Characterization of acoustic cavitation in water and molten aluminum alloy.* Ultrasonics Sonochemistry, 2013. **20**(2): p. 754-761.

107. Tzanakis, I., et al., *Calibration and performance assessment of an innovative high-temperature cavitometer.* Sensors and Actuators A: Physical, 2016. **240**: p. 57-69.

108. Eskin, D.G., *Ultrasonic processing of molten and solidifying aluminium alloys: overview and outlook.* Materials Science and Technology (United Kingdom), 2017. **33**(6): p. 636-645.

109. Takagi, R., S. Yoshizawa, and S.-i. Umemura, *Enhancement of Localized Heating by Ultrasonically Induced Cavitation in High Intensity Focused Ultrasound Treatment.* Japanese Journal of Applied Physics, 2010. **49**(7): p. 07HF21.

110. Caldwell, A.H. and A. Allanore, *Analysis of the partial molar excess entropy of dilute hydrogen in liquid metals and its change at the solid-liquid transition.* Acta Materialia, 2019. **173**: p. 1-8.

111. Ashokkumar, M., *The characterization of acoustic cavitation bubbles – An overview.* Ultrasonics Sonochemistry, 2011. **18**(4): p. 864-872.

112. Leighton, T.G., *2 - Cavitation Inception and Fluid Dynamics*, in *The Acoustic Bubble*, T.G. Leighton, Editor. 1994, Academic Press. p. 67-128.

113. Tzanakis, I., et al., *Characterizing the cavitation development and acoustic spectrum in various liquids.* Ultrasonics sonochemistry, 2017. **34**: p. 651-662.

114. Tzanakis, I., et al., *Comparison of cavitation intensity in water and in molten aluminium using a high-temperature cavitometer.* Journal of Physics: Conference Series, 2015. **656**: p. 012120.

115. Zeqiri, B., et al., *A novel sensor for monitoring acoustic cavitation. Part I: Concept, theory, and prototype development.* IEEE Transactions on Ultrasonics, Ferroelectrics, and Frequency Control, 2003. **50**(10): p. 1342-1350.

116. Xu, W.W., et al., *Synchrotron quantification of ultrasound cavitation and bubble dynamics in Al–10Cu melts.* Ultrasonics sonochemistry, 2016. **31**: p. 355-361.

117. Wei, R., X. Lv, and M. Yang. *Numerical Simulation of Ultrasound-Induced Cavitation Bubbling in a Calcium Ferrite Melt*. in *9th International Symposium on High-Temperature Metallurgical Processing*. 2018. Cham: Springer International Publishing.

118. Matsuda, S., *Absorption of Gases by Metals.* Journal of the Japan Institute of Metals, 1949. **13**(6): p. 10-14.

119. Cheng, J.S., et al., *Flow structures and aspect ratio in liquid metal convection*. 2022: Under consideration for publication in J. Fluid Mech.

120. Cheng, J.S., et al. *UDV methods for characterizing flows in liquid metal batteries*. in *13th International Symposium on Ultrasonic Doppler Methods for Fluid Mechanics and Fluid Engineering*. 2021. Zürich, Switzerland.

121. Cheng, J.S., et al., *Laboratory model of electrovortex flow with thermal gradients, for liquid metal batteries.* arXiv preprint arXiv:2108.01648, 2021.

122. Al-Kuhaili, M.F., *Characterization of copper oxide thin films deposited by the thermal evaporation of cuprous oxide (Cu2O).* Vacuum, 2008. **82**(6): p. 623-629.

123. Özer, N. and F. Tepehan, *Structure and optical properties of electrochromic copper oxide films prepared by reactive and conventional evaporation techniques.* Solar Energy Materials and Solar Cells, 1993. **30**(1): p. 13-26.

—— Appendix A ——

UDV in liquid metal battery experiments

The purpose of understanding the mechanism of UDV measurements in liquid metals is to better apply this technique to address specific scientific problems. One of the practical applications of UDV is to measure the flow structures in liquid metal battery (LMB) layers. In this section, we discuss some specific issues with respect to the improvement of UDV measurements and the handling of liquid gallium in the LMB experiments.

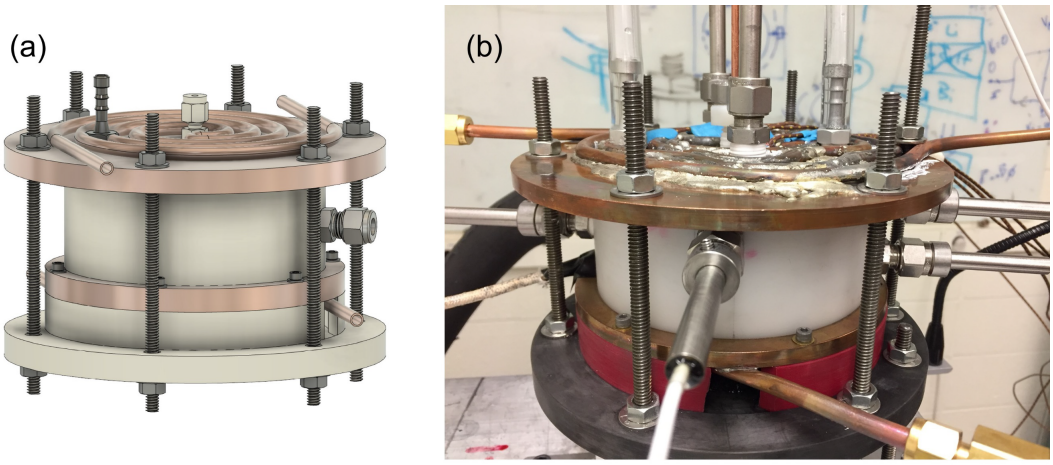

Figure A1. Liquid metal battery experimental setup. (a) Design drawing of the LMB laboratory model. (b) Photo of the real LMB experimental setup. The vessel is composed of copper top and bottom plates and a Delrin sidewall. UDV transducers are used to measure the flow structures of liquid gallium in the vessel.

The experimental configuration of our LMB laboratory model is shown in Figure A1. This system simulates the flow behaviors in the cathode or the anode layer of the LMB by introducing thermal gradients or/and electro-vortex flow in a liquid metal layer. Liquid

gallium is used as the fluid of the electrode layer in this LMB study. The gallium is contained in a cylindrical vessel. Two copper plates are used as the top and bottom layer of the vessel, respectively. The copper plates are also used for temperature control: copper coils are soldered on each copper plate and connected to a thermal baths water circulator to serve as a heat exchanger. The sidewall of the vessel is a hollow cylinder made of Delrin plastic. Multiple holes were drilled on the Delrin sidewall and top copper plate at different positions, for placing the UDV transducers and filling/ draining ports. Two copper rods connected to a power supply are placed in the middle point of the top and bottom plates to introduce currents. More details of the LMB experimental setup and diagnostics are available at [119-121]. Here, we only focus on some tricky issues related to UDV measurements and gallium processing.

Protective coating layer on copper

Although liquid gallium is very user-friendly because of its low melting point and non-toxicity, it tends to react with most metals. In early experiments, we observed that the copper plates used for temperature control whose surface exposed to liquid gallium was attacked by gallium, as shown in figure A2(a). The gallium erosion would destroy the surface smoothness, affect the temperature distribution, and eventually cracks the copper plate. Literature shows that the tungsten layer or copper oxide layer could be used to protect the copper from the attack of liquid gallium [64].

We first tried the tungsten protective layer. The tungsten layer was coated onto the copper plate by the sputtering deposition method. A tungsten target (99.95% purity, Refining Systems, USA) was installed in the sputtering equipment (Denton Sputtering, Denton Vacuum, U.S.A) as the tungsten source. The copper plate was placed in the sputtering

chamber. The sputtering coating process was conducted under 20 A current in an argon atmosphere. After 20 minutes of sputtering, a tungsten layer was successfully coated onto the copper plate, as shown in figure A2(b). However, through our test, we found that the tungsten layer was gradually washed off by water. We also tried changing the surface roughness of the copper plate, but it did not improve the stability of the tungsten layer.

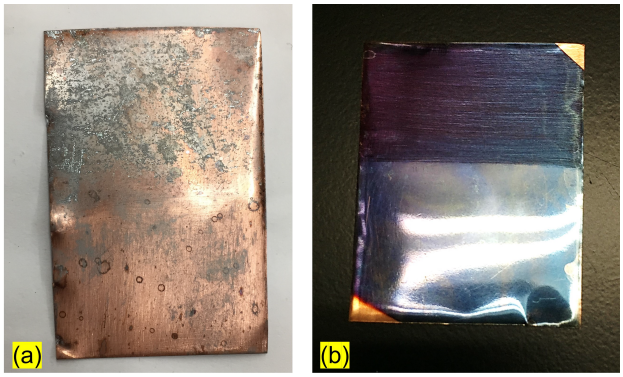

Figure A2. Picture of copper plates. (a) Uncoated copper plate corroded by contact with gallium. (b) Copper plate coated with tungsten. Changing the surface roughness of the copper plate could not improve the stability of the tungsten coating layer.

We then tried the copper oxide protective layer. The thermal evaporation method was used to coat the copper oxide layer on the copper plate. The thermal evaporation coating process was carried out in a Ladd Evaporator (Ladd Research Industries, U.S.A). Copper oxide pellets (CuO, 99.9% purity, AEM Deposition, China) were placed in a tungsten basket, which was held on a conductive stage. The copper plate to be coated was placed above the basket, and both of them were placed in the vacuum chamber of the evaporator. During the evaporation process, the vacuum chamber was vacuumed and maintained at a base pressure of $5*10^{-4}$ Pa. Current was then induced to heat the basket. Once it reaches the evaporation temperature of copper oxide, a copper oxide layer was deposited on the copper plate. To check the composition of the coated layer, we also coated the

oxide layer on a piece of silicon by the same procedure and then examined it under SEM. The results confirmed that a layer of copper oxide was coated successfully, as shown in figure A3. Our experimental observation confirmed that this copper oxide layer is more stable and can prevent gallium attacks effectively. The thickness of the coating layer is estimated to be 0.6 μm so that the effect of the coating layer on the thermal conductivity of the copper plate is negligible.

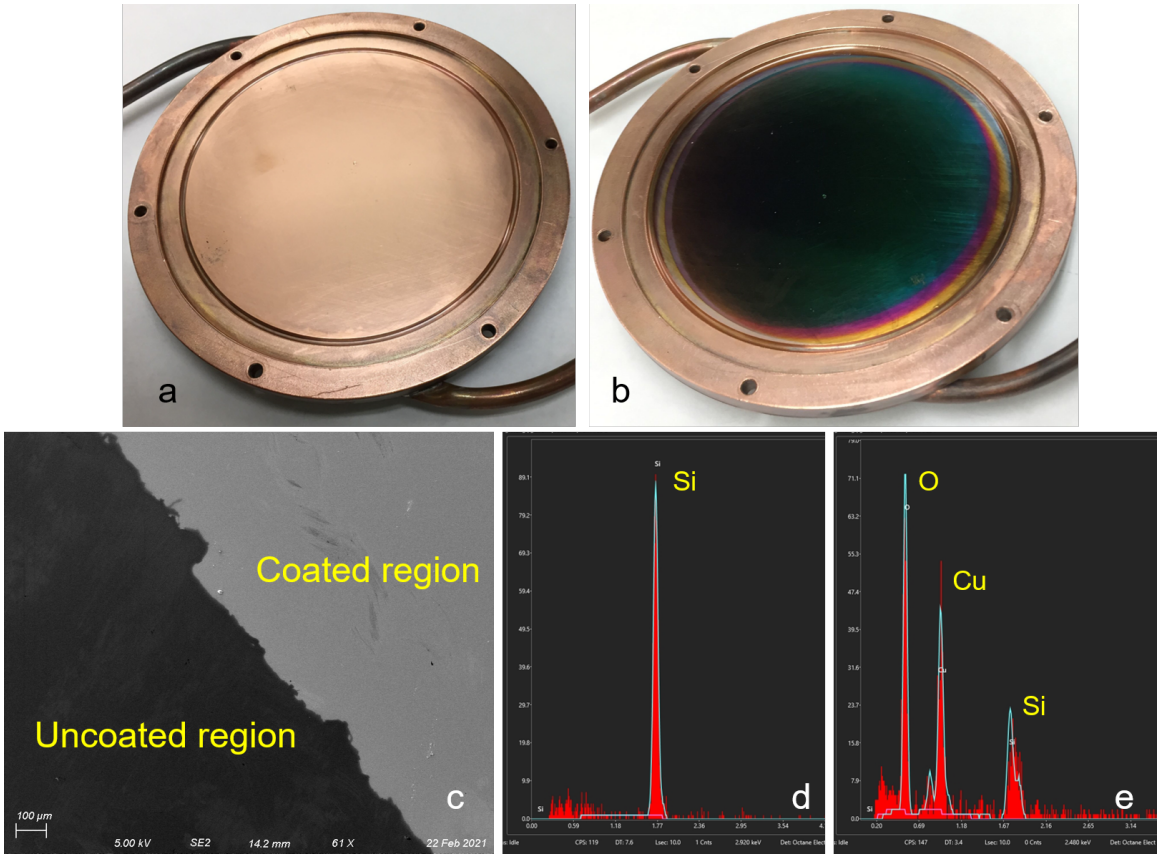

Figure A3. Coating of CuO on copper plate. (a) Before CuO coating. (b) After CuO coating. (c) SEM image of the Si sample. Half of the region was coated with CuO by the same procedure. (d–e) Energy-dispersive x-ray spectroscopy indicated nearly pure Si in the uncoated region and CuO in the coated region.

One of the disadvantages of the copper oxide coating method is that it needs delicate control of the evaporating temperature. A too high or too low evaporating temperature would lead to a change in the copper oxide compound: copper peroxide (CuO_2) might be deposited instead of CuO [122]. An alternative way to coat the CuO layer is available: instead of evaporating copper oxide directly, a pure copper layer could be evaporated first; then placing the copper coating layer in a furnace under a certain temperature and a certain gas atmosphere, the coated copper layer will then be oxidized to CuO. More introduction of the latter method can be found in [123].

The choose of UDV transducer and ultrasound frequency

Totally nine UDV transducers (Signal Processing, Switzerland) were used for measuring flow velocities in gallium from different planes and different directions. Six of them are designed to measure flows through direct contact, and the rest three are designed to measure flows indirectly through the Delrin sidewall. For the direct-contact measurement transducers, we chose the ultrasound frequency to be 8 MHz in order to achieve a smaller wavelength and thus a better spatial resolution. A higher ultrasound frequency could also mitigate the degradation of wetting at the transducer surface when contacting with gallium. The three transducers used for indirect-contact measurement were placed at the chord positions of the sidewall to measure the lateral flow velocities through the Delrin wall. Thus, we chose those three transducers with an ultrasound frequency of 4 MHz, as a low-frequency ultrasound has a lower attenuation rate and thus allows more ultrasound amplitude transmitted through the vessel wall.

The UDV transducer is sealed in a steel housing, and the housing is usually designed to be grounded in order to reduce noises from electromagnetic interference. Since current is

introduced to the liquid gallium layer during the experiment, all UDV transducers in direct contact with gallium must be ungrounded. Therefore, UDV signals measured by direct contact always become noisy when current is introduced. On the other hand, the indirect-contact ultrasound transducers can be grounded to get a better signal-to-noise ratio.

The choose of PRF, Emissions/profile, and TGC

The Pulse Repetition Frequency (PRF) and emission numbers per profile together determine the sampling frequency, measuring range, and velocity resolution of the UDV measurement. During practical measurement, those two parameters are adjusted according to the flow conditions. One principle is to ensure that the sampling frequency is always faster than the variation of the flow velocities. In general, for experiment cases with high-temperature gradient and/or high current, we increase both the PRF and Emissions/profile values to achieve a large measuring range and high sampling frequency; for experiment cases with low-temperature gradient and/or low current, we decrease both the PRF and Emissions/profile values to obtain a higher velocity resolution and a better signal-to-noise ratio.

The Time Gate Control (TGC) function is used to compensate for the ultrasound attenuation in gallium. Rather than a uniform TGC value, we applied custom-defined TGC values based on the measured echo profiled. Our experiments demonstrated that the custom-defined TGC can reduce the measurement noise and increase the measurable distance closer to the transducer surface. However, there will always be a 1-5 mm region in the vicinity of the transducer surface that is unmeasurable due to the ringing effect of the piezo element.

The nine transducers used in the LMB experiments are controlled by the multiplexer function to measure and record data one by one. The UDV parameters and operating time of each transducer can be set individually. The total time of one round of measurement is the sum of operating times from transducer 1 to transducer 9, we call it one block, and the whole measurement consists of multiple blocks. That's said, the interval between two consecutive measurements for the same transducer is the total time of one block. Therefore, in order to record the variation of the flow structures, the time of one block should not be too long. According to different conditions (temperature gradient, current), we usually set the time of one block between 1 second to 3 seconds. The overall measurement duration for one experiment is typically one hour.

For more details about the setting of PRF, Emissions/profile, the multiplexer function, and the specific operating procedure of custom-defined TGC, see Appendix B.

Obtain sufficient wetting for indirect-contact UDV measurement

Measuring flow from the chord position of the vessel always provides additional information different from that measured from the radial direction. For our experimental setup, however, the direct-contact UDV measurement from the chord position of the vessel is not available: due to the curvature of the vessel, the inner wall of the vessel and the transducer surface cannot be aligned in the same plane, so the presence of the UDV transducer would physically disturb the flows. Therefore, we choose the indirect-contact UDV measurement through the Delrin vessel sidewall.

The thickness of the vessel sidewall is 11 mm. As we discussed in Chapter 3, a thick wall disperses more acoustic energy when ultrasound transmits through it. To maximize the transmission of ultrasound waves, the thickness of the area on the wall where transducers

contact is thinned to 0.6 mm. 0.6 mm is also the wavelength of a 4 MHz ultrasound wave in Delrin, thus this thickness can also optimize the ultrasound transmission.

The other important factor for indirect-contact UDV measurement is wetting. Delrin is chosen as the sidewall material because of its excellent machinability. The acoustic wetting between Delrin sidewall and transducer surface is achieved by acoustic gel. The gel should be replenished before each measurement. Unfortunately, the wetting between the Delrin and gallium is not ideal. We measured the contact angle between Delrin and gallium to evaluate their wetting conditions. As shown in figure A4(a), the contact angle of gallium droplet on a machined Delrin surface is 152°, such that the gallium cannot wet the Delrin at all. As we discussed in Chapter 3, poor wetting would hinder the indirect-contact UDV measurement, and our experimental observations confirmed our conclusion: we could not measure any echo signals through the Delrin sidewall.

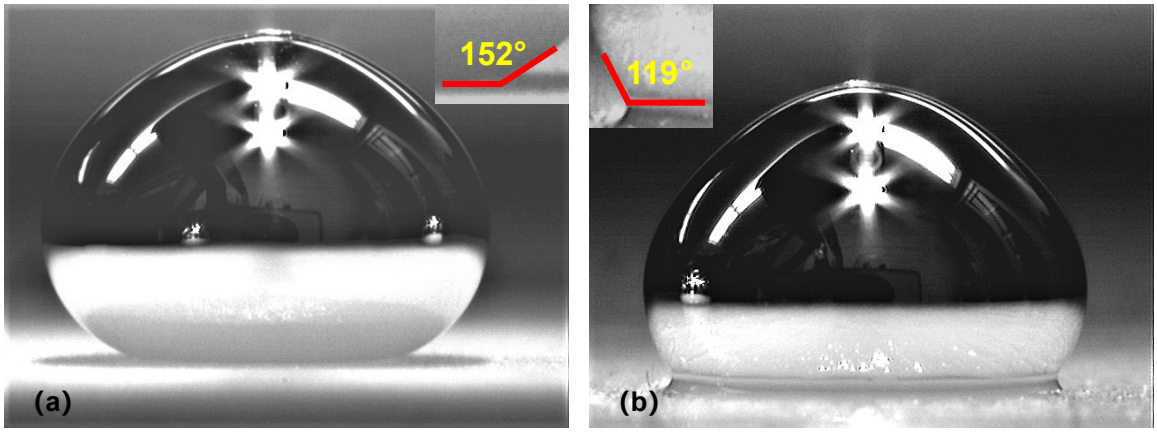

Figure A4. Contact angle measurement of gallium droplet on Delrin plates. (a) Delrin with a machine finishing surface. (b) Delrin with a polished surface and oil treatment. Oil treatment improved the wetting between Delrin and gallium.

We suspected that the poor wettability of Delrin is caused by the rough surface resulting from the machining process. To improve the wetting, we reduced the roughness of the Delrin surface by polishing it with sandpaper. Since Delrin is a soft material, the polishing process has some side effects that small Delrin fibers remain on the surface. To smooth out small fibers and fill in small gaps remaining on the surface, we further applied a thin oil layer on the Delrin surface. After those treatments, the wetting between gallium and Delrin improved that the contact angle is reduced to 119°, as shown in figure A4(b).

Before experiments, we treat the Delrin sidewall with the same procedure: we smooth the inner wall and oil the area on the inner wall where UDV transducers are positioned. The oil used here is a normal machine lubrication oil, which is applied to the wall one day prior to experiments to let it penetrate into the wall and dry over one night. Through the above treatments, we successfully obtained strong and clear UDV signals from the indirect-contact UDV measurement.

Note that as the oil dries, it will be less effective, and we will lose the UDV signals. Besides oil, water or any other medium that could fill the gaps on Delrin can be used. Compared to water, oil can last longer. Usually, the oil is reapplied to the inner wall once a week to maintain a good signal.

Strategy to improve measurement quality

As we demonstrated in Chapter 4, the UDV signal deterioration with time always happens even after a meticulous preparation of experiments. Figure A5 shows an example of a long-time UDV measurement in the LMB experiment. In this example, the UDV signal quality from the direct-contact measurement deteriorated over time, manifested by the increased noisy region near the transducer surface and the disturbed velocity

measurement after 100 minutes. In contrast, the indirect-contact measurement shows a consistently good performance. This observation also confirms the conclusions we draw in Chapter 4, that the indirect contact between the transducer surface and gallium can mitigate the degradation of wetting at the transducer surface.

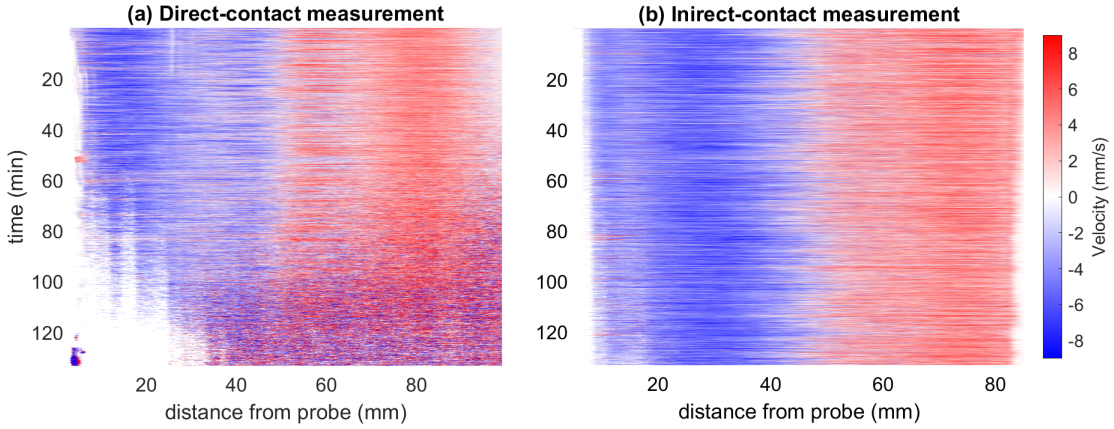

Figure A5. A long-duration measurement of gallium in the LMB experiment. The spatial-temporal velocity maps are measured by (a) a direct-contact transducer and (b) an indirect-contact transducer. The direct-contact measurement shows a more severe deterioration than the indirect-contact measurement.

Although there are problems such as the inevitable signal degradation, direct contact measurement still has some advantages over indirect contact measurement. First, the absolute signal quality of the direct-contact measurement is better as 8 MHz ultrasound has a higher resolution than 4 MHz ultrasound. Second, compared to Delrin, the UDV transducer surface has a better wettability to gallium and does not have to worry about replenishing the oil and acoustic gel. Third, the direct-contact transducer can be easily cleaned after each measurement, whereas the inner wall of the vessel can only be cleaned after disassembling the vessel. Next, we introduce some strategies that can be used to improve the signals quality of the direct-contact measurement.

Filling of gallium

Before experiments, liquid gallium is filled into the vessel through a filling port on the top copper plate. Due to the high surface tension of liquid gallium, the filling process is easy to induce bubbles into the system. If bubbles are attracted to the UDV transducer surface, it would destroy the UDV measurement. To eliminate bubbles, we designed two ports on the top copper plate, and each of them is connected to a plastic tube. During the filling process, the vessel is titled on one side such that one port is higher than the other. The lower port is the one through which we fill gallium into the vessel. The bubbles generated during the filling process will concentrate in the plastic tube of the higher port and thus be removed from the system. After filling, we also use a plastic rod to dredge the two ports in order to remove bubbles remaining inside the vessel. Once the liquid levels of gallium at the two ports are the same, we start to check the performance of each UDV transducer. If any of the transducers perform poorly (weak or noisy echoes), it means there may be bubbles or oxides sticking at the transducer surface. In this case, we have to further dredge the ports or refill the gallium again.

After the filling of gallium, we also need to remove the extra gallium left in the plastic tubes. This step is important because the gallium left in the plastic tubes is subject to an uncontrolled temperature environment: they may thus change the boundary conditions of the system, or even solidify if the environment temperature is too low.

Achieve better wetting for direct-contact UDV measurement

As we mentioned in Chapter 3, the wetting between the UDV transducer surface and gallium is not great. Given the bubbles and oxides generated during the filling process, sufficient wetting between the UDV transducer surface and gallium is not guaranteed. In

an open system, this issue can be easily solved by cleaning the transducer surface. However, in the close system of LMB experiments, the transducer surface can only be cleaned after draining the gallium. Therefore, it is annoying that sometimes a half-hour of gallium filling just results in a poor UDV signal or a failed measurement.

Based on our practical experience, we found that wetting the UDV transducer surface with water prior to the experiment could improve its wetting conditions with gallium. We use a wet towel to wipe the transducer surface right before the experiment. We assume the reason behind this is that the water can fill in the micro-gaps on the transducer surface and results in better wetting with liquid gallium. On the other hand, we also have to ensure that no water droplets remain on the transducer surface after wiping; otherwise, too much water might cause a negative effect, like gallium oxidation.

Turn off ultrasound emission while waiting

After filling the vessel with gallium, we have to check the performance of each UDV transducer to make sure they are working properly. After that, we still have to wait a few minutes for the temperature gradient of the system to stabilize. During this period, we should pause the ultrasound emission. As discussed in Chapter 4, it is ultrasound emission that causes the degradation of wetting at the transducer surface and thus the deterioration of UDV signals. Therefore, pausing the ultrasound emission before measurement starts can optimize the UDV signals quality and prolong the time of high-quality measurement.

The effect of current

During experiments, we realized that introducing current to the system will accelerate the deterioration of UDV signals, especially when the current is high. The reason behind there

is still unclear. To optimize the measurement quality, we should introduce the current after the temperature gradient in the system become stable.

Post-processing of UDV transducer and gallium

After finishing each UDV measurement, we drain the gallium from the vessel through a drainage port. The gallium is reusable and stored in a glass beaker. A lot of gallium oxides will be produced during the experiment and during the pouring process, appearing as wrinkled skin on top of the gallium surface. As too many oxides will disturb the UDV measurement, we remove those extra gallium oxides after each experiment by scratching the gallium surface in the beaker. Scratching off the wrinkled oxide skin, high purity gallium with a shiny mirror-like surface will emerge.

The removed gallium waste is collected in a container. The gallium waste is a mixture of gallium oxide and pure gallium. Pure gallium can be extracted by a combination of chemical and physical treatment. First, we heat the mixture to about 80°C. Then we add NaOH solution (1M) to the container and keep stirring them to let the gallium oxide fully react with NaOH. After tens of minutes, we pour off the excess solution and let the rest gallium solidify over one night. In the next day, we melt the gallium again. This time a black hard layer will form and float on top of the gallium surface, which is a mixture of oxides and sodium gallium compounds. We carefully scratch the gallium surface to remove this layer. By repeating the above processes two to three times, we can obtain some high purity gallium from the waste.

The UDV transducer surface also needs to be cleaned after each measurement. There is always gallium and gallium oxide sticking to the transducer surface after the gallium is drained out of the vessel. We use hot water and cleaner to clean each transducer surface.

Remember that after cleaning, there should be no gallium or water remaining on the transducer surface. We also have to clean the swage fitting used to hold the UDV transducer in place. If gallium droplets are left and solidified inside the fitting, the swage fitting cannot tightly hold the transducer anymore and leakage will happen.

In the last part, we give an example of a successful UDV velocity measurement. The positions of the transducers and the corresponding measurement results are shown in figure A6. By carefully conducting the experiment with the above strategies, we obtained clear and high-quality velocity measurements to analyze the flow structures in liquid metal convection.

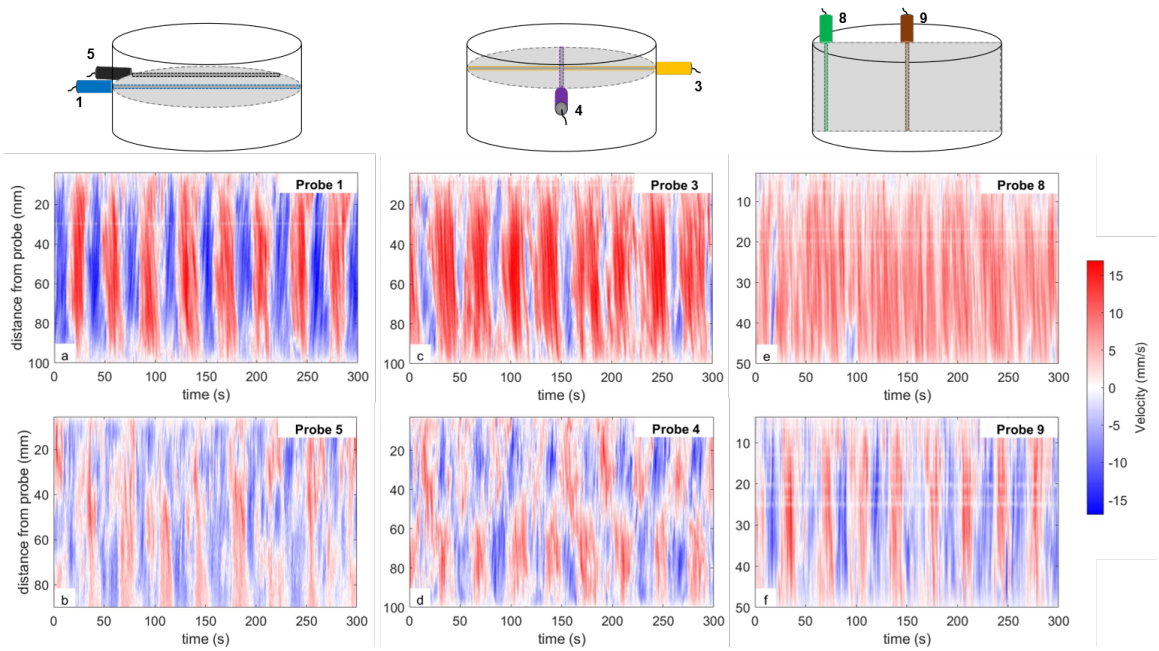

Figure A6. An example of a successful UDV velocity measurement in LMB experiments. The spatial-temporal velocity maps measured from six selected probe positions are displayed. Probe 5 is for indirect-contact measurement, and all the rest are for direct-contact measurement.

—— Appendix B ——

UDV operations and signal quality improvement

Appendix B summarizes some of the author's personal experiences with respect to the operation of the DOP3010 instrument and some tips for improving the signal quality of UDV measurements. It is highly recommended to read the *DOP3000 User's Manual* from Signal Processing first, where the fundamental of Doppler ultrasound velocimetry and various parameters are fully introduced. Here, some key parameters and concerns related to the application of UDV, liquid metals specifically, are discussed. Note that the idea and methods mentioned in this section only focus on improving signal quality and reducing noises in UDV measurements by adjusting parameters during data acquisition. In fact, the experimental design and configuration are also very important, especially the pre-treatment of liquid metals and vessel wall, which are discussed in Appendix A.

PRF and Emissions/profile

In the ultrasound fields, PRF usually means the Pulse Repetition Frequency, which is the frequency the ultrasound pulse is emitted. However, in the DOP software, PRF is expressed in the unit of microseconds (μs). So, it is actually the Pulse Repetition Period (PRP), the interval between two successive emissions, which is the reciprocal of PRF. Therefore, when using the DOP software, one should keep in mind that a smaller number in the input box indicates a higher PRF value, while a larger number in the input box indicates a lower PRF value. More information could be found in section 7.1 from the *DOP3000 User's Manual*.

The PRF defines the maximum measurable depth and velocity. The maximum measurable velocity should always be larger than the velocity to be measured. If the measured velocity value exceeds the measurable velocity range, velocity aliasing will happen, and the excess velocity parts will be folded. When velocity aliasing happens, the *PRF* value (in μs) needs to be reduced to increase the measurable velocity range. One thing that must be mentioned here is that the *PRF* value determines not only the measurable velocity range, but also the resolution of velocity measurement. The DOP outputs velocity values in a signed byte format, which allows 256 different velocity values to display in the interface. So, the velocity resolution is just the measurable velocity range (position + negative) divided by 256. Therefore, increasing the measurable velocity range will sacrifice velocity resolution. On the other hand, if a high resolution is required, then the *PRF* should be set to a large value (in μs) to shorten the measurable velocity range. In most cases, the velocity resolution is high enough for general velocity measurement.

To obtain statistically reliable results, each velocity profile is computed based on correlations between multiple consecutive pulse emissions. The number of emissions required to derive one velocity profile is determined by the parameter *Emissions/profile*. In general, a higher value of *Emissions/profile* produces a more accurate and more “averaged” result, whereas a lower value allows the measurement of flows involving rapid changes. The value of *Emissions/profile* should be chosen according to the type of flow to be measured and the desired time resolution.

The duration of one single emission is determined by the value of PRF. The total time duration of each profile is determined by PRF and Emission/profile together. There is always a trade-off between temporal resolution and measurement accuracy when choosing the values of *PRF* and the *Emissions/profile*. For example, if a flow has a small

velocity but varies frequently, then a large PRF value (in μs) and a small number of *Emissions/profile* should be used. On the other hand, if the to be measured flow is steady but has a large velocity, then a small PRF value (in μs) and a high number of *Emissions/profile* should be used.

In addition to the *PRF* and *Emissions/profiles*, the total duration of one UDV profile also includes the internal data transmission and processing time. More detail could be found in section 7.8 of the *DOP3000 User's Manual*. When multiple ultrasound transducers (multiplexer) are used, extra attention should be paid to reasonably selecting the values of *PRF* and *Emissions/profile* for each channel (see below).

Multiplexer

The DOP3010 allows ten channels to be used independently for velocity measurements. When the multiplexer function is enabled, multiple transducers will emit/receive signals in a certain sequence.

Taking the measurement of liquid metal battery as an example: up to nine channels were used, and the UDV transducers were placed at different positions of the container. For each channel, parameters such as *PRF*, *Emissions/profile*, *burst length*, etc. can be defined individually. The measurement duration of each channel is determined by the input values of *PRF*, *Emissions/profile*, as well as the number of *Acquire*.

As shown in the red box at the bottom of the figure B1, 1 *Acquire* means the current channel will only acquire one profile and then switch to the next channel. X *Acquire* means the current channel will repeat acquiring X profiles before switching to the next channel. When all channels, from channel 1 to channel 9, finish one round of acquisition, it is called one *Block*. In other words, the duration of one *Block* is also the interval between two

consecutive measurements for the same channel. In the liquid metal battery experiments, we prefer a high temporal resolution measurement to capture the variations in flow structures. Therefore, we set only one *Acquire* for each channel in order to shorten the measurement period. The *Acquire* number can also be set to different values for each channel.

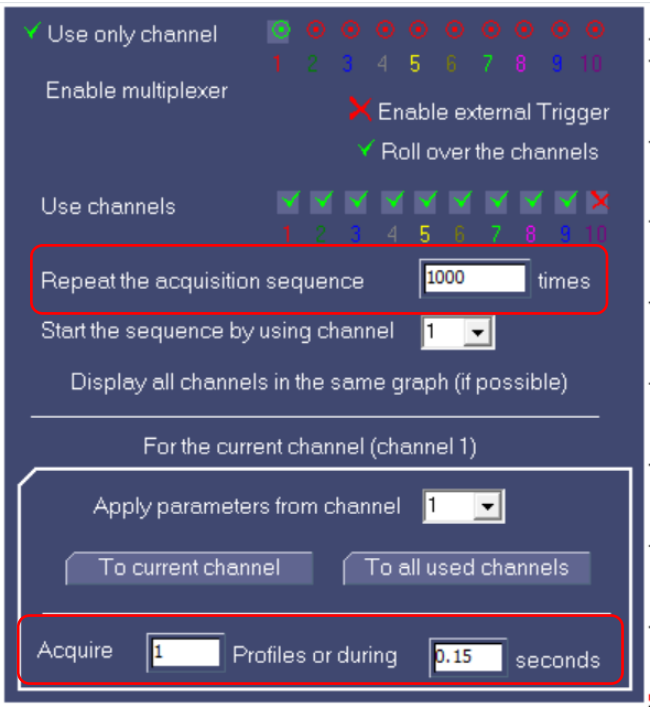

Figure B1. Illustration of the Multiplexer function

The value of the *Repeat acquisition sequence* defines the total number of *Blocks* that will be acquired during one measurement. One should note that once the multiplexer is enabled and recording is started, the recording could not be paused or stopped until all the repeat acquisitions are finished, otherwise the data could not be stored. Whereas for a single channel measurement, one can pause or stop the recording at any time to store the data.

Adjustment of burst length (pulse length)

In UDV, the transducer emits a short ultrasound pulse consisting of several cycles of ultrasound waves. The number of cycles contained in a single pulse is given by the parameter *Burst length*. The *Burst length* and *Emitting frequency* (ultrasound wavelength) together determine the length of the pulse, which is also the longitudinal dimension of the measuring volume. Therefore, to get a higher resolution (small measurement volume), the cycles of *Burst length* should be as small as possible. However, too few cycles do not provide clear ultrasound beams because of a lack of interference between ultrasound waves in the near field. In DOP, although the least number of cycles is 2, it is still recommended to use at least 4 cycles.

Note that the measurement volume is not equal to the actual sampling volume. Due to the intrinsic resolution limitation of the DOP, it has a minimum sampling volume (one cell). If the pulse length is less than the minimum sampling volume of one cell, then the actual sampling volume is determined by the intrinsic resolution of the cell. Therefore, sometimes increasing or reducing the cycles of *Burst length* does not change the real sampling volume.

In addition, a higher number of cycles will increase the intensity of the ultrasound signals, consequently, it will increase the bulk echo intensity and help the ultrasound beam to penetrate thick interfaces (such as the vessel wall). However, a higher number of cycles will also result in a larger measurement volume so that adjacent data points will overlap with each other, thereby decreasing the measurement resolution. Further, a higher number of cycles will increase the depth of the near field so that a larger area near the transducer surface will become unmeasurable.

Accordingly, it is recommended to use 4 or 6 cycles for direct-contact measurement, and 8 or 10 for indirect-contact measurement. If the bulk echo intensity is too low to allow accurate velocity measurement, the number of cycles of *Burst length* should be increased appropriately.

Indirect-contact measurement through a wall or a plate

When conducting the indirect-contact UDV measurement, the DOP provides a function called *US coupling parameters* (as shown in figure B2), which allows us to define parameters of the container's wall that need to be transmitted through and the acoustic coupling medium between the transducer and wall. The *Sound speed* and *Thickness* are given by the selected vessel material. Usually, water or acoustic coupling gel is used as the acoustic coupling medium.

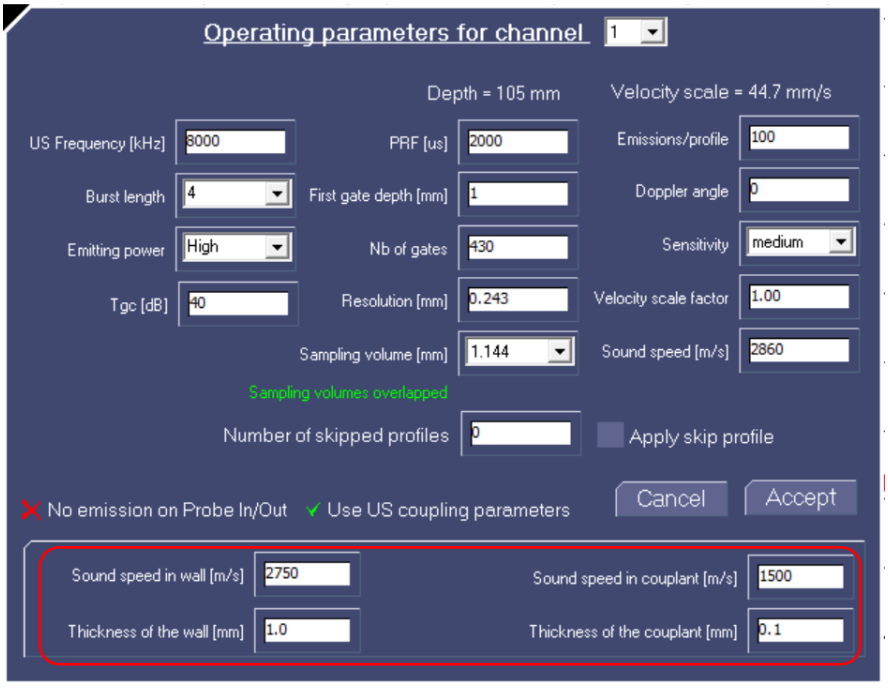

Figure B2. Illustration of the US coupling parameters

By enabling this function, the DOP can reduce some of the noises, caused by the wall, near the transducer surface. However, this effect sometimes might not be very noticeable, because the signal near the transducer surface region is also affected by the near-field and ringing effect.

Standing echoes noise

Ideally, DOP should detect only one strong and high amplitude echo peak at the back wall position. However, standing echoes resulting from the interference between the incoming wave (perpendicular to an interface) and its reflected wave might arise near the back wall of the vessel. If the standing echoes appear behind the back wall position, we can simply ignore them. If they appear in front of the back wall position, then they could prevent the measurement of velocities at those regions. To avoid the appearance of standing echoes, the Pulse Repetition Period (PRP) should be chosen as a multiple of the travel time of the ultrasound through the vessel.

For example, in the liquid metal battery experiments, the vessel diameter is 100 mm, the sound speed of gallium is 2860 m/s; so the travel time is 70 μs. Therefore, the PRF (PRT actually) value can be chosen as a number multiple of 70, such as 1750, 2660, 3500….

Errors reduction and velocity measurement near the transducer surface

In UDV, errors like spurious or null velocity will arise if the bulk echo intensity is too weak. However, those errors could also be introduced if the echo is saturated such that its amplitude exceeds the maximum measurable value of the echo profile. Due to the ultrasound attenuation, the echo saturation always appears at the near transducer surface region. Figure B3 shows an example of UDV measurement in gallium, in which the echoes'

amplitudes at the first 25 mm depth are significantly saturated. If such echo saturation exists, the real flow velocities at those saturated locations could not be measured.

To reduce the velocity errors, the echo amplitude needs to be adjusted to remove the saturation. Specifically, the echo peak amplitude should be less than the maximum measurable value (2000), and the fluctuation in the echo amplitude (due to the movement of scattering particles) can be observed during the echo measurement. There are four parameters in the DOP software that can affect the measured echo amplitude; they are *Burst length*, *Emitting power*, *TGC*, and *PRF*. However, the changes in *Burst length*, *Emitting power*, and *PRF* would also affect the measurement resolution, duration, and quality. Therefore, the adjustment of the TGC level is a better way to remove the saturation effect.

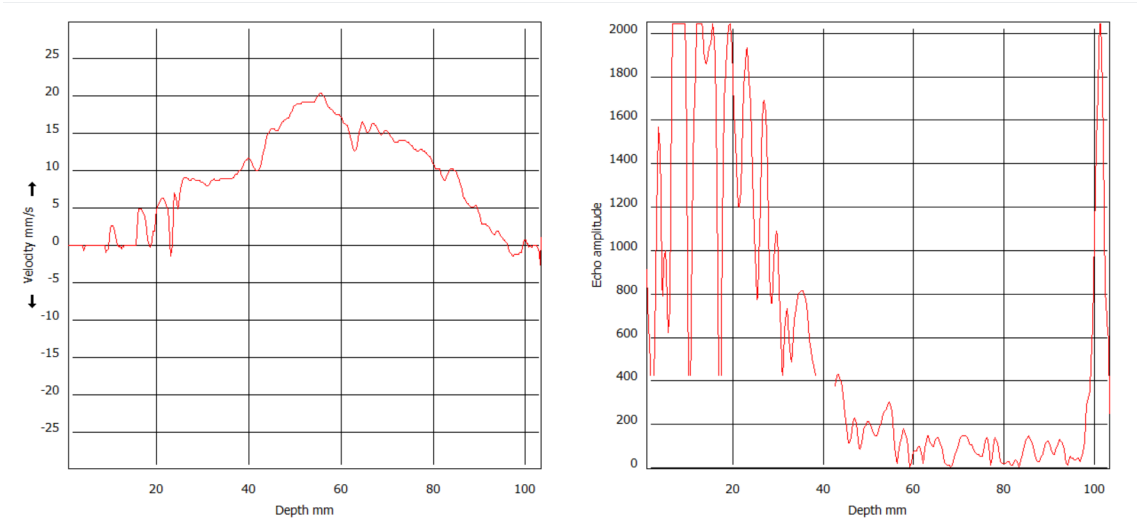

Figure B3. UDV measurement in liquid gallium without TGC adjustment. Significant echo saturation occurs at the first 25 mm depth of the echo profile. Accurate velocity measurement at the corresponding locations is unavailable as many errors appear.

TGC, or Time Gain Control, is an amplification function used to compensate for the attenuation of ultrasound waves when propagating in a medium. In the default setting of DOP, the TGC is set to a uniform level with a maximum value of 40 dB. Although this setting can promise a sufficient echo intensity in the far region, it will introduce echo saturations at the region near the transducer surface. Therefore, it is necessary to adjust the TGC level according to the specific circumstances of the echo profile.

The DOP provides four different modes to define the TGC level, as shown in figure B4. A detail introduction of those four modes can be found in section 7.11 of the *DOP3000 User's Manual*. For UDV measurement in liquid metals, the *Custom* mode is the most useful one, which allows us to define different TGC levels at different regions along the measuring line. Due to the poor wetting between the transducer surface and liquid metals, the echo saturation is usually quite strong in the region near the transducer surface; while due to ultrasound attenuation, the echo amplitudes are very low at the far region. As mentioned above, either too high or too low echo amplitudes will lead to errors in velocity measurement. An often-happened scenario in liquid metal experiments is that a fairly good velocity measurement could be achieved at the far region but almost no velocity could be measured in the near transducer region. Therefore, the *Custom* mode is very suitable for this situation: we can customize the TGC level at different regions.

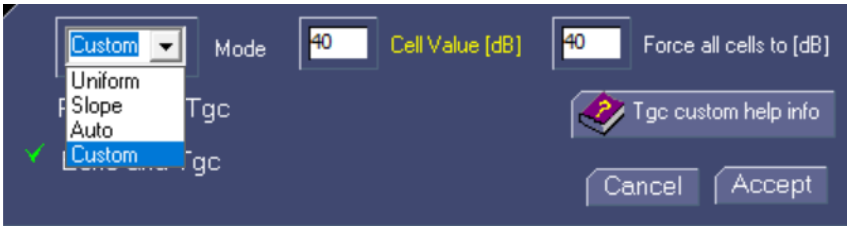

Figure B4. Illustration of the TGC level adjustment

Because of the ultrasound attenuation, the degree of saturation usually increases as the distance approaches the transducer surface. In other words, echoes located on the left of the screen (close to the transducer) require a smaller TGC value to remove the saturation than the echoes located on the right (far from the transducer). Therefore, a recommended routine to define the *Custom* TGC level is:

1. Under the *Custom* TGC mode, input the number 40 (the maximum TGC level) to the right box (*Force all cells to*) to make all cells have the maximum TGC level.

2. Select the whole saturation region by left-clicking the mouse at the very beginning point in the echo profile and right-clicking the mouse at the point where the saturated echo ends. The echo profile in the selected region will turn yellow.

3. Input a number slightly smaller than 40 (like 37 or 35) in the middle box (*cell value*). After this adjustment, some saturated echoes on the far-right of the selected region might be removed; if so, right-clicking the mouse on the echo profile to choose a new saturation ending point; if not, gradually reduce the input TGC number in the middle box until the saturated echoes at the far-right region are removed.

4. Repeat step 3: selecting new saturation ending points and entering smaller numbers of TGC for each new selected region, until all saturations are removed.

Figure B5 shows a UDV measurement in gallium after the custom TGC adjustment, in which all echo saturations have been removed in the echo profile. This time, the velocity measurement at the region close to the transducer surface is available.

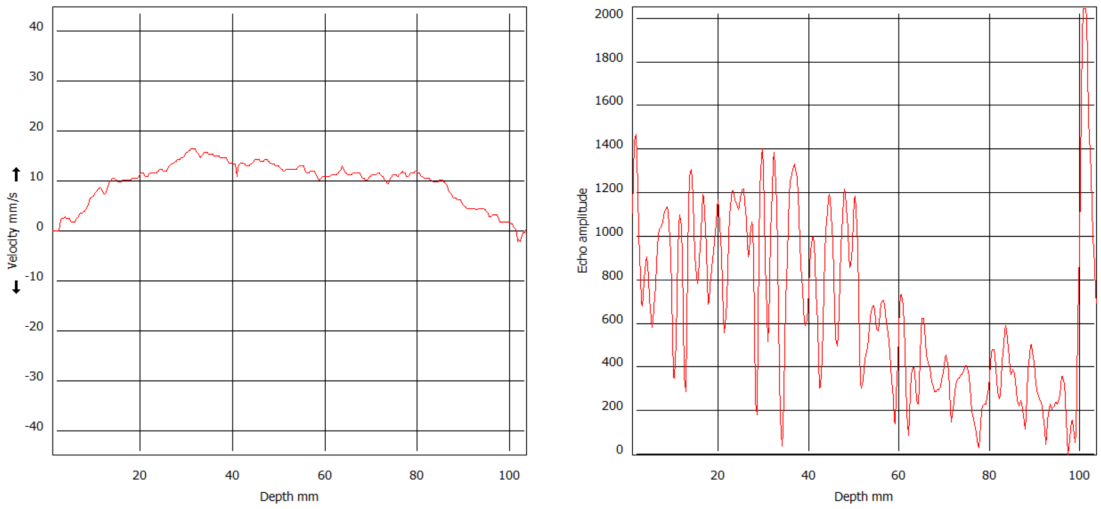

Figure B5. UDV measurement in liquid gallium after TGC adjustment. All saturations have been removed in the echo profile, and accurate velocity measurement could be achieved at the near transducer surface region.

Remember that the TGC level should be reduced gradually, because a too low TGC level will also cause the echo amplitude too weak to be measured. Note that the echo amplitude will further decay with time due to the loss of scattering particles and wetting deterioration at the probe surface. Therefore, it is recommended to adjust the initial echo amplitudes to around 1000-1500 (in arbitrary units), so that the echo intensity is still strong enough after hours of measurement.

In most cases, the above procedure is sufficient to reduce the influence of echo saturation. However, two special cases may be encountered sometimes. For the first special case, some saturated echoes may still present under a TGC value that is sufficient to remove the saturation located on their left but not enough for them. Under this circumstance, we can ignore those echoes at first and continue to finish the above routine procedure; then

we take care of those echoes by individually selecting them and defining an individual TGC value for them.

In the second special case, although an echo amplitude is not displayed at a saturated level in the echo profile, the corresponding velocity measurement might still be incorrect. One strategy for recognizing those incorrect velocities is to closely observe the velocity profile, and find the regions or points where the velocity values fluctuate irregularly or always stay at zero. If we already have a prediction for the shape of the velocity structure to be measured, we can easily find the regions that break the continuity of the whole velocity curve.

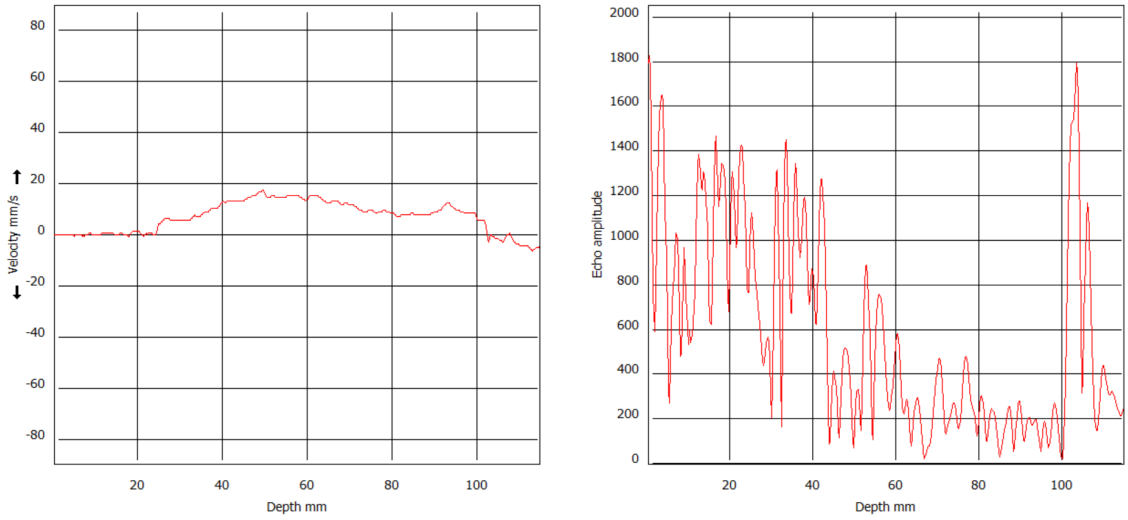

Figure B6. UDV measurement in liquid gallium (special case). The velocity measurement at the first 20 mm depth is incorrect although the corresponding echoes amplitudes are not saturated.

Figure B6 is a good example of the second special case. In that experiment, a rotating flow was measured by the UDV transducer placed at an off-center position. In that configuration, we expect to measure a positive velocity profile with the maximum value at the center. However, in figure B5, the measured velocities at the first 20 mm depth were

incorrect, although the corresponding echoes' amplitudes are not saturated. After locating the incorrect velocity regions, we need to select the corresponding echo regions to adjust their TGC levels. From personal experience, what always happens under this circumstance is that when we slightly adjust the TGC values for those regions, the change in echo amplitude is not apparent. In this case, a large adjustment of TGC to significantly reduce the echo amplitude could fix the errors in the velocity measurement.

Note that some saturations appearing very close to the transducer surface cannot be removed by TGC. Those saturations are caused by the ringing effect, which is inevitable. A small number of *Burst lengths* may help reduce the depth affected by the ringing effect. Nevertheless, there will always exist an echo-saturated region where velocity measurement is unavailable.

Echo noise accumulation

In UDV echo measurement, when the bulk echo intensity is too weak, fake signals may appear that make the echo intensity "looks" stronger. Those fake echoes may build up over time until they suddenly "collapse" and fall back to the real, weak echoes.

I called this echo noise accumulation, but it has not been mentioned in the user's manual. The echo noise accumulation is related to the internal electronic processing of the DOP instrument: when the echo intensity is too weak, offset in the IQ signals would happen (noises arise); when the internal calibration is performed to cancel the offset, echo intensity will back to normal (noises collapse). However, one negative effect of the echo noise accumulation is that an off-phase shift will appear in the velocity measurement when the fake echoes "collapse".

The simplest way to avoid the echo noise accumulation is to maintain a strong bulk echo intensity, either by introducing a vigorous flow or shortening the measurement duration. However, some experiments, like the liquid metal battery experiment, require long-duration velocity measurements with a relatively weak echo intensity.

UDV Energy profile

Another way to avoid the appearance of echo noise accumulation is to use the UDV energy profile instead of the UDV echo profile. The UDV energy profile is a high pass filtered echo profile. It measures only the echo of moving objects inside the beam path (has the velocity component parallel to the ultrasound propagation direction). When the energy profile is applied, the back-wall echo and multiple reflections near the transducer surface cannot be observed anymore, as shown in figure B6.

The UDV energy profile function has been often used in our study due to its advantages. Since the energy profile detects only the echoes from particles moving along the ultrasound beam propagation direction, it was used to track the motion of echoing objects under gravity, as described in Chapter 2. Since the energy profile can avoid the appearance of the echo noise accumulation, it was used to measure the bulk echo decay behaviors in gallium, in which the echo intensity was very weak after a long time of measurement, as described in Chapter 4.

Although the front-wall noises and reverberations do not appear in the energy profile, the influence of echo saturation on velocity measurement still exists. Therefore, it is suggested to display the echo profile first, playing with the TGC to adjust the intensity of those saturated echoes, and then switch to the energy profile.

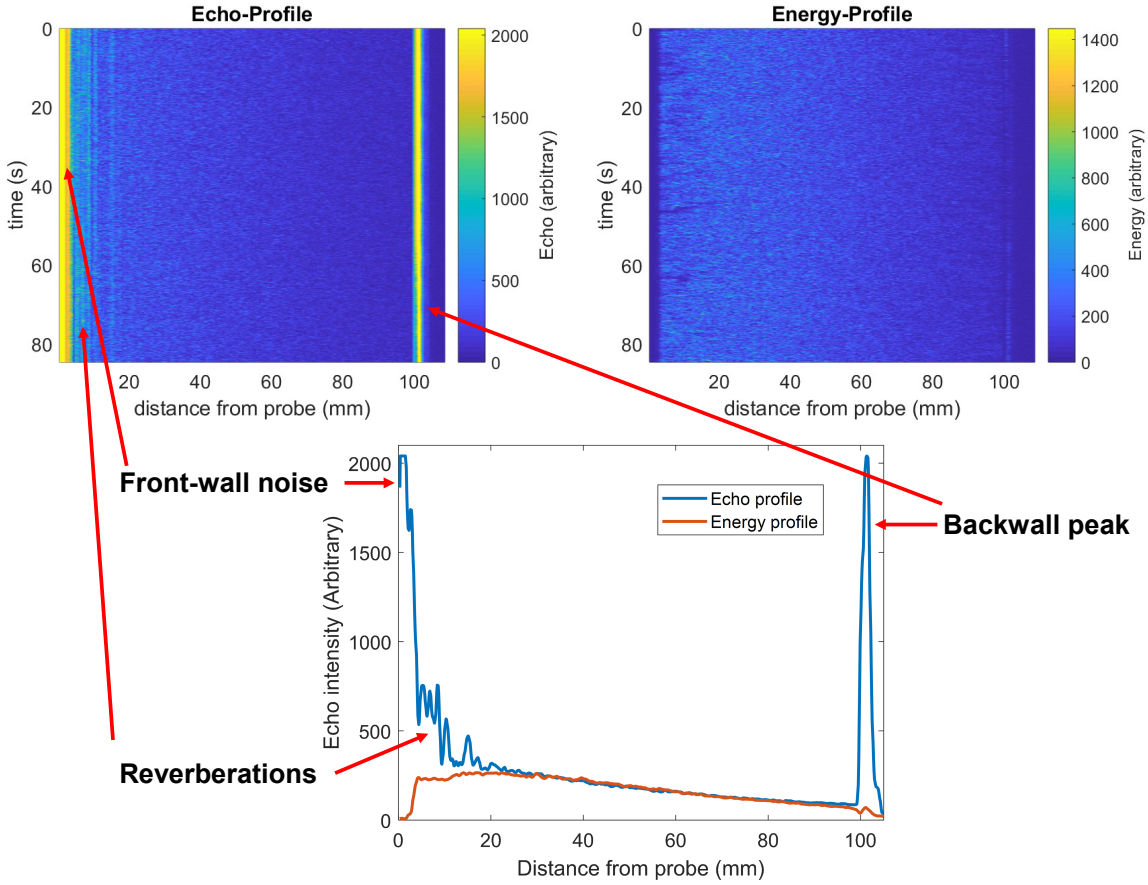

Figure B7. Comparison between the UDV echo profile and energy profile. The bottom plot shows the time-averaged echo intensity curves obtained from the above echo profile and energy profile.